UNIVERSITY OF CALIFORNIA, SAN DIEGO

Effects of Channel Noise on Neural Networks

A dissertation submitted in partial satisfaction of the
requirements for the degree
Doctor of Philosophy

in

Chemistry

by

Brenton A. Maisel

Committee in charge:

Professor Katja Lindenberg, Chair
Professor Rommie Amaro
Professor Patrick Fitzsimmons
Professor Michael Galperin
Professor Francesco Paesani

2018

The dissertation of Brenton A. Maisel is approved, and it is acceptable in quality and form for publication on microfilm and electronically:

_____

_____

_____

_____

_____

Chair

University of California, San Diego

2018

DEDICATION

To everyone who has one way or another supported me along the way.

EPIGRAPH

If we knew what it was we were doing, it would not be called research, would it?

—Albert Einstein

TABLE OF CONTENTS

LIST OF FIGURES

LIST OF TABLES

ACKNOWLEDGEMENTS

This thesis represents not only everything I have learned and worked for the past several years, but is a milestone in my life symbolic of all my accomplishments to date. As such, there are multiple people I wish to thank.

I would first like to thank my thesis advisor, Dr. Katja Lindenberg, for taking me under her wing as a graduate student. I know there was a big adjustment period at the beginning for both of us as neither of us were familiar with this topic, but you did not give up on me. I have grown a tremendous amount working with you, through teaching, writing, and learning. I am a better person today because of you. In addition, I would like to thank the members of my thesis committee: Dr. Rommie Amaro, Dr. Patrick Fitzsimmons, Dr. Misha Galperin, and Dr. Francesco Paesani. It has been a pleasure interacting with and learning from each of you. I admire all of your works and achievements, and I hope to one day be as well-regarded in my field as each of you are in yours.

I would also like to thank several members of the MURI project who were invaluable people throughout my graduate career. First, I thank Sadique Sheik for all of his assistance with programming in Python and whom without this thesis would not have been completed. Thank you for your patience with me as I learned coding from you and for taking so much time out of your busy schedule to help me get to this point. Next, I like to thank Eve Armstrong. I have always enjoyed our conversations whether about the MURI project or about life in general. I appreciate you keeping me sane by relating to everything I had gone through in my graduate career and for being the only person at the conference in Exeter, UK that I knew.

Additionally, there are people I wish to thank who have been influential in my personal growth prior to graduate school. I owe a tremendous amount of gratitude to my undergraduate advisor, Stephen Sieck, who showed me not just what good teaching

looks like but who also gave me the opportunity to teach. I too thank Joseph Mileti who pushed my math capabilities to new heights and who motivated me to find research that blends my math background with applied sciences.

I would next like to thank my family and friends who stuck by my side and offered moral (and financial) support through this entire process. I am eternally grateful to be surrounded by those who love me and care for me.

I thank the U. S. Office of Naval Research (ONR) under Grant No. N00014-13-1-0205 for providing the funding for this research.

Chapter 3, in full, is a reprint of the material as it appears in Physical Review E 2017. Maisel, Brenton; Lindenberg, Katja, Physical Review E, 2017. The dissertation/thesis author was the primary investigator and author of this paper.

Chapter 4, in full, is a reprint of the material currently being prepared for submission for publication to Physical Review Letters. The dissertation/thesis author was the primary investigator and author of this paper.

Chapter 5, in full, is a reprint of the material currently being prepared for submission for publication to journal to be determined. The dissertation/thesis author was the primary investigator and author of this paper.

VITA

2011	B. A. in Mathematics, Grinnell College
2011	B. A. in Chemistry, Grinnell College
2014	M. S. in Chemistry, University of California, San Diego
2016	M. A. in Mathematics (Applied), University of California, San Diego
2018	Ph. D. in Chemistry, University of California, San Diego

PUBLICATIONS

Brenton Maisel and Katja Lindenberg. "Channel noise effects on first spike latency of a stochastic Hodgkin-Huxley neuron", *Physical Review E*, 95, 2017

Brenton Maisel, Sadique Sheik, and Katja Lindenberg. "Channel Noise Effects on Neural Synchronization" (to be submitted)

Brenton Maisel and Katja Lindenberg. "Effects of Gaussian White Noise on Dynamics of a Two Heteroclinic Cycle System" (to be submitted)

ABSTRACT OF THE DISSERTATION

Effects of Channel Noise on Neural Networks

by

Brenton A. Maisel

Doctor of Philosophy in Chemistry

University of California, San Diego, 2018

Professor Katja Lindenberg, Chair

The human brain contains on the order of 10^9 neurons with each neuron having on the order of 10^4 synaptic connections with other neurons. Within each neuron, there are protein channels that dictate when ions can flow through them. It is the flow of these ions that is the basis for action potential generation, and these action potentials are the source of neural communication and information. These channels exist in various configurations some of which are conducting ("open") and some of which are non-conducting ("closed"). Moreover, these channels can stochastically switch between the open and closed states. It is nothing short of remarkable that the brain functions as it does despite the randomness present within each neuron.

What role these microscopic fluctuations, herein known as channel noise, have on macroscopic neural network properties is an open area of neuroscience that has generated a great deal of interest in recent years due to the advancement of computational methods. In this thesis, we first introduce the Hodgkin-Huxley model and mathematical equations which incorporate this channel noise in the Hodgkin-Huxley model. We then study the role of channel noise on properties of small neural networks which begins in Chapter 3. The first property we will look at is how channel noise affects the timing of the first action potential after stimulus onset. This property, known as first spike latency, is believed to be a coding mechanism used by neurons to communicate information between stimuli and brain processing. We will then look at the role of channel noise on neural synchronization. Abnormal synchronization has been strongly correlated with a number of neural disorders such as Alzheimer's disease and Parkinson's disease.

One area of research in neuroscience that is of fundamental interest is the relationship between neural spiking and cognitive processing. For this thesis, in addition to the small neural network models for first spike latency and synchronization, we will consider a recently developed model for cognition and study the model's behavior when subjected to noise. We will conclude with a brief summary of the results obtained as well as discuss ways to extend the research to larger neural network systems.

Chapter 1

Introduction

The human brain is a remarkable and highly complex organ. Despite being a network composed of roughly 100 billion neurons with each neuron connected to roughly 10^4 other neurons, the brain is capable of encoding information about the environment and making a decision within fractions of a second [RWDRvSB99, TFM$^+$96]. For example, we can instantly recognize the faces of our family members out of billions of faces on the planet. How is such a thing even possible? Although the coding mechanism used by neurons remains unclear, it is widely assumed that coding is based on action potentials or spikes. However, exactly which aspects of these spike trains convey the information about the environment? Does the exact timing convey important information or is the rate at which a neuron produces spikes the only important aspect with everything else just noise? The first major section of the thesis will be a study of the effects of fluctuations on spike timing.

As an extension to action potential timing and rates, the study of neural synchronization and how neural networks synchronize their action potential timing between various brain regions arises in many areas of neuroscience such as learning [AM14], both mental health disorders and neurological disorders [ACM14, HBB07, US06], lo-

comotion [RF98], feeding [RES$^+$97], and breathing [TK02]. These networks exhibit oscillatory behavior and the frequencies of these oscillatory behaviors are believed to be associated with various behaviors. For example, the gamma frequency range ($25-100$ Hz) is associated with sensory information processing in areas as seen in the the olfactory system [LD$^+$94] and visual system [GKES89]. The second major section of this thesis will be a study of how fluctuations affect the ability of neurons to synchronize. In order to study both spike timing and synchronization, we need to first understand the biophysical basis of action potentials.

Action potentials are generated when the voltage of the neuron's membrane reaches a certain threshold. Typically, the neuron's resting membrane potential is approximately -65 mV and an action potential forms when the membrane potential reaches a value between -50 and -55 mV [SSR05]. However, fluctuations in the voltage can occur which affect the neuron's spike timing. As we will discuss, this in turn affects both neural coding and neural synchronization, which are strongly tied to mental health disorders. The role of this thesis will be to understand what effects membrane voltage fluctuations have on macroscopic neural network behavior through the study of small neural networks. To understand this concept, we need a mathematical framework to study action potential generation. We begin by reviewing the anatomy and electrophysiology of a neuron.

1.1 Anatomy of the Neuron

A typical neuron can be divided into several regions: dendrites, cell body, axon, and presynaptic terminal. As a simplistic overview, the cell body connects to the dendrites which bring information to the neuron, and the axon which sends information to other

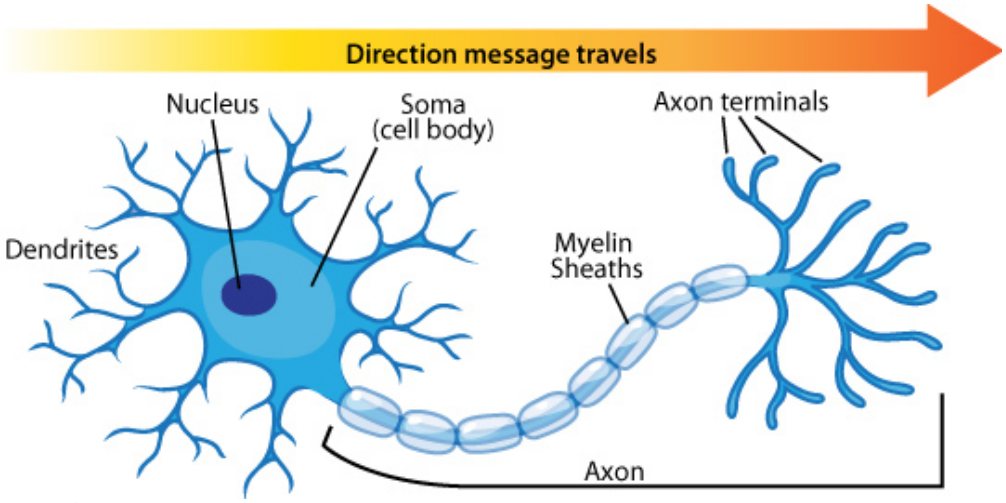

Figure 1.1: Schematic drawing of a neuron with emphasis on its major features. "Nerve Cell" by ASU - Ask a Biologist is licensed under CC BY 3.0 [Szy11] (Used with permission).

neurons. A schematic drawing of a neuron can be seen in Fig. 1.1. Perhaps the most important function of the cell body, also called the soma, is that it contains the nucleus of the neuron and is the site of protein synthesis. These proteins allow neurons to build new axons and dendrites to make new connections with other neurons [LBZ+00].

Dendrites are the branched structures which extend outward from the cell body. These structures receive electrical messages in the form of neurotransmitters from other neurons which come in two forms: excitatory which increase the stimulation of a neuron and lead to neural firing, or inhibitory which decrease neural activity and prevents neural firing. After enough electrical stimulation, the neuron will fire its own action potential which originates at the axon hillock, the junction between the soma and the axon.

Nearly every neuron contains an axon, which is the main conducting unit of the neuron that conveys electrical signals across large distances. The axon also contains several types of proteins (ion channels) which allow for the propagation of action potentials. These will be explored in more detail in the next section. In some cases, the axon may be covered in a mylein sheath which acts as an insulator to the neuron and helps to increase the rate of action potential propagation.

Lastly, the presynaptic terminal contains neurotransmitters enclosed in vesicles. These neurotransmitters get released into an area between two neurons (called the synaptic cleft) which then bind to the dendrites of another neuron. This causes the voltage of this other neuron to change, leading to other action potentials. Further details about this process will be discussed in Section 1.4.

1.2 Physiology of the Neuron

The neural membrane, like other membranes found in cells throughout the human body, consists of a phospholipid bilayer with proteins embedded in it. Some of these proteins act as ion channels which allow ions to flow through the membrane along electrochemical gradients. Other proteins act as pumps and use energy to move ions across the membrane against electrochemical gradients. The most common of these is the sodium/potassium (Na^+/K^+) pump. The cellular membrane and the pump permits the concentration of ions inside the membrane to be different from the outside of the membrane, and this difference is referred to as the membrane potential of the neuron. At equilibrium, the resting potential is typically around -65 to -70 mV.

The course of an action potential is as follows: Upon receiving stimulation from another neuron which increases the membrane potential to a certain threshold, the membrane potential rises quickly in a process called depolarization, and then returns to rest during a repolarization state. Due to differing time scales, the membrane potential overshoots the resting state and enters a hyperpolarized state. The sodium/potassium pump then works to restore the membrane potential back to the equilibrium potential.

Since ions can't pass through the membrane except through protein channels, the membrane essentially acts like a capacitor and generates a current as the voltage changes. The equation for such a current is given by

$$C_m \frac{dV}{dt} = I_{capacitor} \tag{1.1}$$

where C_m is the membrane capacitance (units of $\mu F/cm^2$) and V is the membrane potential in units of mV. Similarly, ionic currents will be generated as ions travel through the proteins. These proteins therefore act as resistors with variable resistance (the reason for variable resistance will be discussed in the next section) which we donate as $R_{ion}(V)$. Therefore using Ohm's Law:

$$I_{ion} = \frac{1}{R_{ion}(V)}(V - E_{ion}) \tag{1.2}$$

By convention, $\frac{1}{R_{ion}(V)}$ is frequently written in terms of conductance $g_{ion}(V)$ as $\frac{1}{R_{ion}(V)} = g_{ion}(V)$ with units of mS/cm^2, and E_{ion} is the reversal potential of the ion channel. The reversal potential is the potential at which there is no net current for that specific ion, and this value is calculated from the Nernst equation [VISGR$^+$12]. The ability to model a neuron membrane as a capacitor with the protein channels as variable resistors allowed for a quantitative biophysical model of a neuron known as the Hodgkin-Huxley model to be developed. This model will be the one we use due to its close connection to biological reality [HH52, BSRSR15, Izh04].

1.3 The Hodgkin-Huxley Model of an Action Potential

Hodgkin and Huxley [HH52] performed experiments on a squid axon and found three types of ion currents: sodium, potassium, and a leak current mainly consisting of chloride ions. These ions flow through the cell membrane of the neuron through specific voltage-dependent ion channels which control the membrane's voltage, one for potassium and one for sodium. The leak current accounts for other channel types not described

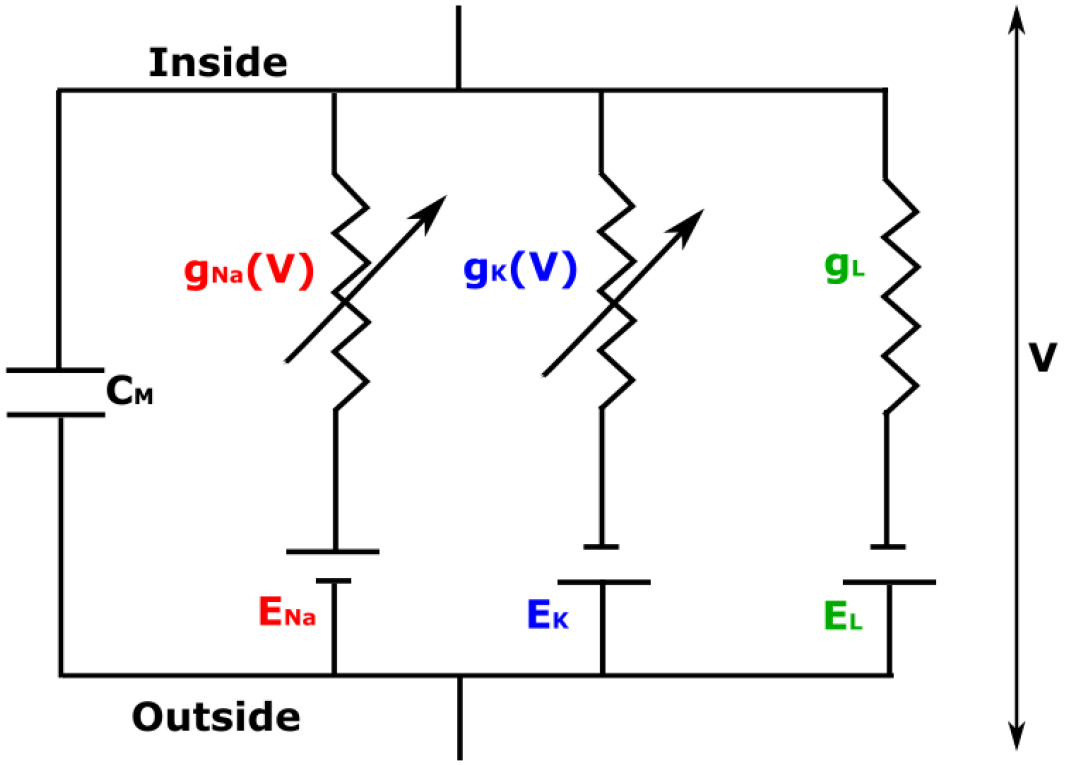

Figure 1.2: Schematic drawing of Hodgkin Huxley model represented as a circuit. The electrochemical gradients driving the flow of ions are represented by batteries (E_{ion}), the protein channels are represented as variable resistors $R_{ion}(V)$ or rather with conductances $g_{ion}(V) = R_{ion}(V)^{-1}$, and the membrane is represented by a capacitor with capacitance C_M.

explicitly. The equivalent circuit diagram is shown in Figure 1.2

Utilizing Ohm's Law and Kirchoff's Law, one obtains the following:

$$\begin{aligned} I_{input} &= I_{capacitor} + \sum_{ion} I_{ion} \\ &= C_M \frac{dV}{dt} + g_{Na}(V)(V - E_{Na}) - g_K(V)(V - E_K) - g_L(V - E_L) \end{aligned} \tag{1.3}$$

where g_L represents the conductance of the leak channel. The key feature of the Hodgkin

Huxley model is that each channel is composed of four gates: the sodium channel is composed of three identical fast-acting activating gates (known as m-gates) and one slow inactivating gate (known as an h-gate). Each channel can be pictured as being a tunnel with four gates arranged one-after-another within it. In order for the individual channel to be open and conduct, all the gates within that channel must be simultaneously open. If even one gate is shut, then the whole channel is shut.

Each gate transitions from an open to a closed state with rate constant $\alpha(V)$ and transitions back with rate constant $\beta(V)$. Let us consider the potassium resistor in Fig. 1.2. The net conductance of potassium channels would be given by $\bar{g_K} \times f_K$ where $\bar{g}_K$ is the maximum potassium channel conductance when all channels are open and f_K is the fraction of open potassium channels. Defining n to be the fraction of open gates n-gates and noting that a potassium channel contains four n-gates, the conductance of the potassium channels in the above circuit should be given by $\bar{g_K} n^4$. A similar expression can be derived for the sodium channels.

Collecting everything, the Hodgkin-Huxley model of a neuron is given by the following sets of differential equations:

$$\begin{aligned} C_M \dot{V} &= I_{input}(t) - \bar{g}_{Na} m^3 h (V - E_{Na}) \\ &- \bar{g}_K n^4 (V - E_K) - \bar{g}_L (V - E_L) \\ \dot{n} &= \alpha_n(V)(1-n) - \beta_n(V) n \\ \dot{m} &= \alpha_m(V)(1-m) - \beta_m(V) m \\ \dot{h} &= \alpha_h(V)(1-h) - \beta_h(V) h, \end{aligned} \tag{1.4}$$

where

$$\begin{aligned}
\alpha_n(V) &= \frac{0.01(V+10)}{\exp[(V+10)/10]-1} \\
\beta_n(V) &= 0.125\exp[V/80] \\
\alpha_m(V) &= \frac{0.1(V+25)}{\exp[(V+25)/10]-1} \\
\beta_m(V) &= 4\exp[V/18] \\
\alpha_h(V) &= 0.07\exp[V/20] \\
\beta_h(V) &= \frac{1}{\exp[(V+30)/10]+1}.
\end{aligned}$$

The transition rate equations with numbers must be experimentally determined. Here, $I_{input}(t)$ is the current input into the neuron and determines the dynamical behavior of the membrane voltage. Frequently, this is decomposed into two terms: an applied current refered to as $I_{app}(t)$, and $I_{syn}(t)$ which is the current input from the potential due to synaptic connections. The values of the parameters along with definitions are found in Table 1.1 [HH52].

Table 1.1: Parameter values used for simulation of the Hodgkin-Huxley model.

Parameter	Definition	Value
C	membrane capacitance	$1\mu F/cm^2$
E_{Na}	sodium reversal potential	$50mV$
E_K	potassium reversal potential	$-77mV$
E_L	leak reversal potential	$-54.4mV$
$\bar{g}_{Na}$	maximal sodium conductance	$120mS/cm^2$
$\bar{g}_K$	maximal potassium conductance	$36mS/cm^2$
$\bar{g}_L$	maximal leak conductance	$0.3mS/cm^2$

A simulation of the set of equations (Eqn. 1.4) is shown in Fig. 1.3. Notice that the dynamics match our earlier physiological description: at low voltage, the m-gates are mainly closed, but upon depolarization, the m-gates open and the voltage increases until the h-gate closes. The membrane then repolarizes as the n-gates open which allows

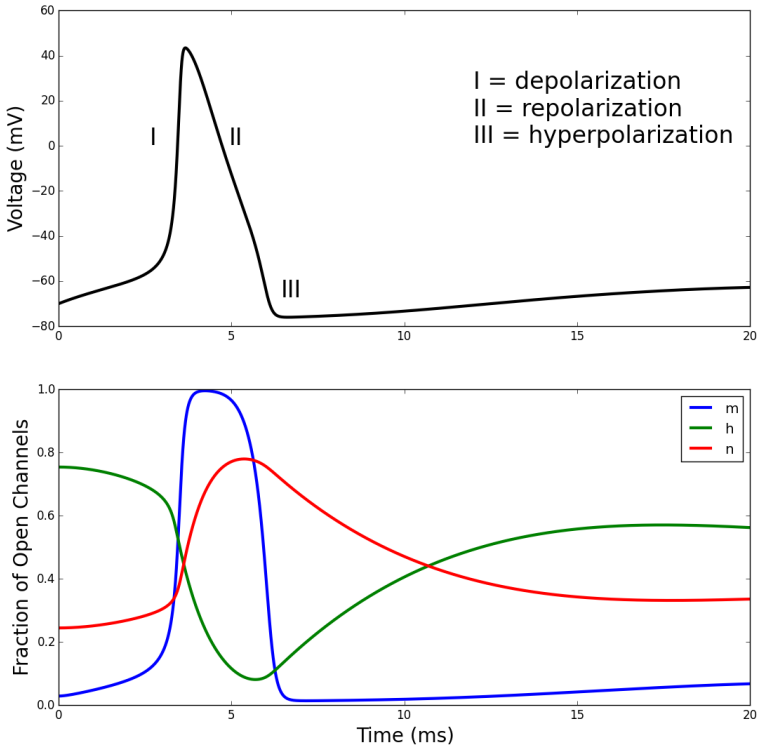

Figure 1.3: (Top) Voltage dynamics of a neuron spike with the different characterizations of a spike: depolarization, repolarization, and hyperpolarization. (Bottom) Dynamics for the gating variable of the Hodgkin-Huxley equation (Eqn. 1.4) during a neuron spike.

potassium to flow through.

With a sufficiently strong applied current, the Hodgkin-Huxley model produces a regular sequence of action potentials [MG01]. However, in vivo experiments of spike trains show far more irregular behavior as shown in Fig. 1.4. Where this irregularity comes from is an open question, but we will discuss several potential sources.

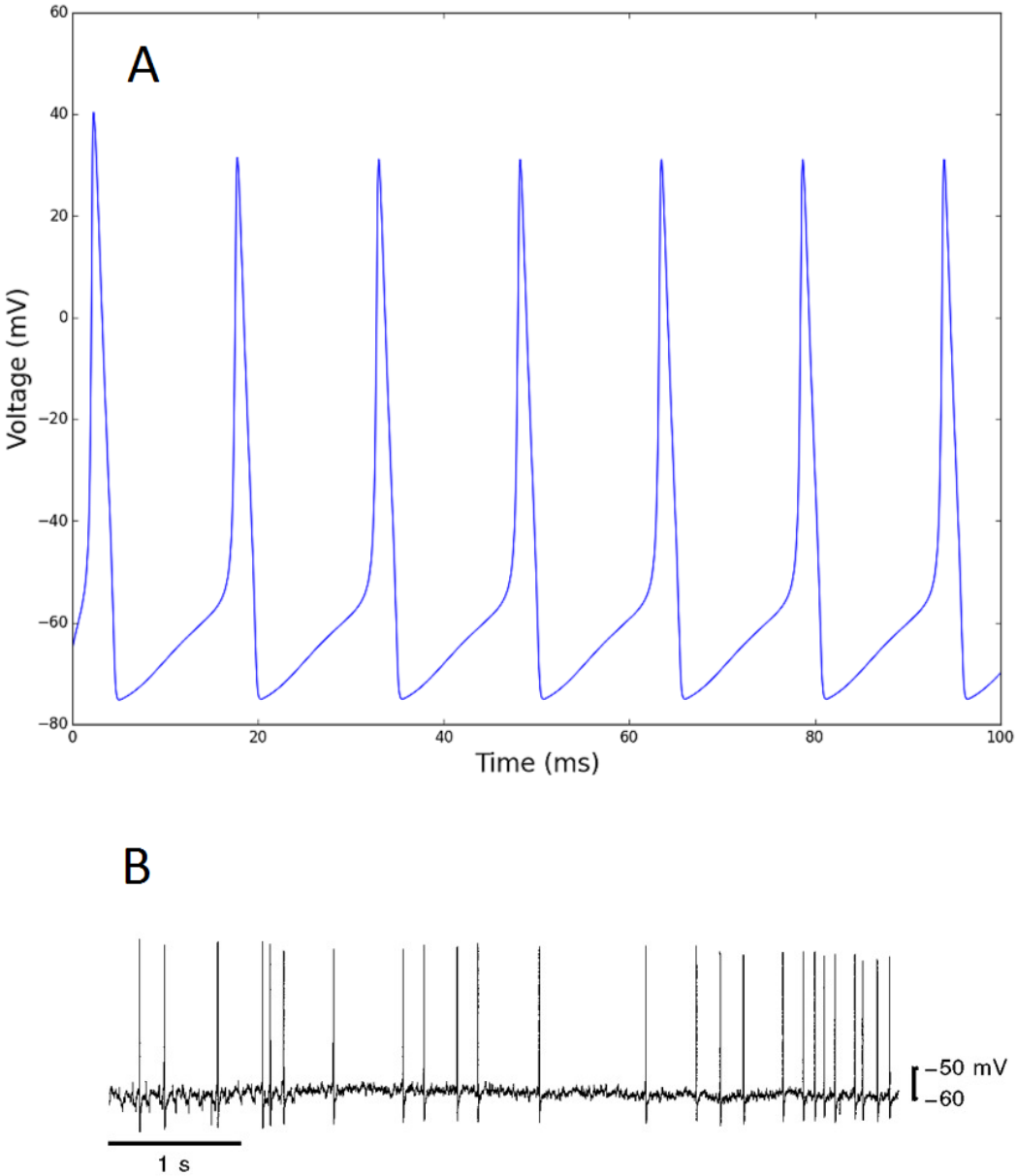

Figure 1.4: (A) Plot of one Hodgkin-Huxley neuron (Eqn. 1.4) with $I_{app}(t) = 10\mu A/cm^2$ starting at resting state. (B) Plot showing irregular firing of action potentials during tissue stretch of guinea pigs (Reproduced with permission from [KCBF99]).

1.4 Neural Communication

The junction between two neurons is referred to as the synapse and is the site of neural communication. The neuron which sends a signal is referred to as the presynaptic neuron and the neuron receiving the signal is referred to as the postsynaptic neuron. A single neuron often connects to more than 10^4 postsynaptic neurons, and estimates place the number of synapses per cubic millimeter of cerebral cortex on the order of 10^9 [ANGSRD08]. There are two types of synapses: chemical and electrical. Neurons which have electrical synapses are connected via gap junctions with impulse traveling in both directions. These are typically found in areas requiring fast responses such as the retina [HFM$^+$04]. We will be more interested in chemical synapses, which are more commonly found in the brain due to their flexibility in neural coding and learning [BWF$^+$08]. A detailed schematic figure of a synapse can be seen in Fig. 1.5.

The basic mechanism of the chemical synpase is as follows: Upon receiving an electrical signal from an action potential, voltage-gated calcium ion channels open in the presynaptic terminal of the neuron. This influx of calcium causes vesicles containing neurotransmitters (chemicals) to fuse with the presynaptic membrane. Upon fusion, neurotransmitter is released into the synaptic cleft via exocytosis. These transmitters then bind to receptor molecules in the postsynaptic membrane which can either open or close the postsynaptic channels. These channel conformation changes can either cause inhibitory or exctitatory postsynaptic potential changes. Upon reaching a threshold, the postsynaptic neuron fires. [MG11, PAF$^+$97]. Although written here in a step-wise fashion, the synapse involves many simultaneous processes such as the production and degradation of neurotransmitter, the release and binding of neurotransmitters to the postsynaptic membrane, and opening of the postsynaptic dendrite channels.

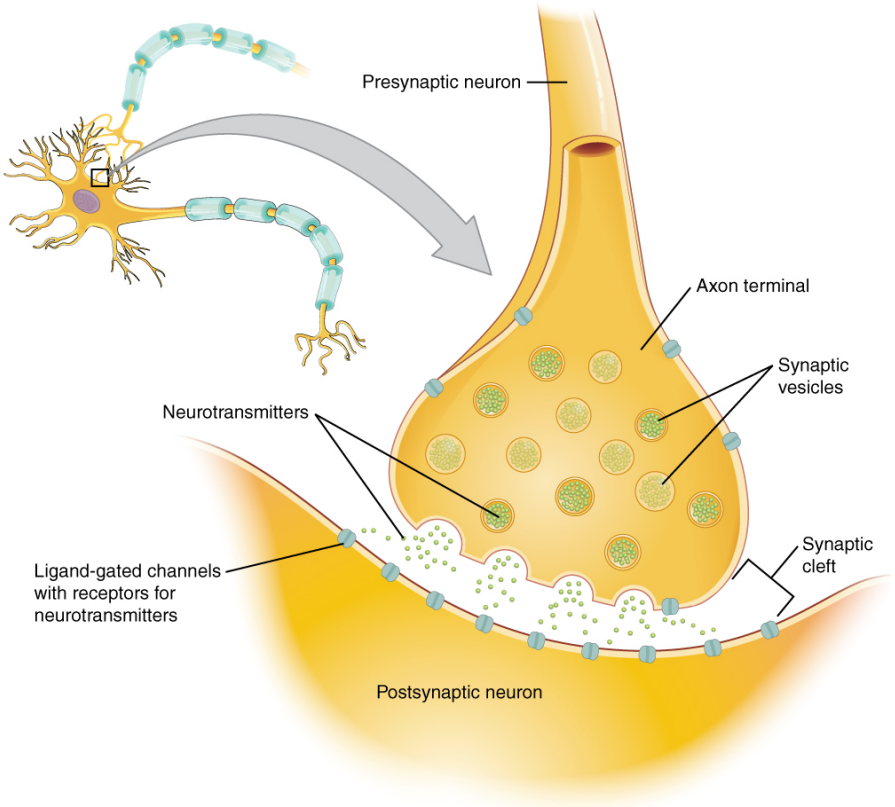

Figure 1.5: Schematic drawing of a chemical synapse. As an action potential arrives, calcium flows into the presynaptic neuron causing vesicles to release neurotransmitters into the synaptic cleft. Upon binding to the postsynaptic neuron, the membrane potential of the postsynaptic neuron changes as ions flow into the postsynaptic neuron from the synaptic cleft. "The Synapse" by Openstax CNX is licensed under a Creative Commons Attribution 4.0 License [Ope14] (Used with permission).

In order to mathematically account for synaptic conduction, we keep things simple by considering a synaptic current that has a Hodgkin-Huxley form, $I_{syn}(t) = g_{syn}(t)(V - E_{syn}) = \bar{g}_{syn} r(t)(V - E_{syn})$ where $r(t)$ is a synaptic gating variable (i.e. the fraction of open channels), g_{syn} is the conductance, and E_{syn} is the synaptic reversal potential. Following the arrival of an action potential at the presynaptic terminal, neurotransmitter molecules, T, are released into the synaptic cleft. Let $[T]$ denote the concentration of neurotransmitter. Since the postsynaptic neural receptors open when transmitter binds, the transition rate for the receptor from a closed state to an open state should be proportional to $[T]$. The rate from open to closed is independent of $[T]$. Thus we have the following scheme:

$$R + T \underset{\beta_r}{\overset{\alpha_r[T]}{\rightleftarrows}} RT$$

where R is the unbound postsynaptic receptor and RT is the bound postsynaptic receptor. Thus, an equation for $r(t)$ can be written as [DMS94, DMS98, GKNP14].:

$$\frac{dr}{dt} = \alpha_r[T](1 - r) - \beta_r r \tag{1.5}$$

The concentration of neurotransmitter should then be a function of the presynaptic membrane voltage as well. When an action potential invades the presynaptic terminal, the transmitter concentration rises rapidly, causing r to increase. Following the release of transmitter, diffusion out of the cleft, enzyme-mediated degradation, and presynaptic uptake mechanisms can all contribute to a reduction of the transmitter concentration [DA$^+$03]. Moreover, the time constant for receptors closing is typically much larger than that of the opening time. Consequently, a common function to describe T is given by:

$$[T](V) = \frac{T_{max}}{1 + e^{-(V - V_p)/K}}$$

where T_{max} is the max value of $[T]$, V is the voltage, K describes the steepness of the sigmoid, and V_p is the value of V at which $[T](V)$ reaches half its maximal value [DA$^+$03, KS98]. For small scale network models, this added synaptic term paints a fuller picture of a neural network. However, for much larger networks, this synaptic term adds extensively to the computational time as one would need to keep track of the voltage of every presynaptic neuron. The tradeoff for an increase in extra information may or may not be worth the longer computational time.

1.5 Membrane Voltage Fluctuations

Like many biological systems, fluctuations in neural systems are abundant. In this section, we will discuss multiple sources of neuronal noise which can be divided into extrinsic and intrinsic categories.

1.5.1 Extrinsic Noise

Extrinsic noise can affect action potential generation. Extrinsic noise is typically thought of as noise from signal transmission between neurons and variability of spike timing due to the neuron being embedded in a network. As an example which we will look at in this work, some experiments suggest that only $10-30\%$ of presynaptic action potentials generate a postsynaptic response which can lead to irregular firing patterns [HSM93, MT96]. In addition, the fact that the number of vesicles and neurotransmitters involved is finite means that they are subject to fluctuations from trial to trial [FK52].

1.5.2 Intrinsic Noise

In addition to extrinsic noise, intrinsic fluctuations are those which cause deviations in the expected voltage but are not associated with a response to stimuli. One such

source of intrinsic noise is thermal noise since voltage across any electrical resistor fluctuates at finite temperature. However, despite the presence of such noise, this noise is of relatively minor influence compared to other neuronal noise sources [MK99a, MK99b].

An alternative source of intrinsic noise, and one which is the focus of this dissertation, is referred to as channel noise. As previously discussed, the ion channels in the Hodgkin-Huxley model transition randomly between an open and closed state with voltage-dependent rate functions. In the Hodgkin-Huxley model, the number of ion channels is assumed to be infinite so that voltage fluctuations due to fluctuations in the number of open channels are neglected. In reality, neurons have finite size and thus have a finite number of channels so that changes in conductivity due to fluctuations in the number of open channels do in fact cause the voltage to fluctuate. To illustrate this fact, let us consider a neuron with N identical stochastic channels in the membrane with the probability of being open denoted as p. Each channel can be thought of as a Bernoulli random variable with probability p of being open. Hence, if each individual channel contributes a current i, then the mean current through the channels is given by iNp and the variance of these current fluctuations is proportional to $Np(1-p)$ [ON14].

Notice that the variance is maximized at $p = 0.5$. In the subthreshold regime, p is typically less than 0.5, so upon depolarization of the neuron the absolute amplitude from ion channel noise increases [H$^+$01]. The relative amplitude, defined by the coefficient of variation, is proportional to $\frac{\sqrt{Np(1-p)}}{Np} = \sqrt{\frac{(1-p)}{Np}}$, and hence the relative amplitude of ion channel noise decreases as p increases upon depolarization. Additionally, the absolute amplitude of fluctuations is on the order of $\sqrt{N}$ whereas the relative amplitude of fluctuations is on the order of $N^{-1/2}$. Hence the relative amplitude of fluctuations decreases for larger populations of ion channels and for infinitely many channels, the relative amplitude of fluctuations is 0.

In the next chapter, we will look at how to adapt the Hodgkin-Huxley model to

account for channel noise.

1.6 Is Channel Noise Important?

Even though we have discussed channel noise as a source of voltage fluctuations in neurons, we have yet to discuss some general effects of this noise on neural network behavior. As discussed by Schneidman with experimental observations, the presence of these channel fluctuations leads to spontaneous spikes in the presence of subthreshold inputs and missing spikes for suprathreshold inputs [SFS98, JA94]. In general, noise is thought to degrade performance, although this is not always the case. For example, the appearance of spontaneous fluctuations is a phenomenon known as stochastic facilitation and has been shown to enhance information processing in neural systems [SM13, Ada03]. An example of a simulation showing this phenomenon is seen in Fig. 1.6. In addition to the aforementioned effects of channel noise, modeling studies have suggested that channel noise exherts influence on spike time reliability [SFS98], firing irregularity [SLYH08, Row07], subthreshold dynamics [WKAK98], and action potential initiation and propagation [CON10, FL07].

Additionally, channel noise has been considered as an important factor for understanding how auditory neurons encode information, and it has been suggested to use channel noise to reproduce more natural responses in neural populations stimulated by cochlear implants [ME96, MRMA04, IR09, GRSB12]. More recently, a study out of Stanford University found experimental evidence that noisy neurons are a critical aspect for learning [ECFW15]. Ultimately, the full range of what channel noise can do for neural networks is an open question, but a plethora of evidence exists showing that microscopic fluctuations from stochastic channel gating can have macroscopic consequences [WRK00, SGH01, DW05, FWL05, WKAK98]. The aim of this thesis is to contribute to

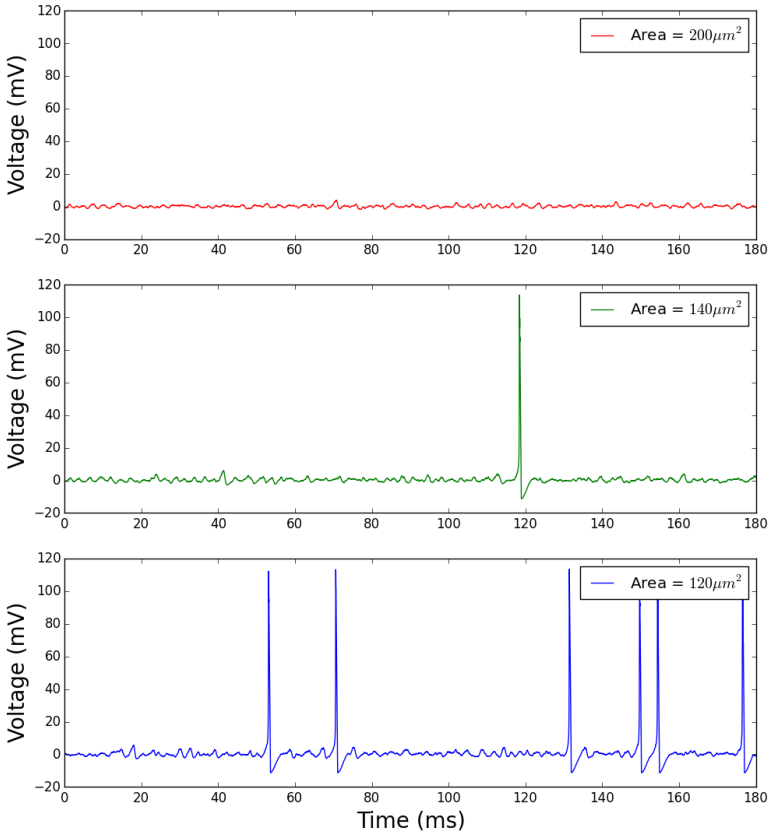

Figure 1.6: Simulations of the Fox and Lu model (Eqn. 2.1) for various membrane area patch sizes. The injected current was $6.0\mu A/cm^2$. Resulting figures show that decreased membrane area (increased magnitude of membrane voltage fluctuations) causes spontaneous spiking for subthreshold input.

the understanding of the impact of channel noise on neural networks.

Chapter 2

Models for Channel Noise

While the Hodgkin-Huxley model is deterministic, real life neural systems are often stochastic entities as noted in the previous chapter. How do we best adapt the Hodgkin-Huxley model to account for these membrane voltage fluctuations due to the channels? Recall that the Hodgkin-Huxley assumes infinitely many channels so that fluctuations in the number of open channels don't affect the membrane voltage. However, since real neurons have finitely many channels due to size constraints, fluctuations in the fraction of open channels can affect the membrane voltage. How noise is introduced into the Hodgkin Huxley model (Eqn. 1.4) in order to capture these fluctuations can have different effects on the dynamics of the model.

2.1 Markov Chain Model

In the Markov Chain Model, each ion channel is considered a distinct object which can exist in several states where each state corresponds to a conformation of the membrane protein. For example, a potassium channel can assume the following configurations with the following transition rates:

$$0 \underset{\beta_n}{\overset{4\alpha_n}{\rightleftarrows}} 1 \underset{2\beta_n}{\overset{3\alpha_n}{\rightleftarrows}} 2 \underset{3\beta_n}{\overset{2\alpha_n}{\rightleftarrows}} 3 \underset{4\beta_n}{\overset{\alpha_n}{\rightleftarrows}} 4$$

where each number corresponds to the number of gates in the channel in the ”open” configuration. In this case, state 4 is the open state whereas the other states are the “closed” states. The channel is considered memoryless (hence, having the Markov property). In general, these transitions occur on a time-scale of nanoseconds, but for modeling purposes, these transitions are considered instantaneous [H$^+$01]. Simulation methods for the Markov Chain Model are often based on Monte Carlo techniques. In general, the simplest way to simulate this model is to first pick a small time step dt. The next step is to convert the transition rate (k) to a transition probability (p^*) by assuming $p^* \approx kdt$. At each time step, one then generates a random number $r \in \text{unif}(0,1)$ for each channel. If $r < p$, then the channel transitions between the open and closed states. No transition occurs if $r > p$. Then, after each time step, one computes the fraction of channels in the “open” configuration and updates the voltage according to the following equation:

$$C_M \dot{V} = I_{input}(t) - \bar{g_K} \frac{N_{o,Na}}{N_{Na}} (V - E_{Na}) - \bar{g_K} \frac{N_{o,K}}{N_K} (V - E_K) - g_L (V - E_L)$$

where $N_{o,K}$ ($N_{o,Na}$) is the number of open potassium (sodium) channels and N_K (N_{Na}) is the total number of potassium (sodium) channels. This method is computationally expensive because it requires the generation of a random number for each channel at each time step.

An alternative method is to use the Gillespie algorithm [Gil77]. In this algorithm, one generates two random numbers: one random number determines when the next transition will occur, and the other number determines which transitions will occur

[SW79, CW96, Gil77] . The simulation then proceeds in time and performs the state transitions. However, the average time step generated is on the order N^{-1} so the algorithm is inefficient for a large number of channels [MRW02].

If possible, one would hope to be able to conveniently place noise terms in order to replicate the Markov Chain Model dynamics with enough accuracy to extract useful information while cutting down on computational costs. We will next introduce several proposed models that sought to do so.

2.2 Current Noise Model

To model fluctuations observed in the Hodgkin-Huxley model, a Gaussian term is frequently added to the end of the voltage equation in Eqn. 1.4. This method is commonly used by computational neuroscientists to model fluctuations in the spike timing [NPR$^+$99, WPDC10, TJ12, TW05, KHZ16]. This noise term is meant to represent the combined stochasticity of the ion channels on the voltage dynamics of the neuron. While this modification is nice for its simplicity, it seems likely that the added noise term should also depend on the voltage or gating variables. As another drawback, there is currently no method for determining how to use an appropriate function to describe the noise intensity [GSB11]. However, for a large membrane area and a constant applied current, the interspike interval distribution generated by the Markov chain model and the distribution generated by the current noise model showed very close agreement [Row07].

2.3 Channel Noise Model

If we consider the case of finitely many potassium channels, for instance, one can apply a system size expansion to the states of the channels. This method was first carried

out by Fox and Lu and we will refer to this model as the Fox and Lu model [FL94]. They derived the following system of stochastic differential equations to account for having finitely many channels:

$$\begin{aligned} C\dot{V} &= I_{input}(t) - \bar{g}_{Na} y_{31}(V - E_{Na}) - \bar{g}_K x_4 (V - E_K) - \bar{g}_L (V - E_L) \\ \dot{\mathbf{x}} &= A_K(V)\mathbf{x} + \frac{1}{\sqrt{N_K}} S_K(V, \mathbf{x}) \dot{\xi}_K \\ \dot{\mathbf{y}} &= A_{Na}(V)\mathbf{y} + \frac{1}{\sqrt{N_{Na}}} S_{Na}(V, \mathbf{y}) \dot{\xi}_{Na}. \end{aligned} \tag{2.1}$$

The matrices A_K, A_{Na}, S_K, and S_{Na} are defined as:

$$A_K = \begin{bmatrix} -4\alpha_n & \beta_n & 0 & 0 & 0 \\ 4\alpha_n & -3\alpha_n - \beta_n & 2\beta_n & 0 & 0 \\ 0 & 3\alpha_n & -2\alpha_n - 2\beta_n & 3\beta_n & 0 \\ 0 & 0 & 2\alpha_n & -\alpha_n - 3\beta_n & 4\beta_n \\ 0 & 0 & 0 & \alpha_n & -4\beta_n \end{bmatrix}$$

$$A_{Na} = \begin{bmatrix} -3\alpha_m & \beta_m & 0 & 0 & \beta_h & 0 & 0 & 0 \\ 3\alpha_m & -2\alpha_m - \beta_m - \alpha_h & 2\beta_m & 0 & 0 & \beta_h & 0 & 0 \\ 0 & 2\alpha_m & -\alpha_m - 2\beta_m - \alpha_h & 3\beta_m & 0 & 0 & \beta_h & 0 \\ 0 & 0 & \alpha_m & -3\beta_m - \alpha_h & 0 & 0 & 0 & \beta_h \\ \alpha_h & 0 & 0 & 0 & -3\alpha_m - \beta_h & \beta_m & 0 & 0 \\ 0 & \alpha_h & 0 & 0 & 3\alpha_m & -2\alpha_m - \beta_m - \beta_h & 2\beta_m & 0 \\ 0 & 0 & \alpha_h & 0 & 0 & 2\alpha_m & -\alpha_m - 2\beta_m - \beta_h & 3\beta_m \\ 0 & 0 & 0 & \alpha_h & 0 & 0 & \alpha_m & -3\beta_m - \beta_h \end{bmatrix}$$

S_K and S_{Na} are the square root matrices of the following diffusion matrices:

$$D_K = \begin{bmatrix} 4\alpha_n x_0 + \beta_n x_1 & -4\alpha_n x_0 - \beta_n x_1 & 0 & 0 & 0 \\ -4\alpha_n x_0 - \beta_n x_1 & 4\alpha_n x_0 + (3\alpha_n + \beta_n) x_1 + 2\beta_n x_2 & -2\beta_n x_2 - 3\alpha_n x_1 & 0 & 0 \\ 0 & -2\beta_n x_2 - 3\alpha_n x_1 & 3\alpha_n x_1 + (2\alpha_n + 2\beta_n) x_2 + 3\beta_n x_3 & -3\beta_n x_3 - 2\alpha_n x_2 & 0 \\ 0 & 0 & -3\beta_n x_3 - 2\alpha_n x_2 & 2\alpha_n x_2 + (\alpha_n + 3\beta_n) x_3 + 4\beta_n x_4 & -4\beta_n x_4 - \alpha_n x_3 \\ 0 & 0 & 0 & -4\beta_n x_4 - \alpha_n x_3 & \alpha_n x_3 + 4\beta_n x_4 \end{bmatrix}$$

$$D_{Na} = \begin{bmatrix} d_1 & -3\alpha_m y_{00} - \beta_m y_{10} & 0 & 0 & -\alpha_h y_{00} - \beta_h y_{01} & 0 & 0 & 0 \\ -3\alpha_m y_{00} - \beta_m y_{10} & d_2 & -2\alpha_m y_{10} - 2\beta_m y_{20} & 0 & 0 & -\alpha_h y_{10} - \beta_h y_{11} & 0 & 0 \\ 0 & -2\alpha_m y_{10} - 2\beta_m y_{20} & d_3 & -\alpha_m y_{20} - 3\beta_m y_{30} & 0 & 0 & -\alpha_h y_{20} - \beta_h y_{21} & 0 \\ 0 & 0 & -\alpha_m y_{20} - 3\beta_m y_{30} & d_4 & 0 & 0 & 0 & -\alpha_h y_{30} - \beta_h y_{31} \\ -\alpha_h y_{00} - \beta_h y_{01} & 0 & 0 & 0 & d_5 & -3\alpha_m y_{01} - \beta_m y_{11} & 0 & 0 \\ 0 & -\alpha_h y_{10} - \beta_h y_{11} & 0 & 0 & -3\alpha_m y_{01} - \beta_m y_{11} & d_6 & -2\alpha_m y_{11} - 2\beta_m y_{21} & 0 \\ 0 & 0 & -\alpha_h y_{20} - \beta_h y_{21} & 0 & 0 & -2\alpha_m y_{11} - 2\beta_m y_{21} & d_7 & -\alpha_m y_{21} - 3\beta_m y_{31} \\ 0 & 0 & 0 & -\alpha_h y_{30} - \beta_h y_{31} & 0 & 0 & -\alpha_m y_{21} - 3\beta_m y_{31} & d_8 \end{bmatrix}$$

and with diagonal entries:

$$d_1 = (3\alpha_m + \alpha_h) y_{00} + \beta_m y_{10} + \beta_h y_{01}$$

$$d_2 = (\beta_m + 2\alpha_m) y_{10} + 2\beta_m y_{20} + 3\alpha_m y_{00} + \alpha_h y_{10} + \beta_h y_{11}$$

$$d_3 = (2\beta_m + \alpha_m) y_{20} + 3\beta_m y_{30} + 2\alpha_m y_{10} + \alpha_h y_{20} + \beta_h y_{21}$$

$$d_4 = 3\beta_m y_{30} + \alpha_m y_{20} + \alpha_h y_{30} + \beta_h y_{31}$$

$$d_5 = 3\alpha_m y_{01} + \beta_m y_{y11} + \beta_h y_{01} + \alpha_h y_{00}$$

$$d_6 = (\beta_m + 2\alpha_m) y_{11} + 2\beta_m y_{21} + 3\alpha_m y_{01} + \beta_h y_{11} + \alpha_h y_{10}$$

$$d_7 = (2\beta_m + \alpha_m) y_{21} + 3\beta_m y_{31} + 2\alpha_m y_{11} + \beta_h y_{21} + \alpha_h y_{20}$$

$$d_8 = 3\beta_m y_{31} + \alpha_m y_{21} + \beta_h y_{31} + \alpha_h y_{30}$$

The vector $\mathbf{x}$ is composed of components x_i, $(i = 1,2,3,4)$, representing the proportion of potassium channels with i open gates of type n. The entries of the vector

$\mathbf{y}$ are denoted as y_{ij}, ($i = 0,1,2,3$ and $j = 0,1$), representing the proportion of sodium channels with i open m subunits and j open subunits of type h. Note that this implies $\sum_i x_i = 1$ and $\sum_j \sum_i y_{ij} = 1$. Moreover, ξ_K and ξ_{Na} are vectors of independent Gaussian white noise terms. While this system is valid for a large number of channels, it has been shown to be a very accurate representation of the Markov chain model even for a small number of channels [GIFSB11]. However, the downside to this model is that closed states are distinguishable and must be accounted for, greatly increasing the dimensionality of the system.

2.4 Subunit Noise Model

In addition to the channel noise model, Fox and Lu derived a system of equations from a system size expansion of the states of the populations of subunits [FL94]. Such a system is given by the following:

$$\begin{aligned} C\dot{V} &= I_{input}(t) - \bar{g}_{Na} m^3 h (V - E_{Na}) - \bar{g}_K n^4 (V - E_K) - \bar{g}_L (V - E_L) \\ \frac{dn}{dt} &= \alpha_n(V)(1-n) - \beta_n(V) n + \sigma_n(V)\xi_n(t) \\ \frac{dm}{dt} &= \alpha_m(V)(1-m) - \beta_m(V) m + \sigma_m(V)\xi_m(t) \\ \frac{dh}{dt} &= \alpha_h(V)(1-h) - \beta_h(V) h + \sigma_h(V)\xi_h(t) \end{aligned} \tag{2.2}$$

where the ξ's are independent Gaussian white noises, and:

$$\sigma_x^2(V) = \frac{\alpha_x(1-x) + \beta_x x}{N}.$$

where N is either N_{Na} when x is m or h, or N_K when x is n. Despite the fact this model is widely used due to its computational efficiency, numerical studies have revealed inaccu-

racies such as weaker voltage fluctuations [Bru09], lower firing rates (and hence longer mean interspike intervals), and overstating information transfer rates when subjected to a brief pulse [SLN10], even as the number of channels increases.

2.5 Differences Between Channel and Subunit Noise Models

The principal difference between the channel noise model and the subunit noise model is that in the channel noise model, one groups subunits together to construct a channel, and then defines the dynamics based on the proportion of channels in each state. In the subunit noise model, one defines the dynamics of the subunits first, and then groups the subunits together to compute the channel conductance. As derived in [GIFSB11], the expected fractions of open channels in the channel noise and subunit noise models are the same in the Markov Chain model. What differs is the variance in the fraction of open channels. Their simulations showed that the variance in the fraction of open channels in the channel noise model is nearly identical to that of the Markov Chain model. However, for the subunit noise model, the variance of the fraction of sodium channels was less than that of the Markov Chain model, and the variance of the fraction of open potassium channels was underestimated in the subthreshold regime and overestimated during spiking.

Chapter 3

First Spike Latency

While it is widely accepted that information is encoded in neurons via action potentials or spikes, it is far less understood what specific features of spiking contain encoded information. Experimental evidence has suggested that the timing of the first spike may be an energy-efficient coding mechanism that contains more neural information than subsequent spikes. Therefore, the biophysical features of neurons that underlie response latency are of considerable interest. In this chapter, we examine the effects of channel noise on the first spike latency of a Hodgkin-Huxley neuron receiving random input from many other neurons. Because the principal feature of a Hodgkin-Huxley neuron is the stochastic opening and closing of channels, the fluctuations in the number of open channels lead to fluctuations in the membrane voltage and modify the timing of the first spike. The results will show that when a neuron has a larger number of channels, (i) the occurrence of the first spike is delayed and (ii) the variation in the first spike timing is greater. We also show that the mean, median, and interquartile range of first spike latency can be accurately predicted from a simple linear regression by knowing only the number of channels in the neuron and the rate at which presynaptic neurons fire, but the standard deviation (i.e. neuronal jitter) cannot be predicted using only this information.

We then compare our results to another commonly used stochastic Hodgkin-Huxley model and show that the more commonly used model overstates the first spike latency but can predict the standard deviation of first spike latencies accurately. We end the chapter by suggesting a more suitable definition for the neuronal jitter based upon our simulations and comparison of the two models.

3.1 Introduction

How information is encoded and decoded by neurons is a fundamental question of neuroscience. Although the coding mechanism used by neurons remains unclear, it is widely assumed that coding is based on action potentials or spikes. The most widely assumed coding mechanism is known as rate coding which emphasizes that information that neurons encode about the environment is found in the mean firing rates of neurons [VGT05]. There are three ways to calculate the mean: as the average over the distribution of firing rates over a population of neurons at a fixed time, or as an average of the distribution of firing rates of a single neuron over a long time window, or as an average over a large number of runs of a single neuron [GKNP14]. Such coding mechanisms are not without flaws. Averaging over an extended time window is unfeasible: behavioral experiments have shown that a fly can react to stimuli and change flight directions in only 30-40ms [RWDRvSB99] and humans can recognize visual scenes in under 150ms [TFM$^+$96], so there is simply not enough time for the brain to average over an extended time period. Furthermore, it is easier experimentally to record a single neuron and average over N runs than it is to record N neurons in a single run, so experimental evidence rests on the assumption that there are populations of neurons with similar properties. Based on these issues of timing and the requirement that neurons in a population be essentially identical, the idea of "rate coding" by all of these methods has been routinely criticized

[BRVSW91, ABMV93, APBV94].

An alternative coding mechanism, known as first spike latency coding, has been used as a meaningful strategy to understand information encoding by neurons. First spike latency is defined as the time of the first spike relative to stimulus onset. In [TFM$^+$96], Thorpe argues that the brain does not have time to evaluate more than one spike from each neuron for each step of processing behavioral responses to a stimulus. Therefore, the first spike should contain most of the relevant information, and several groups have shown that most of the information about a new stimulus is conveyed very quickly [OR87, RT95, PPD01, Hei04]. In 2004, the first direct evidence showing first-spike coding in humans was released [JB04]. In this experiment, Johansson et al. applied objects of various shapes to fingertips at various angles and forces. They showed that the first spikes contained reliable information about the direction of fingertip force and object shape. Moreover, it provided information faster than rate coding did. While we do not claim that either rate coding or first spike latency coding is the correct one (and recent publications suggest that both methods are used for information encoding in animals [APD06, ZSN$^+$15, VHIAD07, DvHK$^+$08]), we focus on first spike latency as an informative mathematical problem and potential coding mechanism.

In this chapter, we investigate the first spike latency of a Hodgkin-Huxley neuron with stochastic perturbations. Our goal is to understand how channel noise affects the timing of first spike latency. Neurons in networks receive input from other neurons within the network. Experimental studies have shown that synapses transmit signals in an unreliable fashion due to stochastic release of transmitters, and so not every presynaptic spike elicits a postsynaptic response [BS09, AS94, HL98]. Experimental evidence shows that only $10-30$ percent of presynaptic spikes may elicit any postsynaptic response [HSM93, MT96]. Thus the stochastic perturbations we will examine come from two sources: the intrinsic channel noise due to the stochastic opening and closing of membrane

protein channels, and extrinsic network noise as a result of other neurons sending signals in an unreliable fashion.

This chapter is organized as follows: In Sec. 3.2 we give a mathematical description of the stochastic Hodgkin-Huxley neuron with unreliable synaptic input as well as discuss how we analyze first spike latency from a statistical perspective. Then in Sec. 3.3 we analyze how the parameters of the model affect these first spike latency times and the distribution of the times. In addition, we study what effect the number of channels in a Hodgkin-Huxley neuron has on the first spike latency. We then conclude with some closing remarks in Sec. 3.4.

3.2 The Model

The deterministic dynamics of the Hodgkin-Huxley model [HH52] were given in Eqn. 1.4. The channel conductances $\bar{g}_K$ and $\bar{g}_{Na}$ are the products of two factors: an individual channel conductance on the order of picosiemens and the number of channels in the area A (given by N_{Na} for the number of sodium channels and N_K for the number of potassium channels). The sodium channel density is therefore the value N_{Na}/A and likewise N_K/A for potassium channel density which we will use when discussing the stochastic model. For this chapter and the remainder of this dissertation, we assume that the sodium channel density is given by $60\mu m^{-2}$ and the potassium channel density by $18\mu m^{-2}$, where these values are derived from biophysical neuron parameters [GIFSB11, FM85]. Note that this means that we can rewrite $N_{Na} = 60A$ and $N_K = 18A$ in Eqn. 2.1 where A is the membrane area so we can simply vary this one parameter and observe what effects this causes on neural networks.

As previously mentioned, we are interested in understanding how first spike latency is affected by channel noise and stochastic input from other neurons in a network.

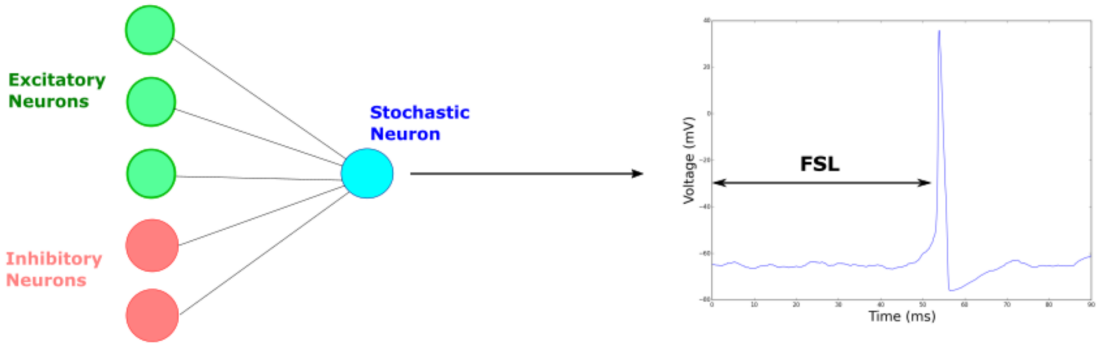

Figure 3.1: Schematic network and first spike latency definition of stochastic Hodgkin-Huxley neuron with unreliable synaptic input from a network of excitatory and inhibitory neurons.

A schematic drawing of the model we will use is shown in Fig. 3.1.

Generally, a presynaptic neuron connects to over 10^4 postsynaptic neurons, and estimates are that the brain is composed of 100 billion neurons, so each neuron connects to many others and is connected to many others [GKNP14]. To simplify matters, we assume that our Hodgkin-Huxley neuron receives current from presynaptic neurons which spike at some rate λ. We let λ be the same for each presynaptic neuron. We express such a presynaptic current as follows:

$$I_{syn}(t) = Q\left[\sum_{k=1}^{N_e}\sum_{l} h_k^l \delta(t-t_k^l) - \sum_{m=1}^{N_i}\sum_{n} h_m^n \delta(t-t_m^n)\right]. \tag{3.1}$$

In this equation, N_e is the number of excitatory presynaptic neurons, N_i the number of inhibitory presynaptic neurons, $Q = C\Delta V$ represents the charge associated with each voltage change ΔV, t_k^l is the discharge time of the l^{th} spike at the k^{th} excitatory presynaptic neuron, and similar notation represents the inhibitory presynaptic neurons [UOG12]. To account for the fact that not every presynaptic spike elicits a postsynaptic response [BS09, AS94, HL98], we introduce the random variable h_k^l where $h_k^l = 1$ with probability p (the probability of a successful postynaptic response) and $h_k^l = 0$ with probability $1-p$ (the probability of no postsynaptic response). As we indicated earlier,

experimental evidence suggests that reasonable values for the parameter p are in the range $0.1 - 0.3$ [HSM93, MT96].

First we choose the values for the parameters in the $I_{syn}(t)$ expression [Eq. (3.1)]. Each excitatory presynaptic neuron which induces a voltage change to our Hodgkin-Huxley model instantaneously increases the voltage by a value of Q which for this model will be set to $0.5mV$. This value is near experimental observations for neurons in the rat visual cortex and the cat visual cortex [Koc04, GGMK09, TLK07, RS99, JMPR71]. Experiments have shown that mammalian vestibular nucleus neurons fire spontaneously in the awake animal at baseline firing rates of $30 - 100$ Hz (and can increase to several hundred Hz) [TS97, GMdL10] (in humans 40 Hz is considered a typical firing rate associated with consciousness) [Gol99]. Thus in order to see the trend of first firing times as a function of the spiking rate of presynaptic neurons, we focus on the interval of $30 - 100$ Hz. We further assume that the number of presynaptic neurons is 2000 (since only a fraction of the 10^4 presynaptic neurons will provide input) and the excitatory to inhibitory ratio of the presynaptic neurons is $N_e : N_i = 4 : 1$, the ratio found in the mammalian cortex [BS13]. While we do not claim that these parameter values are exact across all species, they are biologically plausible values which allow us to examine how the first spike latency time is affected by underlying parameters in the model.

In the limit of infinitely many channels, m^3h and n^4 accurately model the fraction of open channels. Real neurons, on the other hand, only have finitely many channels, so fluctuations in the number of open channels have an effect on the membrane voltage. The channel noise model developed by Fox and Lu, which we will use here, is a stochastic version of the Hodgkin-Huxley system which accounts for fluctuations in the fraction of open channels. The Fox and Lu system to account for finitely many channels is given by twelve stochastic differential equations shown in Eqn. 2.1[FL94, GIFSB11]. While the Fox and Lu system is valid for a large number of channels, it has been shown to be

a very accurate representation of the Markov chain model even for a small number of channels [GIFSB11]. In addition to its accurate approximation of the Markov Chain model, it is also computationally less expensive.

We are interested in understanding the time to first spike and the variability of this spiking time across trials. A spike occurs when the voltage $V(t)$ crosses some threshold θ. Hence we define the random variable T as

$$T = \inf\{t \geq 0 | V(t) \geq \theta\}. \tag{3.2}$$

We consider θ to be a fixed constant of approximately $35mV$, although the exact value is not important since it shifts the spike time by only a fraction of a milisecond. In order to study typical first firing times, many studies have looked at the expectation of T, denoted by $\langle T \rangle$, and the trial-to-trial variability (or jitter) of T defined as the standard deviation of T. These values generally provide useful information when the distribution is not skewed. However, based on our simulations of Eq. (2.1), the distribution of spike times is heavily skewed (see Fig. 3.2). For this reason, we choose instead to compare median values as a better measure of the central tendency of data and to use the interquartile range (IQR) as a better measure of trial-to-trial variability, where the interquartile range is defined to be the difference between the first quartile and third quartile of a data set. Median first spike latencies and IQRs have begun to be used more in biological experiments [LM11, SSR15], but actual simulations comparing these values to those of means and standard deviations have, to the best of our knowledge, not been done.

The parameters of Eq. (2.1) that we vary in these simulations are the presynaptic firing rates, the probability of successful transmission of presynaptic spikes to our Hodgkin-Huxley neuron, and the number of channels in the neuron. As the number of channels grows, the dynamics of the stochastic Hodgkin-Huxley neuron converges to

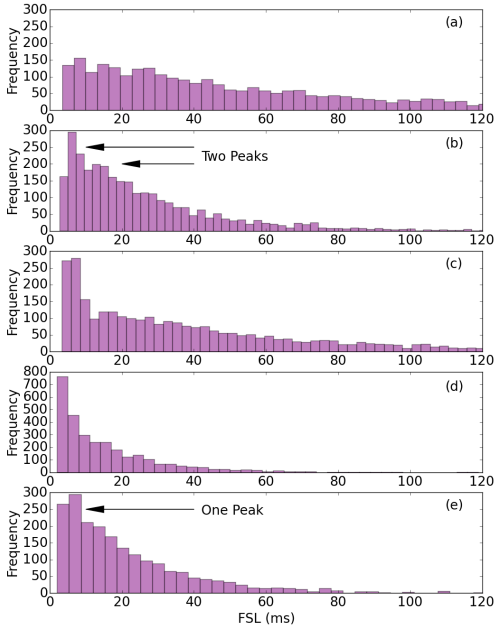

Figure 3.2: Examples of the distribution of first spiking times obtained from the set of equations Eq. (2.1) showing positive skewness. Parameters used for low noise plots (panels (a) and (c)) were $N_{Na} = 1800$, and $N_K = 540$ while for high noise plots (panels (b) and (d)), they were $N_{Na} = 600$, and $N_K = 180$. For low rate plots (panels (a) and (b)), the parameters for the synaptic input current were $\lambda = 25$ Hz and $p = 0.10$, while for high rate plots (panels (c) and (d)), the parameters were $\lambda = 100$ Hz and $p = 0.30$. Panel (e) shows no channel noise with high synaptic input.

that of the deterministic Hodgkin-Huxley model. From the structure of the stochastic Hodgkin-Huxley model [Eq. (2.1)], it is clear that fewer channels lead to stronger fluctuations since the magnitude of fluctuations changes as $A^{-1/2}$. Furthermore,it is a known fact that if X and Y are two independent Poisson random variables each have rates λ_X and λ_Y respectively, then $X+Y$ is a Poisson random variable having rate $\lambda_X + \lambda_Y$. Hence in this case, we have N_e independent excitatory presynaptic neurons with each firing at rate λ, and this is statistically equivalent to having one excitatory presynaptic neuron firing at rate λN_e. To account for the less than certain successful transmission from the presynaptic neuron, we modify this rate term to be $\lambda N_e p$, where p is the probability of a successful transmission. Since N_e is a fixed parameter, we can eliminate one parameter

by considering λp as a single parameter and thus viewing the probability term p as rescaling the rate. Thus, the two parameters we will look at are the product λp which we will refer to as the "effective rate," and the number of channels (N_K and N_{Na}) which we showed can be controlled by the membrane area A. The parameters we use for the numbers of channels can be found in Table 3.1.

Table 3.1: Membrane area and corresponding number of channels

Membrane Area	Number of Channels	
(μm^2)	N_{Na}	N_K
5	300	90
10	600	180
20	1200	360
30	1800	540

3.3 Results and Discussion

All simulations were based on the system of stochastic differential equations Eq. (2.1). We used the Euler-Maruyama method [Hig01, Gar88] with time step $\Delta t = 50\mu s$ and with 2000 presynaptic neurons providing spike train inputs at rate λ. Initial conditions were given by the resting state of the neuron shifted so that $V(0) = 0$ mV. The mean first spike latency is defined as $\langle t \rangle = \frac{1}{N}\sum_{i=1}^{N} t_i$, where N is the number of trials (we used $N = 1000$) and t_i is the time of the first spike for the i^{th} trial. The standard deviation (or jitter) is defined as $J = \sqrt{\langle t^2 \rangle - \langle t \rangle^2}$ [UOG12, OUPG09, BDB$^+$06]. The median is defined as $t_{(\frac{N}{2})}$ and the interquartile range is defined as $t_{(\frac{3N}{4})} - t_{(\frac{N}{4})}$ where $t_{(j)}$ is the j^{th} order statistic.

We first discuss the behavior seen in Fig. 3.2. The histograms shown in Fig. 3.2 are based on $2,000$ simulations of Eq. (2.1). The input current into the Hodgkin-Huxley neuron determines its firing rate. Ignoring the stochasticity of the input current for the moment, the neuron is in the silent regime (i.e. no firing) for $I < 6.27\mu A/cm^2$, in a bistable

regime where the fixed point coexists with a stable limit cycle for $6.27\mu A/cm^2 < I < 9.78\mu A/cm^2$, and in a periodic firing regime for $I > 9.78\mu A/cm^2$. Taking the stochasticity into account, the average stimulating current $\bar{I}_{input}$ determines the dynamical regime of the neuron. Following Luccioli et al. [LKT06], the average stimulating current is given by $\bar{I}_{input} = C\lambda p\Delta V(N_e - N_i)$. With the parameters defined earlier, this simplifies to $\bar{I}_{input} = (0.6\mu A \cdot s/cm^2)\lambda p$. Therefore, the low input current panels in Fig. 3.2 [panels (a) and (b)] present a stochastic neuron in the silent regime, and the high input current [panels (c) and (d)] illustrate a stochastic neuron in the periodic firing regime.

In our model, there are two mechanisms that lead a neuron to fire: the stochastic synaptic current and the intrinsic channel noise. Therefore, we expect to see some juxtaposition of the distributions from both sources in the first spike latency distributions in Fig. 3.2 [WR83, LKT06]. The multipeak distributions in panel (b) (low firing rate panel) shows this clearly: each peak is primarily due to one or the other of the two firing mechanisms. Further evidence of the reasoning behind the multipeaks can be observed in panel (e) in which the channel noise has been eliminated. With the absence of this extra source of noise, the histogram lacks a multipeaked distribution. The very small fluctuations in the channel noise lead to a distribution with a very long tail as seen in panel (a). This tail overlaps with and masks the low synaptic input peak. This behavior is similar to that illustrated by Luccioli et al. for the low rate behavior [LKT06]. Increases in the average synaptic current and in the amplitude of intrinsic channel noise lead to faster first spike latency, which is consistent with the fact that a neuron fires as soon as a threshold value is reached. The associated shift in the distribution toward a faster first spike latency and less heavy tails is seen in panels (c) and (d) of Fig. 3.2. As both of these current increases lead to a shortening of the first spike latency, the multipeaks tend to merge at the low end and the resulting distributions are smoother than in the low firing rate cases illustrated in panels (a) and (b). As we will see in the next sections,

some statistical properties of these distributions can be accurately modeled by a linear regression depending on the synaptic input rate and the intrinsic channel noise.

Our next goal is to compare the mean with the median and the IQR with the standard deviation of the distribution of first spike latencies for different channel areas and effective rates (recall that the effective rate is the quantity λp, where λ is the Poisson rate of each presynaptic neuron and p is the probability of successfully producing a postsynaptic response).

3.3.1 Mean/Standard Deviation vs. Median/IQR

As previously stated, the skewness of the data suggests using the median and IQR to analyze typical first spike latencies and the IQR to study their variability rather than using the mean and standard deviation. For each of the channel areas in Table 3.1, we plotted the resulting values of means, medians, IQRs, and standard deviations, see Fig. 3.3. We then calculated the Pearson Correlation Coefficients r [SJ60] to measure the strength of linear correlation between the statistics of interest and the effective firing rate, the results of which are shown in Table 3.2. Recall that values close to 1 (-1) indicate a very strong positive (negative) linear relationship between two variables.

Table 3.2: Pearson Correlation Coefficients r of the relationship between Effective Rate and Statistical Measures for various Membrane Areas

Membrane Area	Mean	Median	IQR	Standard Deviation
5	-.9376	-.9690	-.9070	-.6959
10	-.9783	-.9764	-.9362	-.6955
20	-.9583	-.9757	-.9515	-.6061
30	-.9659	-.9710	-.9529	-.7335

Since neuronal first spike latency is heavily determined by firing rates of input neurons [BGB09], we would like to be able to predict the median firing time knowing the effective rate. For this reason, the Pearson's Correlation Coefficient gives us a quantitative

idea about how linear the data is, and thus values close to $r = -1$ suggest we can closely estimate that statistical property of the first spike latency. We first note that the mean and median values are both strongly correlated with the effective rate, with the median first spike time slightly more correlated with the effective rate. The values of the mean first spike latency are greater than those of the median first spike latency, which results from the positive skewness of the data. One naturally expects that when there is an increase in input from the presynaptic neurons, the postsynaptic neuron should fire sooner. In fact, that trend is observed in Fig. 3.3, where we show data from simulations when the membrane area is $10\mu m^2$ and $30\mu m^2$ as a representative sample of statistical behavior. We can therefore see that the effective rate can be used as a good predictor for determining the values of the mean and median first spike latencies. This is a key result of this chapter: despite the randomness of the presynaptic input and the randomness of the intrinsic channel noise, a simple linear regression yields high accuracy for predicting a number of statistical properties of the distribution of first spike latencies for a biologically plausible range of values.

The results in Table 3.2 suggest that IQR is a better measure for the spread of the first spike latencies than the standard deviation, and that the effective rate more accurately predicts the spread of data in terms of IQR compared to the standard deviation because of the proximity of the correlation coefficient to -1. The reason is that the combination of the stochastic opening and closing of channels along with unreliable synaptic input can cause large outliers due to noise being able to drive voltage away from the threshold thereby delaying the time to first spike. These outliers have a much stronger effect on the standard deviation than on the IQR. For this reason, the effective rate does a poorer job estimating the neuronal jitter than it does estimating the IQR as a measure of the spread

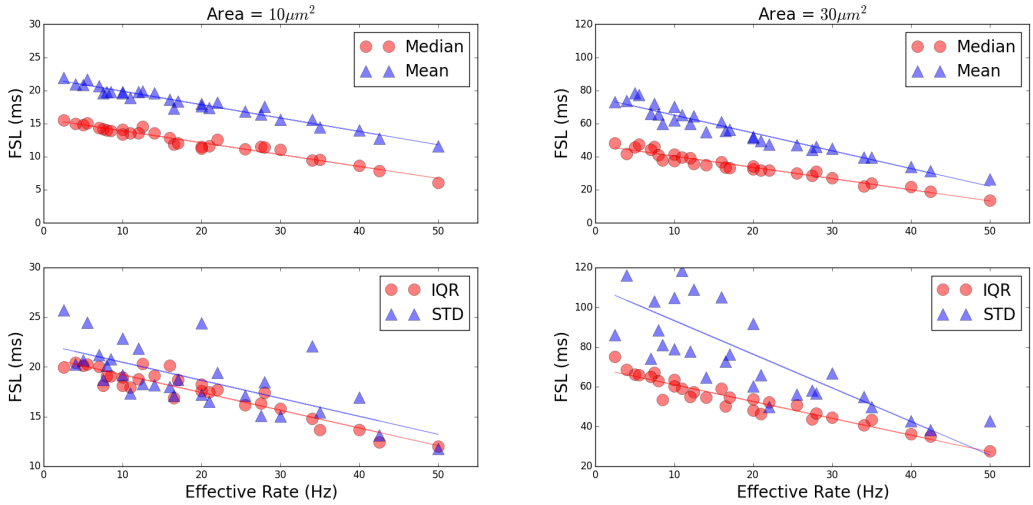

Figure 3.3: Plots of the mean, median, IQR, and standard deviation (STD) of the first spike latency (FSL) based on results of 1000 simulations of the set of equations Eq. (2.1) for each value of effective rate for two channel areas ($10\mu m^2$ and $30\mu m^2$). The plots show that the mean, median, and IQR are modeled exceptionally well by a linear function, whereas the standard deviation is not.

of the data. We also see that for a fixed channel area, there is much more variability in the measurements of standard deviation for smaller effective rates, but that the spread decreases as the effective rate increases. This is due to the fact that when the effective rate is higher, the postsynaptic neuron receives more input and therefore the voltage drifts toward the threshold more quickly, thereby reducing the probability of an outlier.

3.3.2 Effect of Channel Number on FSL

We now explore the effect of changing the number of channels on the distribution of first spike latencies. As a result of Eq. (2.1), increasing the number of channels reduces the fluctuations in voltage due to the stochastic opening and closing of the gates. Figure 3.4 shows the median first spike latency as the channel area increases for various values of the effective rate. For clarity, we do not include every effective rate value used in the previous section, but we use a sufficiently broad range in order to understand trends

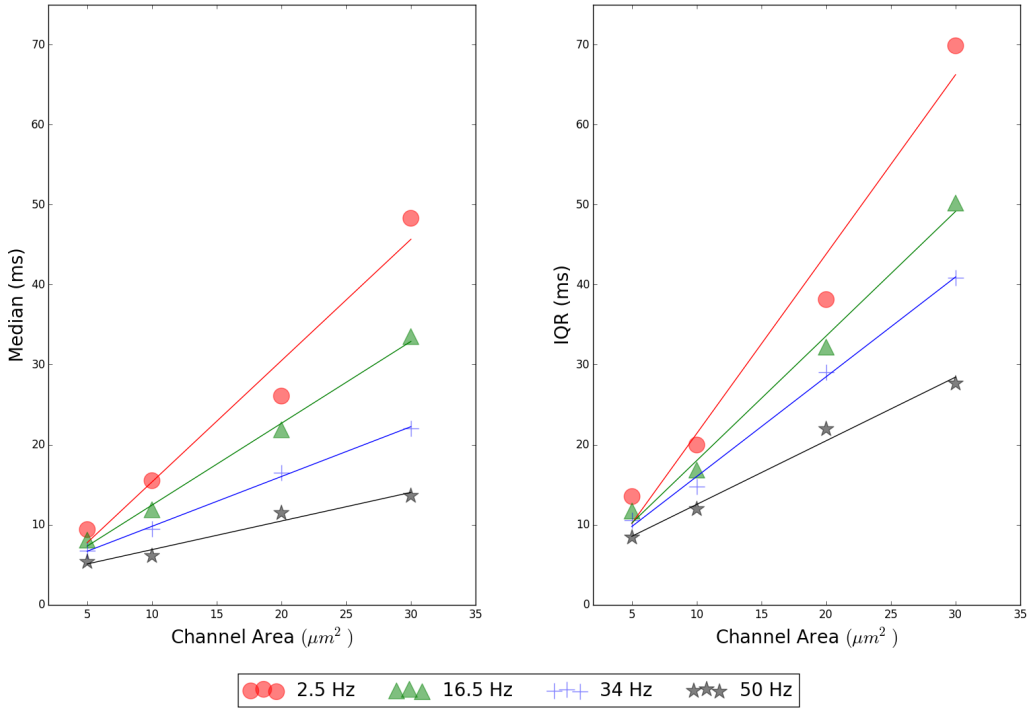

Figure 3.4: Median first spike latency and IQR for various effective firing rates as a function of the change in the number of channels in the Hodgkin-Huxley neuron. For clarity, only a subset of all the effective rates was used, but this subset was chosen to give a representative sample for a range of effective rates. Lines show best fit linear regression for various effective rates. Top line to bottom line show best linear fits for circles, triangles, pluses, and stars respectively.

in the behavior of first spike latency times.

We recall that the number of sodium channels is $60 \times A$ where A is the channel area (in units of μm^2), and the number of potassium channels is $18 \times A$. That is, the total number of channels is directly proportional to the channel area. From the structure of Eq. (2.1), we know that the Wiener processes are scaled by a factor of $N^{-1/2}$, where N is the number of channels. By increasing the channel area, the variance of the Wiener processes decreases by a factor proportional to $N^{-1} \propto A^{-1}$, and so a larger number of

channels of a neuron leads to a smaller effect of the stochastic opening and closing of the gates within the channels.

We first discuss the effect of channel noise on the median first spike latency. From Fig. 3.4, we see that as the number of channels increases, there is a delay in the median time to spike as well as an increase in the spread of firing times. Conversely, when there are fewer channels, the median times until first firing are close to each other regardless of synaptic input rate. Because there are more excitatory than inhibitory neurons, and because the extitatory presynaptic neurons provide a net positive voltage increase, there is a net drift for the postsynaptic membrane voltage to increase from the resting states towards the firing threshold. The simulations show that the presence of noise helps to accelerate this voltage increase. Additionally, we note that when the noise is weaker (i.e., when there is a larger number of channels), the median firing time can nevertheless be short for strong enough synaptic input. Because there are two sources of stochastic effects, the channel noise and the synaptic input fluctuations, it follows that when the channel noise in the neuron is weak, the synaptic input becomes the primary factor for voltage fluctuations. This effect is observed in Fig. 3.4 where we see larger gaps between the median first spike latencies for larger membrane areas.

As discussed in the previous section, we find the IQR to be a better measure of the spread of first spike latency statistics than the standard deviation. For this reason, we show the IQR instead of the standard deviation in Fig. 3.4. The effects observed for the median first spike latency are essentially the same as those for the IQR.

3.3.3 Comparison to Subunit Noise Model

An alternative model to incorporate stochasticity into each gating variable is referred to as the subunit noise model, where each gating variable equation in the original Hodgkin-Huxley model is perturbed by Gaussian white noise as shown in Eqn. 2.2. This

set of stochastic differential equations was first proposed by Fox and Lu as a Langevin equation description for the dynamics of the subunits, and was derived by applying a system size expansion to the states of populations of subunits [FL94]. Such a system is represented by the set of stochastic differential equations in Eqn. 2.2. The subunit noise model has been used extensively to account for fluctuations in the gating variables and hence in the fraction of open channels [SLYH08, Cas03, JKCK05, OE05, FVPB08]. One reason for its popularity is that it maintains the original structure of the Hodgkin-Huxley model (with the addition of noise terms). Despite its widespread use, numerical studies have revealed inaccuracies such as voltage fluctuations that are too weak [Bru09], firing rates that are too low (and hence mean interspike intervals that are too long), and overstated information transfer rates [SLN10]. Such discrepancies can be explained as follows: the quantities m, h, and n represent the fraction of open subunits, whereas the quantities that influence the membrane potential are the products m^3h and n^4, the fraction of open channels. In the limit of infinitely many channels, m^3h and n^4 correctly model the fraction of open channels, but for finitely many channels, there is no guarantee that fluctuations in these terms will model fluctuations in the total fraction of open channels. In other words, the subunit noise model assumes that $\langle m^3h \rangle = \langle m \rangle^3 \langle h \rangle$, which is not correct for a neuron with only finitely many (small number of) channels.

Let us consider a case study of the subunit noise model Eq. (2.2) using an area of $30\mu m^2$. The plots of the median, mean, standard deviation, and IQR are shown in Fig. 3.5. The Pearson correlation coefficients are: mean (-.9781), median (-.9694), standard deviation (-.9714), and IQR (-.9528). The standard deviation for the subunit noise model has a much stronger linear correlation with the effective rate λp of presynaptic neuron firing than the channel noise model. As discussed in [Bru09], the fluctuations in membrane voltage due to the intrinsic noise are much weaker than those resulting from the synaptic input from presynaptic neurons. Because the inputs from the presynaptic neurons

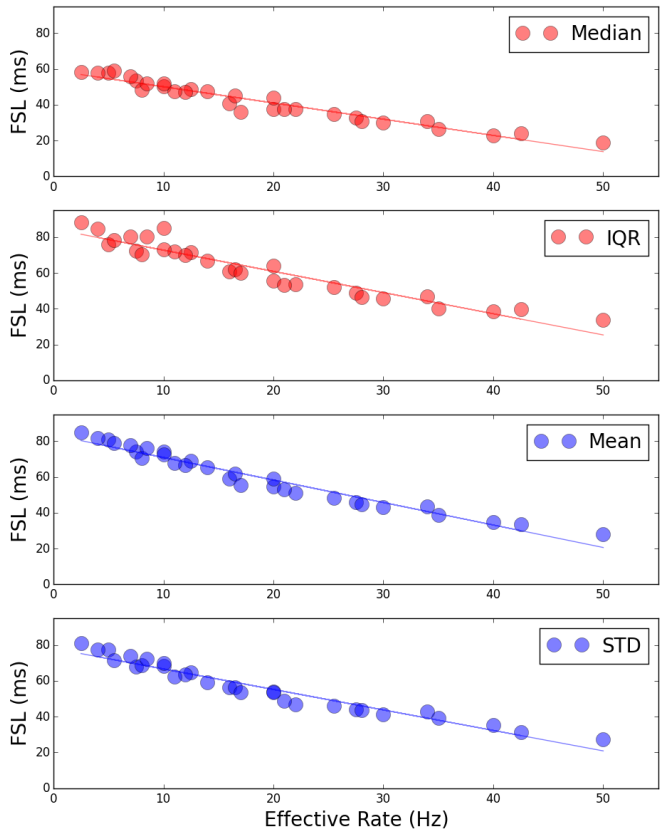

Figure 3.5: Plots of the subunit noise model Eq. (2.2) comparing the median (top plot), IQR (second plot), mean (third plot), and the standard deviation (bottom plot) for different values of the effective rates λp when noise perturbs subunit fractions. The parameter for the area of the neuron is $A = 30\mu m^2$.

cause the membrane voltage to have a net drift toward the threshold, the probability of having a first spike time which deviates greatly from the mean spiking time is very small. Therefore, we expect the values for the mean, median, IQR, and standard deviation to have strong correlation values, which is observed in Fig. 3.5.

Moreover, for a membrane area $A = 30\mu m^2$, the subunit noise model typically has a larger mean, median, and IQR but a smaller standard deviation than the channel noise model (with the value of the IQR larger than that of the standard deviation). As pointed out in [SLN10], the subunit noise model has a longer mean spike interval (i.e.

lower firing rate). For that reason, we expect an overall delay in the time until the first spike and hence we see an increase in the mean and median first spike latency, and this delay is observed in our simulations. We also observed that although some trials had a large first spike latency, they did not deviate as far from the central tendency of the distribution as they did in the channel noise model. The delay in the mean and median first spike latency as well as the observation of large first spike latency times which are relatively closer to the median of the distribution compared to the channel noise model explains the increase in IQR and the lower value for standard deviation in the former.

Although the subunit noise model maintains the original structure of the Hodgkin-Huxley neuron model, the subunit noise model and the channel noise model show widely different behaviors for the standard deviation of first spike latencies for different effective rates and channel areas. As previous literature has shown [Bru09, SLN10], the channel noise model maintains high accuracy for predicting the original Markov Chain model whereas the subunit model does not. Our numerical results imply that the traditional definition of neuronal jitter (standard deviation) is not an appropriate statistical measure of first spike latency. The fact that standard deviation is well-predicted in the inaccurate subunit noise model and poorly predicted in the more accurate Fox and Lu model [Eq. (4.1)] suggests that the traditional definition of neuronal jitter is ill-suited for describing variations in the first spike latency.

3.4 Conclusions

In this chapter, we have sought to examine the effects of channel noise on first spike latency. Because real neurons have finitely many channels, the stochastic opening and closing of these channels leads to fluctuations in the membrane voltage that are not accounted for in the deterministic Hodgkin-Huxley model. In order to account for these

fluctuations, we used the Fox and Lu system size expansion model because (a) it is a highly accurate approximation to the gold standard Markov Chain, and (b) it is a far more computationally efficient model than the Markov Chain [FL94, GIFSB11]. We first looked at statistical descriptions of the first spike latency, and we demonstrated that the median/IQR were better statistical descriptions of the first spike latency distribution than the mean/standard deviation. We noted that the distribution of spike times is positively skewed, which leads to poor predictions of the neuronal jitter (defined as the standard deviation of the spike latency distribution). Moreover, we established the surprising result that statistics of the first spike latency distribution could be accurately predicted by a simple linear regression despite the presence of both intrinsic channel noise and the randomness of synaptic input from other neurons in the network. Our work suggests that despite the randomness within the model, accurate measures of parameters of a stochastic neural system can lead to highly accurate predictions of first spike latencies through a simple linear function.

We then analyzed the effect of channel noise on the median first spike latency and on the IQR of first spike latencies. We showed that as the channel number increases, the effective firing rate becomes the determining factor in the distribution of first spike latencies. This is due to the fact that increasing the channel number decreases the amplitude of the fluctuations in the membrane voltage, so the residual fluctuations in voltage are increasingly due to the randomness of presynaptic neural firing. The results from our simulations agree with previous literature that channel noise contributes importantly to spike timing by increasing fluctuations in spike timing but decreasing first spike latency [VROS03]. An application of such a result is in "stochastic facilitation," or the improvement of information processing due to noise. As we previously noted, we showed that the presence of channel noise in a neuron causes spiking to occur more quickly. Bi and Poo showed that when the postsynaptic neuron fires within 20ms after the

presynaptic neuron fires, the synaptic efficacy increases, leading to long-term potentiation [BP98]. Our results would suggest that the fluctuations of the membrane potential due to the stochastic opening and closing of membrane channels helps facilitate spike-timing dependent plasticity.

Lastly, we showed that the standard deviation may be an inappropriate definition for studying first spike latency variations. To understand why, we compared the channel noise model to that of a subunit noise model in which the individual gating variables themselves are perturbed with independent Gaussian white noise. The subunit noise model was first introduced by Fox and Lu as a simplification of their system size expansion [FL94]. The subunit noise model is more commonly used due to the fact that it retains the original structure of the Hodgkin-Huxley model. As we noted earlier, the subunit noise model assumes that $\langle m^3 h \rangle = \langle m \rangle^3 \langle h \rangle$, which is generally not true when the system contains finitely many channels. This assumption leads to weaker voltage fluctuations and lower firing rates [SLN10, Bru09]. Our simulations show that compared to the channel noise model, the subunit noise model increases the mean and median time to first spike but decreases the neuronal jitter. The neuronal jitter can be predicted far more accurately from knowing the effective rate in the subunit noise model than in the channel noise model. In other words, using standard deviation as a definition for neuronal jitter is accurate only for the subunit noise model and not for the channel noise model. However, this may lead to serious errors in model applications because the channel noise model is much more accurate (closer in replicatng dynamics of the Markov Chain model) than the subunit noise model for describing neurons with biological channel noise. For this reason, we suggest that the IQR rather than the standard deviation is a more appropriate measure of the spread of first spike latencies.

To summarize, the main contributions of this chapter are (a) to demonstrate that the median and IQR are better statistical measures to describe the first spike latency

distribution than the mean/standard deviation, (b) to demonstrate that a simple linear regression is highly accurate for estimating the IQR, mean, and median first spike latency from knowing only the effective firing rate for different numbers of channels, and (c) to provide evidence that using standard deviation as a measure of neuronal jitter may be improperly applied as a result of using the more common subunit noise model despite its inaccuracy by producing weaker voltage fluctuations than predicted by the Markov Chain model.

In the next chapter, we will look at the effects of channel noise on the synchronization of a small neural network. Research has shown a strong correlation between abnormal synchronization and brain disorders including epilepsy, Parkinson's disease, Alzheimer's disease, and schizophrenia. Studying the effects of channel noise on synchronization provides a mathematical framework towards understanding how neurons regulate synchronization in the presence of noise [US06, HBB07, ACM14].

3.5 Acknowledgments

We wish to acknowledge Sadique Sheik for his assistance in developing numerical simulations. We gratefully acknowledge support by the U. S. Office of Naval Research (ONR) under Grant No. N00014-13-1-0205.

Chapter 3, in full, is a reprint of the material as it appears in Physical Review E 2017. Maisel, Brenton; Lindenberg, Katja, Physical Review E, 2017. The dissertation/thesis author was the primary investigator and author of this paper.

Chapter 4

Neural Synchronization in Channel Noise Models

In the previous section, we were interested in the timing of the first spike and how channel noise affected that value. The relative timing of neuronal spikes can also matter for neural responses. In fact, some evidence points to synchronization as a necessary component of neural networks since it is strongly tied to the implementation of cognitive processes, whereas abnormal degrees of neuronal synchronization has been linked to a number of brain disorders such as epilepsy and schizophrenia. Here we examine the effects of channel noise on the synchronization of small Hodgkin-Huxley neuronal networks. As a reminder, real neurons have finitely many channels which lead to fluctuations in the membrane voltage and modify the timing of the spikes, which may in turn lead to large changes in the degree of synchronization. In this chapter, we demonstrate that with the addition of channel noise, neurons in the network reach a steady state synchronization level that depends only on the number of neurons in the network. The channel noise only affects the time it takes to reach the steady state synchronization level. In addition, we supply the code used to study synchronization in Appendix C.

4.1 Introduction

Neurons influence each other through excitatory and inhibitory synaptic connections, and as a result, neurons in a network are rhythmically activated and inhibited through their synaptic connectivity [Buz06]. Most of the brain's cognitive functions are based on synchronized interactions of a large number of neurons distributed across different brain areas [vWBD12, Fri05, FA11, SG05, Sin93]. For example, when monkeys learn categorical information (e.g., how to distinguish between groups of negative and positive objects), experiments have shown increased neural synchronization between the prefrontal cortex and the striatum [AM14].

In addition to the cognitive roles of synchronization, abnormal synchronization has been linked to a number of brain disorders such as epilepsy, schizophrenia, Alzheimer's disease, and Parkinson's disease [ACM14, HBB07, US06]. For example, epilepsy has commonly been associated with excessive synchronization of neural populations [JdCJ$^+$13, US06] whereas schizophrenia has been associated with impaired neural synchronization [SNN$^+$03, US10]. In combination with cognitive function, it is clear that the balance between synchronized and asynchronized neural oscillations plays a pivotal role in healthy brain activity.

In order to model neuronal synchronization, many studies have focused on networks of Hodgkin-Huxley neurons. As we've previously noted, while the Hodgkin-Huxley model assumes that there are infinitely many channels so that fluctuations in the number of open channels remain undetected, real neurons have only finitely many channels and hence experience intrinsic noise through the stochastic opening and closing of sodium and potassium protein channels in the neural membrane. This stochasticity leads to fluctuations in the membrane potential which can alter spike timing of neurons. We refer to this stochasticity as channel noise, and its role in neural synchronization is

the focus of this chapter.

In this study, we investigate the synchronization of a small network of noisy Hodgkin-Huxley neurons. In order to account for perturbations in the Hodgkin-Huxley model, some studies have used the current noise model (Eqn. 2.2) and added an external perturbation to the Hodgkin-Huxley equations to assess the role of noise in synchronization [BBL$^+$16, LBB$^+$12, PYT13]. This method, however, lacks justification that it accurately models the stochastic opening and closing of channels. As an alternative, we will use the Fox and Lu model (see Eqn. 2.1) to understand how channel noise affects the synchronicity of neurons in a network.

This chapter is organized as follows: In Sec. 4.2, we present a mathematical description of the stochastic Hodgkin-Huxley neuron with a synaptic connectivity term. Then in Sec. 4.3, we analyze how channel noise affects the synchronization of a network of neurons, and derive a formula to estimate the degree of synchronization based upon the size of the neural network. We then conclude with some closing remarks.

4.2 Model

To study synchronization of neurons influenced by channel noise, we will again use the Fox and Lu system size expansion to describe the voltage of each neuron. The Fox and Lu equations are given by:

$$\begin{aligned} C\dot{V} &= I_{inj}(t) + I_{syn}(t) - \bar{g}_{Na} y_{31}(V - E_{Na}) \\ &- \bar{g}_K x_4 (V - E_K) - \bar{g}_L (V - E_L) \\ \dot{\mathbf{x}} &= A_K(V)\mathbf{x} + \frac{1}{\sqrt{N_K}} S_K(V, \mathbf{x}) \xi_K \\ \dot{\mathbf{y}} &= A_{Na}(V)\mathbf{y} + \frac{1}{\sqrt{N_{Na}}} S_{Na}(V, \mathbf{y}) \xi_{Na} \end{aligned} \tag{4.1}$$

where the matrices A_K, A_{Na}, S_K, and S_{Na} are defined in Eqn. 2.1. We are interested in a neural network in which the connections between neurons are unidirectional and the local dynamics are described by the Fox and Lu system size model (Eqn. 4.1). The I_{syn} term represents current input from the chemical synapses of other neurons in the network. Such a term is given by the following set of ordinary differential equations [DMS94, BBL$^+$16, GR93]:

$$I_{syn} = \frac{(V_r - V_i)}{\omega} \sum_{j=1}^{N} \varepsilon_{ij} s_j$$
$$\dot{s}_i = \frac{5(1-s_i)}{1+\exp(-\frac{V_i+3}{8})} - s_i$$

Here, V_r is the synaptic reversal potential set to $20mV$ [PYT13], s_i is the post-synaptic potential, ε_{ij} represents the synaptic coupling strength between the j^{th} presynaptic neuron and the i^{th} postsynaptic neuron, and ω is the number of presynaptic connections. The remaining parameter, I_{inj}, determines whether or not action potentials occur [LKT06]. For small values of $I_{inj}, (I_{inj} < 6.27\mu A/cm^2)$, the deterministic Hodgkin-Huxley model resides in a silent regime in that action potentials are not generated. When the injected current is greater than $9.78\mu A/cm^2$, the deterministic Hodgkin-Huxley model enters the repetitive firing regime. Between these values, known as the excitable region, the model shows bistability between silence and repetitive firing.

In this chapter, we are interested in how channel noise affects the synchronicity of neuron spiking at different firing rates. In order to study neural synchronicity, we need a quantitative measure of synchronization.

4.2.1 Kuramoto Order Parameter

Recall that we previously discussed that a neuron starts in a resting state, proceeds through an action potential, and returns to rest. The important aspect of this process is that the neuron proceeds through a periodic orbit to return to the state it once was in. In this view, we can think of the neuron as a phase oscillator. In a phase oscillator model, we view the state of the system as going around a simple loop, in this case the unit circle. The phase, denoted by θ, exists in the interval $[0, 2\pi]$. We shall consider the phase to be $\theta(t) = 2\pi m + 2\pi \frac{t - t_m}{t_{m+1} - t_m}$ where m enumerates the spikes and t_m is the time of the m^{th} spike. Note that this equation means that the phase starts at 0 when the first spike occurs, and the phase increases linearly until the next spike occurs at $\theta = 2\pi$.

A simple way to describe the unit circle is to embed it into the complex plane. If a complex number is on the unit circle, then it can be expressed as $e^{i\theta}$ where $i = \sqrt{-1}$ and θ is the angle between the positive real axis and the vector from the origin to the point on the unit circle. We define the order parameters simply by averaging the complex numbers that represent the phase of the oscillators on the unit circle. For N phase oscillators with phases θ_j, $j = 1, 2, \ldots, N$, the position of each oscillator is given by $e^{i\theta_j}$. The average of these positions is given by the complex number $z = \frac{1}{N} \sum_{j=1}^{N} e^{i\theta_j}$.

Consider the simple case of $N = 2$. We'd like to consider mapping the complex number z into a value on $[0, 1]$ so that 0 represents neurons completely asynchronous and 1 represents completely synchronized. If two neurons are completely synchronized, their positions on the unit circle would be the same, and hence the length of the vector that points from the origin to the average location of the points on the unit circle would be 1. Likewise, if they are completely asynchronous, then they are on exact opposite sides of the unit circle, and the average length of the vector would be 0.

Thus, the appropriate mapping we will use is given by the following order parameter:

$$R(t) = |z| = \left| \frac{1}{N} \sum_{j=1}^{N} \exp(i\theta_j) \right| \tag{4.2}$$

where $\theta_j(t)$ is the phase of the jth neuron defined by $2\pi m + 2\pi \frac{t - t_{j,m}}{t_{j,m+1} - t_{j,m}}$ [ABV$^+$05, BBL$^+$16]. In this equation, $t_{j,m}$ denotes the time when neuron j emits spike m ($m = 0, 1 \cdots$). Eqn. 4.2 is designed in such a way that the first spike begins at $\theta = 0$ and the phase increases linearly until the next spike occurs at $\theta = 2\pi$. If all neurons are completely synchronized, then $\theta_1(t) = \cdots = \theta_N(t)$, and hence: $R = \left| \frac{1}{N} \sum_{j=1}^{N} \exp(i\theta_j) \right| = \left| \frac{1}{N} N \exp(i\theta_1) \right| = |\exp(i\theta_1)| = 1$. Therefore, as discussed above, R values are closer to unity when neurons have more synchronized spike times.

4.3 Results

All simulations were based on the system of stochastic differential equations Eq. 4.1. We used the Euler-Maruyama method [Hig01, Gar88] with time step $\Delta t = 10\mu s$. Unless noted otherwise, initially each neuron in the network was assumed to be in the resting state.

4.3.1 Frequency-Current Relationship

To understand how the number of channels affects the firing rate of a Hodgkin-Huxley neuron, we analyze the relationship between firing frequency of a stochastic neuron and the input current. In the squid axon modeled by Hodgkin and Huxley, the ratio of sodium channel density to potassium channel density is approximately $60\mu m^{-2}$: $18\mu m^{-2}$, and we use these values for our simulations [FM85]. Defining A to be the membrane area, the total number of sodium channels is given by $60 \times A$ and the total number of potassium channels is $18 \times A$. From Eqn. 4.1, the parameter A controls the

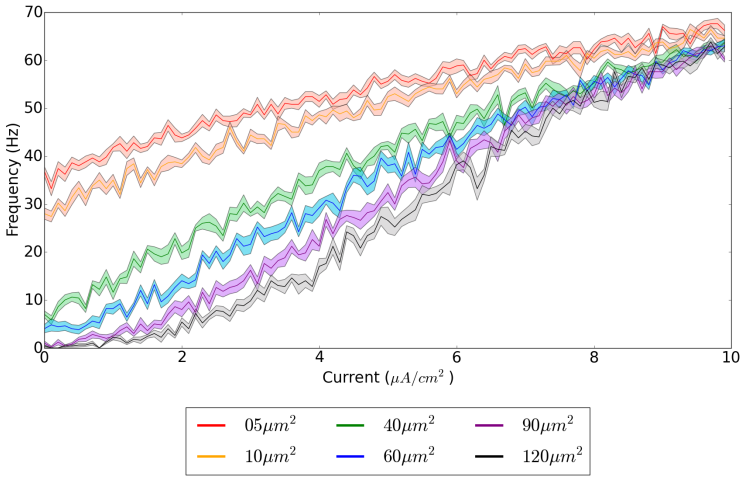

Figure 4.1: Relationship between input current and firing frequency for varying membrane areas. Solid lines show the mean firing frequency averaged over 50 simulations. Shaded areas show one standard deviation of firing frequency from the mean.

magnitude of fluctuations from the channel noise as $A^{-1/2}$. Therefore, smaller membrane area results in larger fluctuation magnitude whereas larger membrane area results in smaller fluctuation magnitude. The resulting firing frequencies as a function of input current for different membrane areas are given in Figure 4.1.

The results show that in the absence of input current, the size of the membrane area is what primarily determines the rate of spontaneous firing. As the input current increases, the firing rates for all different areas converge towards each other and the firing rate becomes independent of the membrane area. With an increase in current, the neurons enter the repetitive firing regime so fluctuations in the membrane voltages should produce only minor changes in the frequency of spikes. Therefore, channel noise has a larger effect on the firing rate at low input currents in agreement with previous literature [SW79, CD83, SD93].

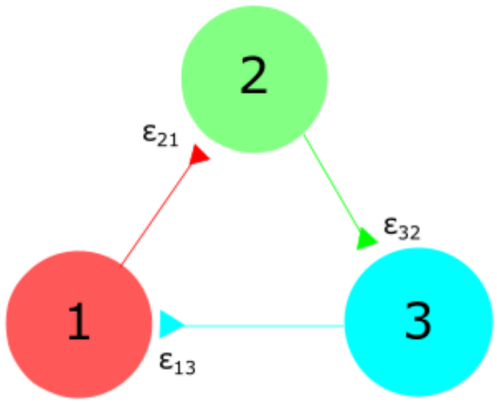

Figure 4.2: Schematic drawing showing three unilaterally connected excitatory neurons with coupling strengths $\varepsilon_{13}, \varepsilon_{21}$, and ε_{32}

4.3.2 Channel Number Effect on Synchronization

To understand how the number of channels affects the synchronicity of neurons, we consider a simple three member neural network with unidirectional excitatory connections and local dynamics given by Eqn 4.1. Such a system is shown in Figure 4.2. In this example, we assume the connections to have identical coupling constants $\varepsilon_{13} = \varepsilon_{21} = \varepsilon_{32} = 0.10$ and zero otherwise.

Because the neurons all start with the same initial condition, we have that $R(0) = 1$ regardless of the value of the membrane area, i.e. all the neurons begin completely synchronized. However, as time passes, the degree of synchronization changes. Fig. 4.3 shows simulations of the three neuron neural network with varying membrane area. Although the degree of synchronization for smaller area changes more rapidly than in the case of larger membrane area, the degree of synchronization appears to reach the same steady state value and hover around this value. From this simulation, the channel area only affects the time to reach the steady state synchronization value but not the steady state synchronization value itself. Since changing membrane area changes the firing rate (see Fig. 4.1), this suggests that there is an inverse relationship between the firing rate and time it takes to reach a steady state synchronization level (and consequently, a direct

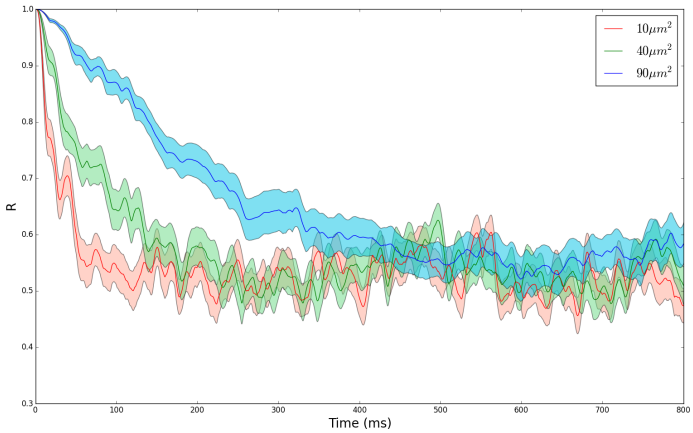

Figure 4.3: Simulations of Eqn. 4.1 using the system shown in Fig. 4.2 for varying membrane areas. Bold lines represent the mean after 50 simulations while shaded areas show one standard deviation from the mean. Injected current was $10.0\mu A/cm^2$.

relationship between membrane area and time to reach steady state.)

4.3.3 Comparison to Independent Poisson Neurons

We wish to compare the observed steady state value in Fig. 4.3 with the predicted value of Eqn. 4.2 when the neurons are completely independent Poisson neurons. We will then extend this result to a larger network afterwards. In large network modeling, the distribution of spike times is highly irregular, and modeling neurons in the network as a Poisson process is widely used [Zad96, GKNP14, Izh03]. As shown in Figure 4.1, for a given input current, channel noise affects the firing rate of a neuron. Therefore, we can understand the relationship between channel noise and synchronization by studying the relationship between synchronization and firing rate.

To compare the steady state synchronization level observed in simulations with that of independent Poisson neurons, our aim is to calculate the expectation of our order parameter $R(t)$, which we denote as $\langle R(t) \rangle$. For simplicity, let us initially assume we have two neurons N_1 and N_2 whose spike times follow a Poisson distribution with rate parameter λ, and

$$\begin{aligned}\langle R(t)\rangle = \langle\sqrt{R(t)^2}\rangle &= \frac{1}{2}\langle\sqrt{|e^{i\theta_1(t)}+e^{i\theta_2(t)}|^2}\rangle \\ &= \frac{1}{2}\langle\sqrt{2+2\cos(\theta_1(t)-\theta_2(t))}\rangle\end{aligned}$$

To compute this expectation, we are required to find the joint distribution of θ_1 and θ_2. Since we are assuming the Poisson neurons are independent, we only need to find the density function of θ_1.

From the definition of θ, only the random term $\frac{t-t_m}{t_{m+1}-t_m}$ has any bearing on the order parameter. Therefore to understand the distribution of θ, we only need to understand the distribution of $\frac{t-t_m}{t_{m+1}-t_m}$. Since we observe some steady state of synchronization in the simulations after time passes, consider a time t where t is large enough so that at least one spike has occurred before time t. Let X be a random variable describing the length of time between our time t and the time of the most recent spike before time t. Moreover, let Y be the length of time between time t and the next spike after time t. Notice that the ratio $\frac{X}{X+Y}$ corresponds directly with the $\frac{t-t_m}{t_{m+1}-t_m}$ term in the definition of θ. We need to add one constraint to X. Because X is the length of time between t and the previous spike, the maximum value X can take is t (otherwise a spike had to occur before time 0, which can not happen). Therefore, $\frac{t-t_m}{t_{m+1}-t_m}$ can be modeled by $\frac{\min\{X,t\}}{\min\{X,t\}+Y}$. Since the spike times of the neurons are being treated as Poisson processes, the wait time between spikes is an exponential distribution with rate parameter λ. Therefore, we have that Y has an exponential distribution with rate parameter λ, X also has an exponential distribution with rate parameter λ, and X and Y are independent of each other.

Let us employ a small trick to simplify matters. Exponential distributions have the scaling property, which means that if X has an exponential distribution with rate λ, then X has the same distribution as $\lambda^{-1}\xi$ where ξ is an exponential random variable with

rate 1. Thus, Y also follows the distribution $\lambda^{-1}\eta$ where η is an exponential random variable with rate 1. Putting everything together, we have:

$$\begin{aligned}\frac{t-t_m}{t_{m+1}-t_m} \sim \frac{\min\{X,t\}}{\min\{X,t\}+Y} &= \frac{\min\left\{\lambda^{-1}\xi,t\right\}}{\min\{\lambda^{-1}\xi,t\}+\lambda^{-1}\eta} \\ &= \frac{\min\{\xi,\lambda t\}}{\min\{\xi,\lambda t\}+\eta}\end{aligned}$$

Assuming λt is large enough, we can approximate the distribution of θ to be that of $\frac{\xi}{\xi+\eta}$ where ξ and η are independent exponential random variables with rate parameter 1. To find the density function of θ, we only need to determine the density function for $\frac{\xi}{\xi+\eta}$. This is known to be a uniform distribution, but we will provide a short proof for the purpose of completeness [S$^+$02]. To calculate this density function, we will find the cumulative distribution function and take its derivative. Note that $0 < \frac{\xi}{\xi+\eta} < 1$, so let us pick an arbitrary $a \in (0,1)$ to use for calculating the distribution function. We use $f_\xi(x)$ to mean the density function of ξ in the derivation. We have:

$$\begin{aligned}P\left(\frac{\xi}{\xi+\eta} \le a\right) &= P\left(\frac{\xi+\eta}{\xi} \ge \frac{1}{a}\right) \\ &= P\left(\eta \ge \xi\left(\frac{1}{a}-1\right)\right) \\ &= \int_0^\infty P\left(\eta \ge s\left(\frac{1}{a}-1\right)\right) f_\xi(s)ds \\ &= \int_0^\infty e^{-s\left(\frac{1}{a}-1\right)} e^{-s} ds \\ &= \int_0^\infty e^{-\frac{s}{a}} ds \\ &= a\end{aligned}$$

This means that $\frac{\xi}{\xi+\eta}$ has the exact same distribution as a uniform random variable

on $(0,1)$ as expected. Consequently, the density function of θ is just 1. Returning to our calculation of the expectation of synchronization:

$$\begin{aligned}\langle R(t)\rangle &= \frac{1}{2}\langle\sqrt{2+2\cos(\theta_1(t)-\theta_2(t))}\rangle \\ &= \frac{1}{2}\int_0^1\int_0^1\sqrt{2+2\cos(2\pi x_1-2\pi x_2)}dx_1dx_2 \qquad (4.3)\end{aligned}$$

This double integral can be solved exactly by utilizing a simple substitution and recognizing that we are integrating over one period of the cosine function,

$$\begin{aligned}\langle R(t)\rangle &= \frac{1}{2}\int_0^1\int_0^1\sqrt{2+2\cos(2\pi x_1-2\pi x_2)}dx_1dx_2 \\ &= \frac{1}{8\pi^2}\int_0^{2\pi}\int_0^{2\pi}\sqrt{2+2\cos(x_1-x_2)}dx_1dx_2 \\ &= \frac{1}{4\pi}\int_0^{2\pi}\sqrt{2+2\cos(x_1)}dx_1 \\ &= \frac{2}{\pi}\end{aligned}$$

Remarkably, we have shown that in the long-term limit of weakly coupled neurons, the expected steady state synchronization level has no dependence on the firing rate (membrane area) of the neurons and will confirm, as already implicit, that it only depends on the number of neurons in the network. In order to obtain a solution for the two-neural-network system, we needed to make a few assumptions: (a) the neurons in the network were weakly coupled to approximate them as independent of each other, and (b) the quantity λt is sufficiently large. Expanding on the second point, recall that we approximated $\min\{\xi,\lambda t\}$ by ξ. Since ξ is exponentially distributed with rate parameter 1, then $P(\xi\leq\lambda t)=1-\exp(-\lambda t)$. Because of the exponential decay dependence on λt, this means that λt does not have to be very large before one can approximate $\min\{\xi,\lambda t\}$

by ξ with high probability. With the application to neurons, this implies that when the firing rate of neurons is higher (small membrane area), we should expect less time to reach a steady state synchronization level. Conversely, with a lower firing rate (large membrane area), we should expect a longer time to reach steady state synchronization. The high and low firing rates correspond with lower and higher channel noise magnitude respectively. Therefore, this derivation provides justification for the observation in Fig. 4.3 that larger channel noise magnitude in neurons results in faster desynchronization.

To expand the result above to a larger neuron network, note that the only place where changes will occur is in the term under the radical. That term results from simplifying $\sqrt{R(t)^2}$, and a formula for $\langle R(t)\rangle$ as follows:

$$\langle R(t)\rangle = \frac{1}{N}\int_0^1 \sqrt{N + \sum_{\substack{j,k=1 \\ j\neq k}}^{N} \cos\left(2\pi x_j - 2\pi x_k\right)} dx_1 \ldots dx_N \tag{4.4}$$

Unlike the two neural network case, higher dimensional cases of Eqn. 4.4 must be evaluated numerically. Numerical estimations for the steady state synchronization predicted by Eqn. 4.4 for different numbers of neurons N can be found in Table 4.1

Table 4.1: Steady state synchronization values estimated from Monte Carlo simulations of Eqn. 4.4

Number of Neurons (N)	Steady State Synchronization Value
2	0.636
3	0.525
4	0.450

The comparison between the values obtained above and numerical simulations is shown in Fig. 4.4. As shown in Fig. 4.4, our estimation of the steady state synchronization values as determined by Eqn. 4.4 is quite accurate, demonstrating that in the presence of channel noise, the synchronization of our neural network behaves just as that of independent Poisson neurons.

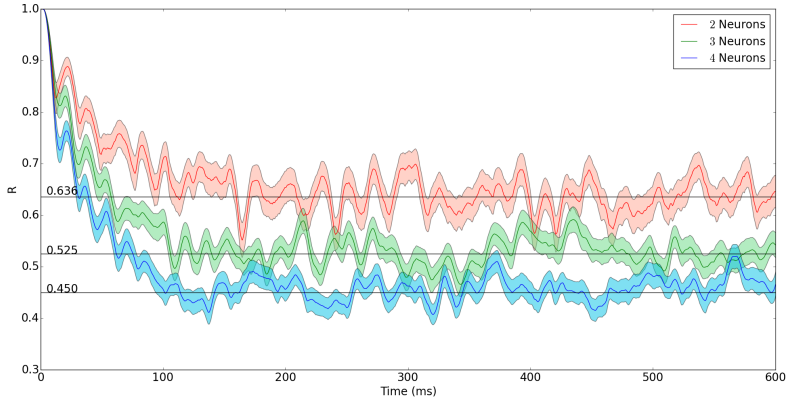

Figure 4.4: Simulations showing synchronization parameter behavior for neuron networks of $2, 3$, and 4 neurons. Straight lines show estimated steady state synchronization values as determined by Eqn. 4.4. Each neuron in the network had an area of $40\mu m^2$ and an injected current of $8.0\mu A/cm^2$. Bold lines represent the mean after 100 simulations while shaded areas show one standard deviation from the mean.

It is also worth noting that based on our results, the connectivity of neurons in the network has no bearing on the steady state synchronization as long as the coupling is weak. To emphasize, the importance of synchronization of the network is not on the connectivity of neurons, or the initial states of the neurons, but only in the number of neurons involved in the network. The role of noise is to help change the rate at which the network reaches a steady state synchronization level but does not appear to change the level itself. To generalize this result a bit further, we will consider two additional cases. We will examine what happens if we change the connectivity strengths so that the connections are no longer equal, and we will change the areas so each one is affected by a different magnitude of channel noise. These results are shown in Fig. 4.5.

For the case of asymmetric coupling constants, we considered the network in Fig. 4.2 with all neurons having a membrane area of $40\mu m^2$ and coupling constants of $\varepsilon_{21} = 10, \varepsilon_{32} = 10^{-1}$, and $\varepsilon_{13} = 10^{-3}$. For the case of various channel noise magnitudes, we considered all synaptic connections to be 0.10, and each neurons 1, 2, and 3 had membrane area of $10\mu m^2$, $40\mu m^2$, and $90\mu m^2$ respectively. In both cases, the expected

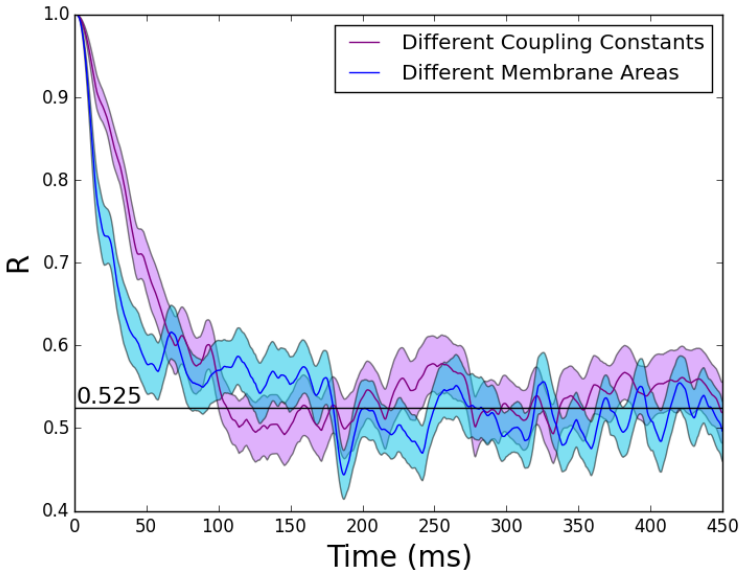

Figure 4.5: Simulations of the network shown in Fig. 4.2 to control for symmetrical parameters. For the coupling constant plot, we use the parameters $\varepsilon_{21} = 10, \varepsilon_{32} = 10^{-1}$, and $\varepsilon_{13} = 10^{-3}$ with each neuron having a membrane area of $40\mu m^2$. For the membrane area plot, we considered each neuron having a different membrane area with either $10\mu m^2$, $40\mu m^2$, and $90\mu m^2$. All coupling constants for the different membrane area simulation were set to 0.10.

steady state deviation again approaches that of independent Poisson neurons, and this was observed over a wide range of value. This result suggests that the resulting formula for the expected steady state synchronization obtained for independent Poisson neurons is applicable not just to Poisson neurons or a symmetric Hodgkin-Huxley network, but generalizes to Hodgkin-Huxley networks which have asymmetric coupling and differing membrane areas.

4.3.4 Large Membrane Area

In the derivation of our formula, we have approximated the spiking pattern as a Poisson distribution due to the irregularity of spike times in neural networks. One might expect that if the area of the neurons is very large so that the magnitude of fluctuations is very small, and hence the dynamics of the stochastic model align very closely with the deterministic behavior, then the synchronization would not reach the steady state but instead retain a synchronization value close to 1 (i.e. completely synchronized) due to how close the stochastic and deterministic dynamics are and the fact that the neurons are coupled. It feels as if one could ignore the fluctuations due to channel noise when the number of channels is extraordinarily large. Surprisingly, the answer to this is no. To examine this, we have considered an area of $300\mu m^2$ (equivalent to $18,000$ sodium channels and $5,400$ potassium channels) whose results are shown in Fig. 4.6.

Despite the similarity of the the stochastic and deterministic dynamics (Fig. 4.6), there are slight mismatches in spike timing due to the stochasticity of the Fox and Lu model. These slight mismatches accumulate over a lengthy period of time, and hence the order parameter decreases over time, albeit slowly. Even with the magnitude of the fluctuations from the channel noise being very small so that the spike timing is reasonably predictable, the degree of synchronization still decreases to the steady state value predicted by Eqn. 4.4. Our simulations and results suggest that channel noise

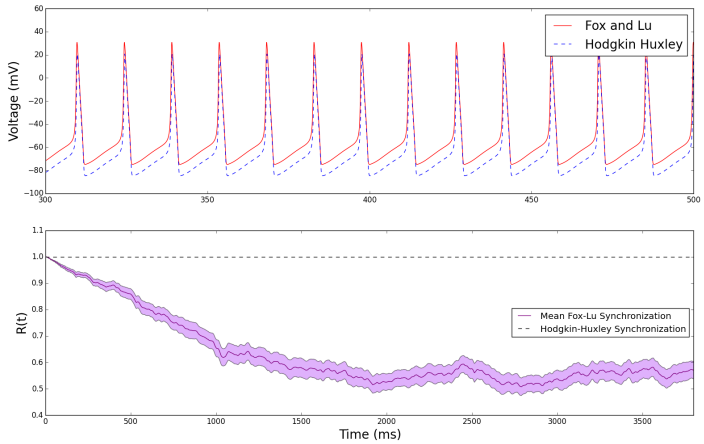

Figure 4.6: (a) Comparison of membrane voltages for the deterministic Hodgkin-Huxley model and Fox and Lu model with membrane area of $300\mu m^2$. Both plots were conducted with input current of $10.0\mu A/cm^2$. Membrane voltage for the Hodgkin-Huxley model was offset by 10 mV for clarity. (b) Order parameter for the system shown in Fig. 4.2 where all three neurons are either deterministic or stochastic with an area of $300\mu m^2$. The bold line shows the mean order parameter value over 50 realizations, and the shaded area shows one standard deviation from the mean.

should be accounted for in the modeling of real neuron synchronization regardless of the magnitude of fluctuations.

4.3.5 Current Noise Model

We next model the network shown in Fig. 4.2 where each neuron is described by the current noise dynamical equations (Eqn. 2.2). The input current in this equation can be thought of as two components: a deterministic input current and a noisy input. Since there is no noise intensity term, one may not expect the steady state synchronization of the current noise model, if there even is one, to match the steady state synchronization for the Fox and Lu channel noise model. While a steady state synchronization value appears to exist as shown in Fig. 4.7, it is vastly greater than the synchronization value predicted by the Fox and Lu channel noise model. In addition, the time to reach the steady state synchronization is extraordinarily fast relative to the channel noise synchronization.

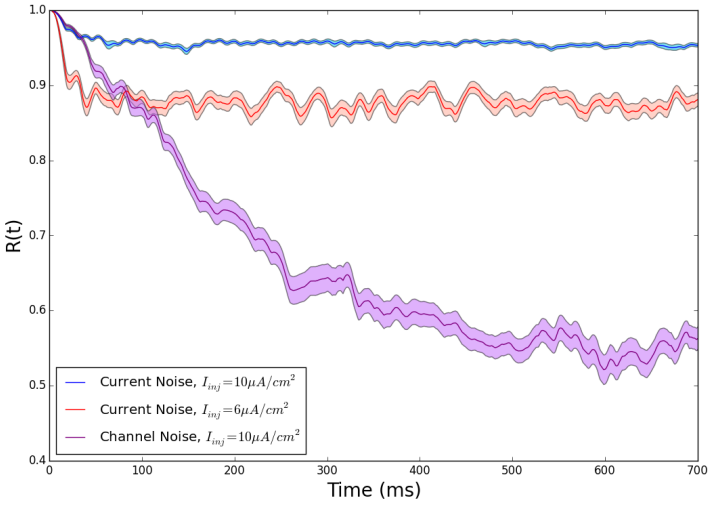

Figure 4.7: Plots of the synchronization parameter as a function of time for the network shown in Fig. 4.2 under different conditions. The three conditions shown are where each neuron is modeled by the current noise model with $I_{inj} = 6\mu A/cm^2$ and $10\mu A/cm^2$, and the channel noise model with area $90\mu m^2$ and injected current of $10\mu A/cm^2$. Solid lines show the mean synchronization over 200 simulations, and shaded regions represent one standard deviation from the mean.

Despite the similarities of the interspike interval distributions of the current noise model and Markov Chain model, the synchronization behavior is significantly different. Our simulations suggest that while the current noise model may be useful measures for some neural properties such as interspike interval [Row07], it is not an accurate measure for studying synchronization properties of stochastic Hodgkin Huxley neurons.

4.3.6 Subunit Noise Model and Expected Time to Reach Steady State

In this section, we compare the synchronization results of using the subunit noise model compared to that obtained by the Fox and Lu channel noise model. In the channel noise model, a system size expansion is applied to the dynamics of the channels. Alternatively, one can apply a system size expansion to the dynamics of the subunits which leads to the system of equations given by Eqn. 2.2. Here, the dynamical equations closely resemble those of the deterministic Hodgkin Huxley model. In the

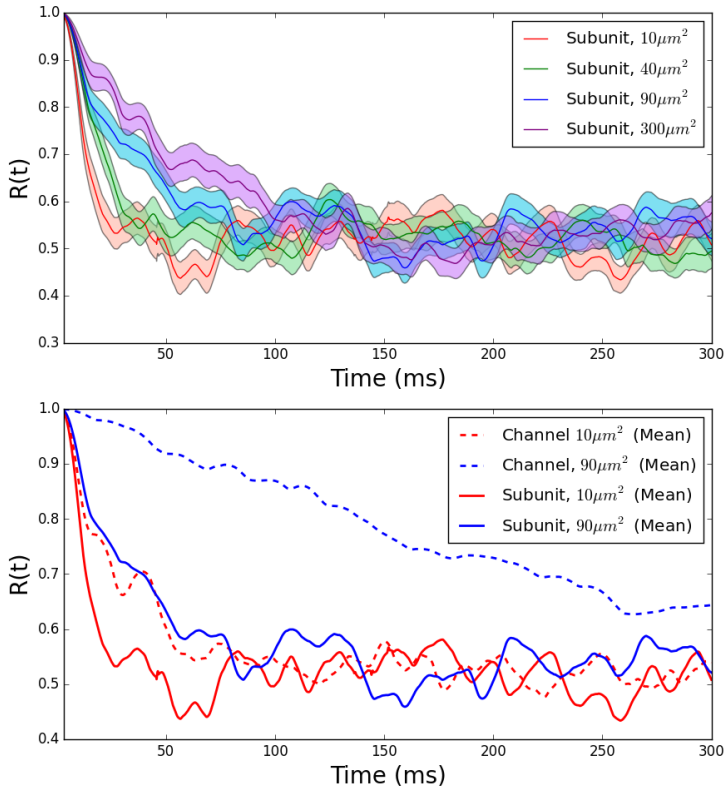

Figure 4.8: (Top) Order parameter dynamics for the subunit noise model as a function of time for changing membrane area. Solid lines show the mean order parameter over 50 simulations where shaded regions show one standard deviation from the mean. (Bottom) Comparison of the order parameter dynamics for channel noise and subunit noise models for different membrane areas. Lines show that mean dynamics over 50 realizations.

limit of infinitely many channels, both the subunit noise model and channel noise model dynamics converge to that of the Hodgkin-Huxley model. Despite inaccuracies in the spike timing exhibited by the subunit noise model we discussed earlier [Bru09, SLN10], it remains possible that the order parameter for a network of neurons represented by the subunit noise model reaches the same steady state value predicted by Eqn. 4.4 that was calculated for the channel noise model. To test this, we simulated the network in Fig. 4.2 where each neuron is modeled by the stochastic differential equations in Eqn. 2.2. The results of these simulations are shown in Fig. 4.8.

For the channel noise model, the expected steady state synchronization for the three neuron network was calculated to be 0.525 based on Eqn. 4.4. The subunit noise model, despite the differences in spike timing, remarkably reaches the same steady state synchronization level as the channel noise model regardless of the magnitude of fluctuations (dictated by the membrane area). In other words, Eqn. 4.4 is valid not just for the channel noise model but the subunit noise model as well. However, Eqn. 4.4 only predicts the value that the long-term synchronization reaches, and tells nothing about the time it takes to reach that steady state value. As shown in Fig. 4.8, when the fluctuation magnitude is large (i.e. smaller membrane area), the time to reach the steady state synchronization is similar between both subunit and channel noise models. As the membrane area grows larger, it takes the channel noise model significantly more time to reach the steady state synchronization level, even though both models will eventually reach that level. A more detailed analysis of the time to reach the steady state can be seen in Fig. 4.9

For these simulations, we consider the time to reach the steady state when our order parameter is within 0.02 of the value calculated by Eqn. 4.4. Most notably, the time to reach the steady state increases with increasing membrane area for both the subunit and channel noise models but at substantially different rates. Therefore in both cases, the stochastic order parameter dynamics converge to the deterministic order parameter dynamics in the limit of infinitely many channels. The rate of convergence is what is different between these two models. Based on previous literature, the subunit noise model has lower firing rates compared to the Markov Chain model, and hence the relative timing in spiking across several neurons is much further apart, and hence the neurons become desynchronized much more quickly, a notion confirmed by Fig. 4.9 [SLN10]. It also worth noting that these lower firing rates persists even as the number of channels grows very large which helps to explain why the time to reach the steady state synchronization

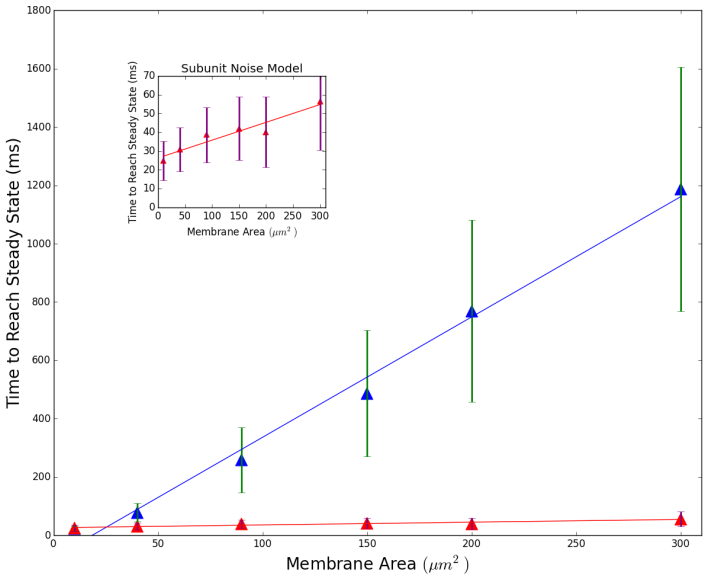

Figure 4.9: Plots comparing the time to reach the steady state synchronization value (defined as within 0.02 of the value calculated by Eqn. 4.4) for both the subunit and channel noise models. The subplot shows a zoomed version of the subunit noise model plot. Error bars indicate one standard deviation away from the mean.

value is much faster than the Fox and Lu model, even when the number of channels is very large [ZJ04, Bru09].

4.4 Conclusion

In this chapter, we have sought to examine the effects of channel noise on neural network synchronization. Because real neurons have finitely many channels, the stochastic opening and closing of these channels leads to fluctuations in the membrane voltage that are not accounted for in the deterministic Hodgkin-Huxley model. In order to account for these fluctuations, we used the Fox and Lu system size expansion model because (a) it is a highly accurate approximation to the gold standard (but computationally expensive) Markov Chain model, and (b) it is a far more computationally efficient model than the Markov Chain model [FL94, GIFSB11]. We first looked at the relationship

between firing frequency and input current in the presence of different magnitudes of channel noise. These simulations showed that channel noise had a larger effect on the firing rate in the absence of input current, but the effect was weakened as input current increased. We then looked at numerical simulations to qualitatively describe the effect of channel noise on neural network synchronization. We observed in Fig. 4.3 that (a) the neural networks hovered around a steady state synchronization level after some time, and (b) that increasing channel noise shortened the time it took to reach that synchronization level. In addition, we were able to derive a formula based on independent Poisson neurons to accurately estimate the long term expected steady state synchronization level. The key result is that even with a tiny amount of channel noise in coupled Hodgkin-Huxley equations, the steady state synchronization behaves identically to independent Poisson neurons. In addition, the derivation required λt to be large where λ is the firing rate. This requirement illustrates two features: that (a) as firing rate decreases (i.e. number of channels increases), the time to reach the steady state synchronization level increases, and (b) as firing rate increases, the steady state synchronization is reached faster. This observation was confirmed by the simulations shown in Fig. 4.3. Our work suggests that despite the randomness within the model, channel noise causes neural networks to reach a steady state level of synchronization, and the steady state value only depends on the number of neurons in the network as suggested by Fig. 4.4.

We next considered two cases, one where the coupling constants were all different and one of them was much stronger than the others, and one where the membrane areas of each neuron were different but the coupling constants were the same. In both of these cases, we observed the same behavior of the synchronization level reaching the same value as predicted by independent Poisson neurons. We then considered the network in Fig. 4.2 where the membrane area was very large for each neuron, and each neuron was in the repetitive firing regime. The purpose of doing this was to observe the synchronization

behavior when the stochastic dynamics are very close to the deterministic dynamics. Even when the dynamics are extremely similar, the small amount of channel noise causes a big change in the degree of synchronization. While three coupled Hodgkin-Huxley neurons (without noise) remain completely synchronized, the small amount of channel noise causes them to desynchronize as observed in Fig. 4.6. The reason for this is that the small variation in the timing of the spikes causes the phases of the neurons to gradually drift apart.

We then considered two alternative models to account for fluctuations in the membrane voltage due to stochastic ion fluctuations: the current noise model and the subunit noise model. As noted by Goldwyn et al [GSB11], the subunit noise model does two things: understates the variance of the fraction of open sodium channels and overstates the variance in the fraction of open potassium channels during neuronal spiking. Because of the increase in variance in the fraction of open potassium channels, the timing between spikes can vary much more than the Fox and Lu model, and as previously noted, the subunit noise model can also miss spikes that the Markov Chain model produces. The combination of these factors leads to spike timing being much less regular, and hence there is a faster decrease in the degree of neuronal synchronization.

Finally, we showed that there seems to be an approximately linear relationship between the membrane area and the expected time to reach the steady state synchronization level. This result shows that in the limit of infinitely many channels, the steady state synchronization we expect to reach from Eqn. 4.4 is never reached. This is in agreement with the simulation shown in Fig. 4.6 where as the channel number grows to infinity, the stochastic dynamics converge to the deterministic dynamics, and the order parameter doesn't change for all time. However, for any finite number of channels, the simulation suggests that the expected steady state will be reached eventually. Ultimately, our work in this chapter strongly supports the notion that valuable insight can be gained

by incorporating channel noise in the study of neural synchronization. In future work, we hope to compare our results obtained for the Fox and Lu model to other stochastic neuron models used to simulate channel noise.

4.5 Acknowledgements

We gratefully acknowledge support by the U. S. Office of Naval Research (ONR) under Grant No. N00014-13-1-0205. We also wish to acknowledge Patrick Fitzsimmons for his help in deriving a formula for the steady state synchronization level.

Chapter 4, in full, is a reprint of the material currently being prepared for submission for publication to Physical Review Letters. The dissertation/thesis author was the primary investigator and author of this paper.

Chapter 5

Heteroclinics: A Model For Cognition

Much of the work done up to this point has been at the level of small neural networks. One of the ultimate goals of computational neuroscience is to relate the randomness observed in neural networks to actual cognitive processes. In general, this is quite difficult to do, but some theoretical framework has been proposed as a possible explanation for experimental observations. The underlying guiding principle for modeling cognition is called winnerless competition, a system described by a dynamical set of equations in which each interacting unit or state in the system becomes a "winner" for a temporary time interval. While we do not claim this model is absolute for describing cognitive behavior, we have taken some initial steps to understand how noise affects winnerless competition. We will first begin with biological motivation for using winnerless competition as a model for neuroscience, followed by mathematical definitions of structures we will use to study winnerless competition, and then study how one-dimensional noise (e.g. environmental noise such as temperature fluctuations) affects winnerless competition compared to four-dimensional noise (e.g. fluctuations as a result of neurons being in different network environments) for a set of dynamical equations which gives rise to winnerless competition.

5.1 Biological Motivation

Many kinds of mental activities such as perception and cognition are sequential in nature in terms of information processing[RKS03, ZSR$^+$10]. Sensory signals from the environment are processed through the activation of specific groups of neurons, and how these neurons encode information is dependent upon both the quality and quantity of the stimulus. After the neurons are activated, neural encoding has been observed to occur in a sequential pattern. For example, in [AKR08, JFS$^+$07], it was shown that by using a Hidden Markov Model, an ensemble of neurons in the rat gustatory cortex could be categorized into states where each state represents some firing pattern of the neurons composing the ensemble. Surprisingly, when a specific stimulus was introduced, the ensemble went through a sequence of various states, and although the time scales of switching between these states differed from trial-to-trial, the sequence was always preserved. Figure 5.1 shows the result of this experiment.

Consequently, this experimental evidence along with others [JFS$^+$07, BKH$^+$03, LSF$^+$01] has led to the recognition that nonlinear dynamics plays a key role in qualitatively modeling cognitive activities including decision making, attention, and working memory [Fri97, RHVA08, RHL08, RTV13, BR09]. Thus, some features that may possibly be incorporated into a model of cognitive behavior should involve these biological features: 1) a sequential switching between states with fast transitions between them, and 2) this sequential switching should occur regardless of the initial conditions of the dynamical model (robustness). The sequential switching has been called "winnerless competition" and has also been used as a model for cognitive behavior [RHVA08, RMSB10, RVTA14]. A stable heteroclinic channel is a mathematical object that utilizes these features for modeling a dynamical system that undergoes transitions between various states [Fri97, RHL08, AZR04].

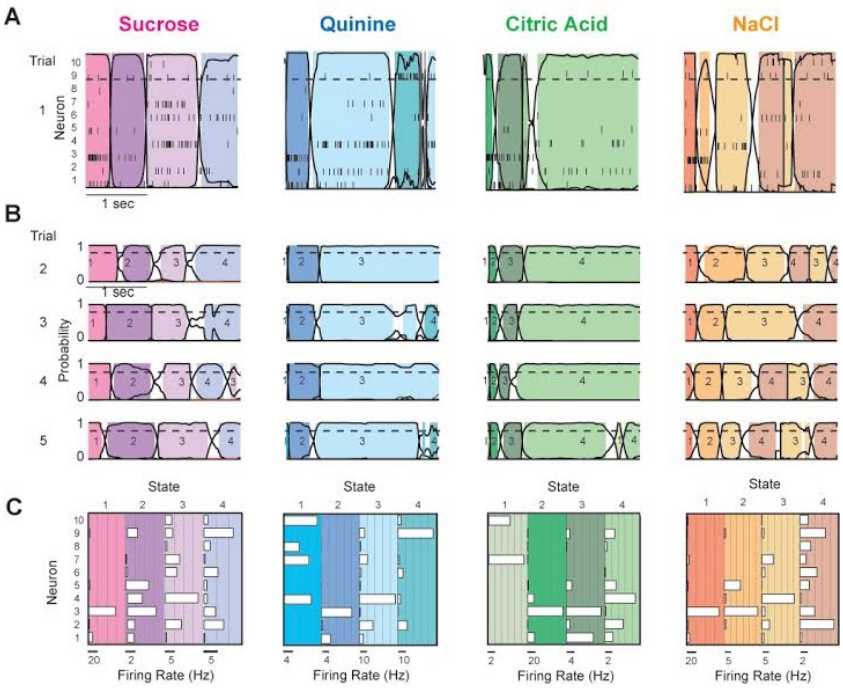

Figure 5.1: Coherent state sequences in Gustatory Cortex (GC) ensembles. (A) Representative single trials of the response of one GC ensemble to each basic taste stimulus (top) reveal simultaneous changes in firing rates in several neurons. Each tick mark represents an action potential, and each row is a different simultaneously recorded neuron. Overlaying the population raster plots is the HMM output: black continuous lines show the probability of each state occuring as a function of time (x axis), and shaded regions are periods during which one particular state (each color represents a specific state) exceeds 0.8 likelihood (horizontal dashed line). In nonshaded periods, no state was dominant. (B) Four more trials of the response of the same ensemble to each taste, showing reliability of state sequence and trial-to-trial variability of transition time. Numbers within each colored region label the state number. (C) Histograms showing firing rates of each neuron (open horizontal bars) in each state for each taste. Each box summarizes the firing patterns of the neurons in each state for the above taste; the number of the state is listed above. [Scale bars (below each shaded panel) show spikes per sec; y axis shows neurons numbered from 1 to 10.] (Figure, and adapted caption, used with permission from [JFS$^+$07])

5.2 Mathematical Description

We will define a heteroclinic cycle in terms of a heteroclinic sequence. Formally, a heteroclinic sequence of a continuous time dynamical system $\dot{x} = f(x)$ is the union of a sequence of finitely many fixed points $\{Q_1, \cdots, Q_n\}$ and a set of trajectories connecting them. A heteroclinic sequence occurs when Q_1 is a local source, Q_n is a local sink, and all other fixed points are saddles. The trajectory connecting the j^{th} fixed point to the k^{th} we denote by γ_{jk}. Thus the union of both the fixed points and the trajectories connecting them, $\Gamma \equiv \bigcup_{k=1}^{n} \left(Q_k \cup \gamma_{k,k+1}\right)$, is defined to be the heteroclinic sequence. This union is denoted as a heteroclinic cycle when the sequence is closed off, i.e. there exists a trajectory connecting the first and last fixed point in the sequence, thereby requiring all fixed points to be saddles.

5.3 The Model

Heteroclinic cycles generally arise in a limited number of dynamical systems [Kru97], and this fact has been exploited outside of neural networks for the design and fabrication of very sensitive sensor devices that operate at low power [BGP00, Pal03, PILK12]. One particular interesting problem worth studying is whether or not noise can cause trajectories to reach saddle points previously unattainable in a deterministic dynamical system. This is an important question as it provides insight into the robustness of heteroclinic cycles to biological sources of noise. The sample model of the heteroclinic system we will look at can be seen pictorially in Fig. 5.2.

In order to actually write an equation from Fig. 5.2, we use the following result from Hirsch as the basis for the model [Hir82, Hir85, Hir88]:

Suppose the system $\dot{x}_i = x_i M_i(x)$, $x \in \mathbb{R}^n_+ = \{x \in \mathbb{R}^n | x_i > 0 \text{ for each } i\}$ satisfies the following:

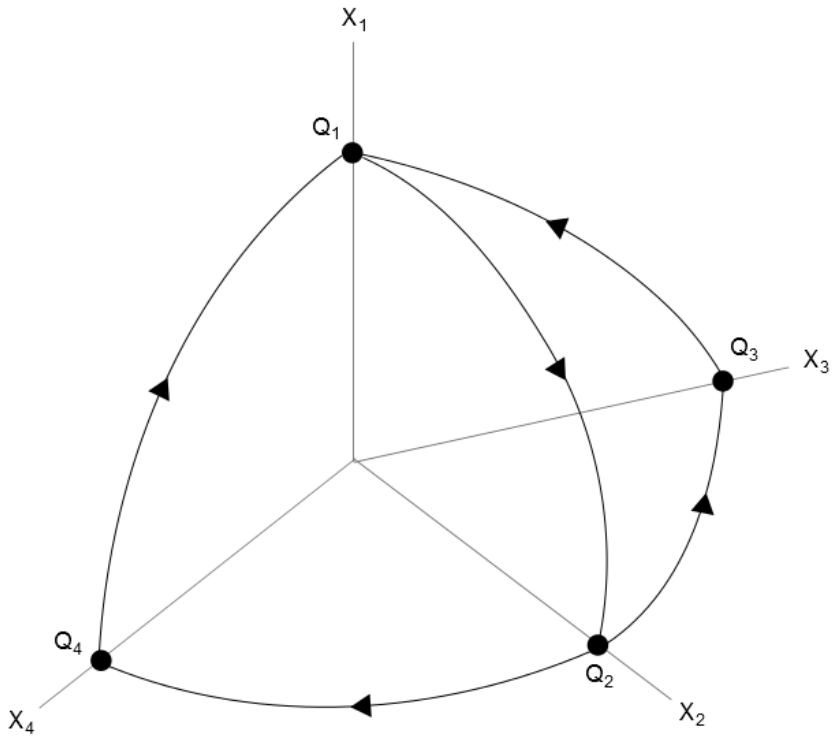

Figure 5.2: Schematic of a four-dimensional heteroclinic system in the positive $\mathbb{R}^4$ cone with two heteroclinic cycles sharing an edge (γ_{12}). One cycle is formed by the fixed points Q_1, Q_2, and Q_3 (denoted as Q_3 cycle) while the other is formed by Q_1, Q_2, and Q_4 (denoted as Q_4 cycle). In the figure, Q_2 acts as a decision point and the arrows show the direction of flow.

1. $\frac{\partial M_i}{\partial x_j} < 0$
2. $M_i(0) > 0$
3. $M_i(x) < 0$ for $|x|$ sufficiently large

Then there exists an invariant hypersurface $\Sigma \subset \mathbb{R}^n_+$ such that:

1. Σ attracts every point in $\mathbb{R}^n_+ \setminus \{0\}$
2. Each line in $K = [0,\infty)^n \subset \mathbb{R}^n$ through the origin meets Σ at a unique point.
3. Σ is homeomorphic to the standard $(n-1)$-dimensional unit simplex $\Delta_{n-1} = \{x_i : x_i \geq 0, \sum_{i=1}^n x_i = 1\}$

Thus, we look for an equation of the form $\dot{x_i} = x_i M_i(x)$ which satisfies the conditions of Hirsch so that we may use the edges of the hypersurface as our heteroclinic cycle. One such example is the following:

$$\begin{aligned}
\dot{x_1} &= \left(x_1\left(1-x_1^2-x_2^2-x_3^2-x_4^2\right) - c_{21}x_1x_2^2 + e_{31}x_1x_3^2 + e_{41}x_1x_4^2\right) \\
\dot{x_2} &= \left(x_2\left(1-x_1^2-x_2^2-x_3^2-x_4^2\right) + e_{12}x_2x_1^2 - c_{32}x_2x_3^2 - c_{42}x_2x_4^2\right) \\
\dot{x_3} &= \left(x_3\left(1-x_1^2-x_2^2-x_3^2-x_4^2\right) - c_{13}x_3x_1^2 + e_{23}x_3x_2^2 - c_{43}x_3x_4^2\right) \\
\dot{x_4} &= \left(x_4\left(1-x_1^2-x_2^2-x_3^2-x_4^2\right) - c_{14}x_4x_1^2 + e_{24}x_4x_2^2 - c_{34}x_4x_3^2\right) \qquad (5.1)
\end{aligned}$$

with $c_{ij}, e_{ij} > 0$ for all i and j. In general, if the saddle value defined as c_{ij}/e_{ji} is greater than unity at each fixed point, then the cycle is attracting. Many proofs involving stochastic models which are similar in structure to Equation 5.1 require every interaction parameter to be greater than 0 (see [MB12, ZY09] for examples). In order to study fluctuations on Equation 5.1, we perturb the intrinsic growth rates of the activity levels

of each interacting unit by additive white noise to model how units interact with the environment [SFV03]. Thus, Equation 5.1 with noise becomes:

$$\begin{aligned}
\dot{x_1} &= \left(x_1\left(1-x_1^2-x_2^2-x_3^2-x_4^2\right)-c_{21}x_1x_2^2+e_{31}x_1x_3^2+e_{41}x_1x_4^2\right)+\sigma_1x_1\dot{W}_t \\
\dot{x_2} &= \left(x_2\left(1-x_1^2-x_2^2-x_3^2-x_4^2\right)+e_{12}x_2x_1^2-c_{32}x_2x_3^2-c_{42}x_2x_4^2\right)+\sigma_2x_2\dot{W}_t \\
\dot{x_3} &= \left(x_3\left(1-x_1^2-x_2^2-x_3^2-x_4^2\right)-c_{13}x_3x_1^2+e_{23}x_3x_2^2-c_{43}x_3x_4^2\right)+\sigma_3x_3\dot{W}_t \\
\dot{x_4} &= \left(x_4\left(1-x_1^2-x_2^2-x_3^2-x_4^2\right)-c_{14}x_4x_1^2+e_{24}x_4x_2^2-c_{34}x_4x_3^2\right)+\sigma_4x_4\dot{W}_t
\end{aligned} \tag{5.2}$$

where each σ_i represents the strength of noise. Due to the symmetry of white noise, we can assume $\sigma_i > 0$ for all i. As in many biological models, only non-negative solutions are physically relevant. Moreover, Eqn. 5.2 admits several interesting properties with proofs found in Appendix B provided the following two properties are satisfied (referred to as the hypothesis):

1. $\sigma_i > 0$ for each i
2. For all i, j with $c_{ij} > 0$ and $e_{ij} > 0$, we have $c_{ij} \geq e_{ji} - 2$

With the hypothesis satisfied, the following are true:

1. Under the hypothesis, for each $x_0 \in \mathbb{R}^4_+ = \left\{(x_1,x_2,x_3,x_4) \in \mathbb{R}^4 : x_1,x_2,x_3,x_4 > 0\right\}$, there is a unique positive solution $x(t)$ to equation (5.2) on $t \geq 0$, and the solution will remain in $\mathbb{R}^4_+$ with probability 1.
2. Under the hypothesis, for $p \leq 2$, $E\left[|x(t)|^p\right] \leq K < \infty$
3. The solution $x(t)$ is stochastically bounded

5.4 Numerical Results

In this section, we provide some numerical results to complement the theorems we prove in the appendix about the stability of Equation 5.2 as well as study the behavior of switching cycles. The simulations were based on Equation 5.2 and the parameter values shown in Table 5.1. Simulations were done using a fourth order Runge-Kutta method adapted for stochastic differential equations with time step $\Delta t = 0.01$ [Gar88]. We observed similar behavior for smaller time steps. Note that cases 1-4 satisfy the hypothesis of the theorems we proved whereas case 5 does not. We include case 5 because Ambruster, Stone, and Kirk observed interesting behavior in the additive noise case, namely that trajectories spent time going back and forth between cycles and spent intermittent blocks of time in each cycle [ASK03]. In the figures, we show perturbations by both a one-dimensional noise and where the system is perturbed by four independent Brownian motions. For all plots, we used $\sigma_i = 1.0$ unless noted otherwise. Explanations of how parameters affect the underlying ODE system (Equation 5.1) can be found in [KS94].

Parameters	Case #1	Case #2	Case #3	Case#4	Case#5
c_{13}	4.2	0.5	4.8	6.2	6.2
c_{14}	4.2	3.3	3.2	4.2	1.0
c_{21}	4.3	4.3	1.3	7.3	7.3
c_{32}	4.4	4.9	10.0	2.4	2.4
c_{34}	4.4	3.8	2.0	12.7	12.7
c_{42}	4.4	3.7	10.0	5.7	5.7
c_{43}	4.4	3.0	2.8	5.0	5.0
e_{12}	1.9	3.5	1.8	0.5	1.5
e_{23}	2.5	2.5	2.5	2.5	2.5
e_{24}	2.2	2.0	2.0	2.0	2.0
e_{31}	2.0	1.0	1.0	1.0	3.0
e_{41}	4.0	4.8	2.5	4.8	4.8

Table 5.1: Table of parameter values for differing cases of asymptotic behavior of the two cycle system

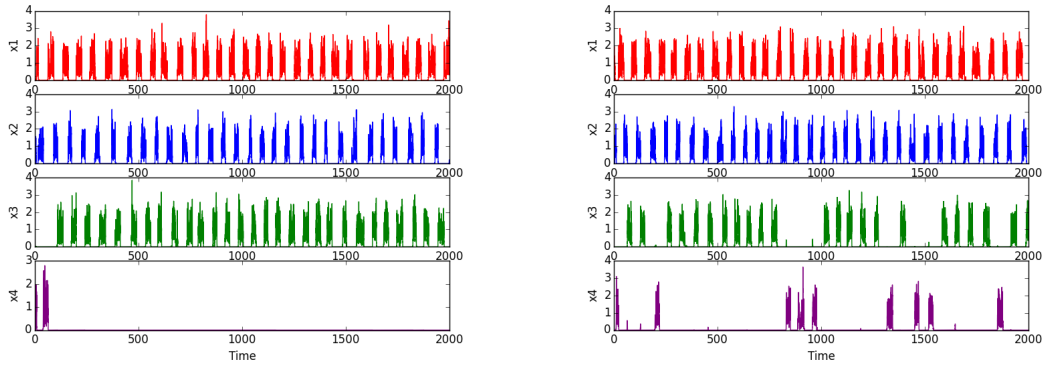

Figure 5.3: Plots of stochastic trajectories with parameters from Case 1 where Gaussian white noise is one-dimensional (left figure) and four-dimensional (right figure).

Case 1 (Figure 5.3) gives an example of parameters where noise in the one-dimensional case is not enough to cause a trajectory to switch cycles, but increasing the dimension of the noise causes random switches between the cycles. Although the underlying ODE is still attracted to the Q_3-cycle, four-dimensional noise readily drives trajectories to the other cycle when a trajectory passes near the Q_2 fixed point.

In Case 2 (Figure 5.4), the parameters show a case where noise has minimal long-term effects on trajectories switching. Although the trajectory begins within the Q_4 cycle, it quickly switches to the Q_3 cycle and noise is unable to bring it back to the Q_4 cycle. The underlying ODE system with these parameters allows the Q_3 cycle to attract almost all trajectories starting near the network. In this instance, the Q_3 cycle is called essentially asymptotically stable, defined as follows [Mel91]:

A flow-invariant set X is essentially asymptotically stable (e.a.s) if there exists a set C such that given any $a \in (0,1)$ and any open neighborhood U of X, there is an open neighborhood $V \subset U$ such that:

1. all trajectories starting in $V \backslash C$ remain in U and are asymptotic to X
2. $\mu(V \backslash C)/\mu(V) > a$ where μ is Lebesgue measure

In other words, the measure of initial conditions not asymptotically stable to the

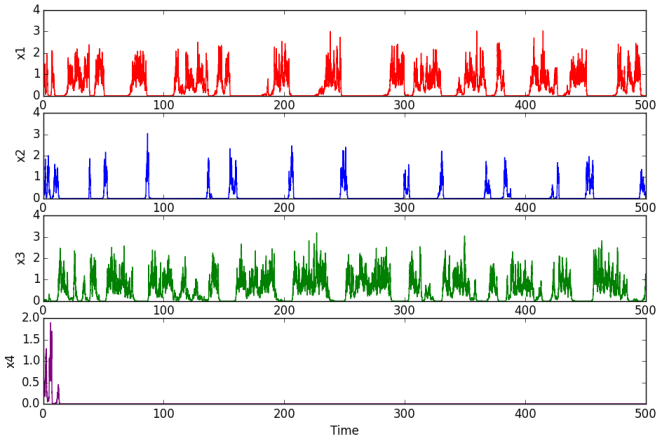

Figure 5.4: Plots of stochastic trajectories with parameters from Case 2 where Gaussian white noise is four-dimensional. Here, $\sigma_i = 1.5$ for each i. Very similar behavior was seen in the one-dimensional case in that we did not observe switching between cycles.

network is small. For the parameters of case 2, the Q_3 cycle is e.a.s. and attracts almost all trajectories near it even in the presence of noise. In this simulation, we show only a four-dimensional noise as simulations with one-dimensional noise exhibited nearly identical behavior.

In case 3, the Q_3 cycle is not e.a.s. but almost all trajectories started anywhere in the network are eventually attracted to it. The results of this simulation are shown in Figure 5.5. Notice that even though almost all trajectories are eventually attracted to the cycle, four-dimensional noise is strong enough to cause trajectories to briefly escape the cycle whereas one-dimensional noise is not.

In case 4, neither cycle is e.a.s. but both cycles attract open sets of initial conditions. We used an initial condition of $[x_1(0), x_2(0), x_3(0), x_4(0)] = [0.2, 0.5, 0.2, 0.6]$. With these parameters and this initial condition, the Q_3 cycle attracts the ODE trajectory, but because both cycles attract open sets of initial conditions, we expect that noise may cause a trajectory which is initially attracted to the Q_3 cycle to spend longer periods of time in the Q_4 cycle. In fact, Figure 5.6 shows this behavior in the four-dimensional

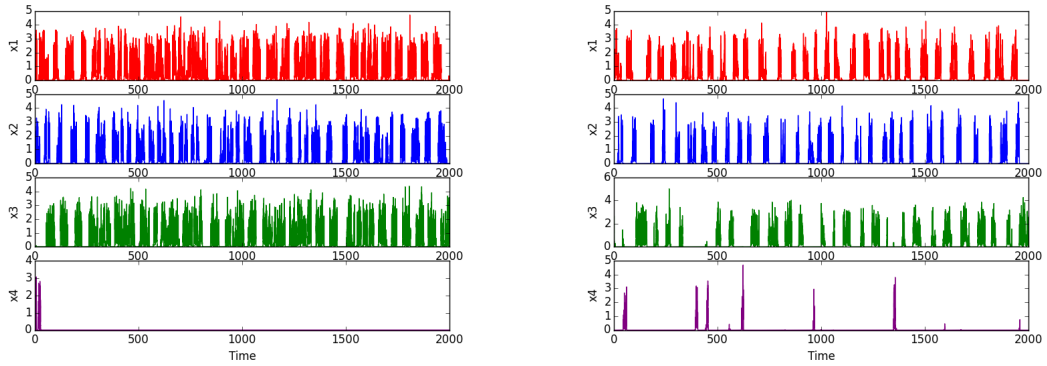

Figure 5.5: Plots of stochastic trajectories with parameters from Case 3 where Gaussian white noise is one-dimensional (left figure) and four-dimensional (right figure).

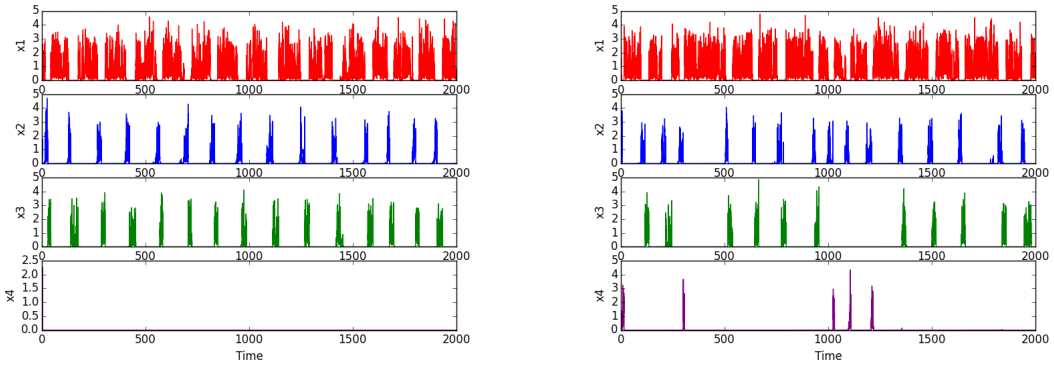

Figure 5.6: Plots of stochastic trajectories with parameters from Case 3 where Gaussian white noise is one-dimensional (left figure) and four-dimensional (right figure). Here, $\sigma_i = 1.5$ for all i.

noise case where trajectories pass near Q_4 and remain in the Q_4 cycle for a period of time before jumping back to the Q_3 cycle.

In case 5, notice that the parameters do not satisfy our hypothesis. As we stated before, there is a unique local solution $x(t)$ on $t \in [0, \tau_\varepsilon)$ where τ_ε is the explosion time because the coefficients are still locally Lipschitz continuous. We also are no longer guaranteed finite first and second moments, and so the solutions may have a lot more variability. With these parameters, both cycles attract large sets of initial conditions. An example of an initial condition where the Q_3 cycle is attractive is $(0.2, 0.3, 0.7, 0.2)$ and the Q_4 cycle attracts the initial condition $(0.2, 0.3, 0.2, 0.7)$. Figure 5.7 shows the results

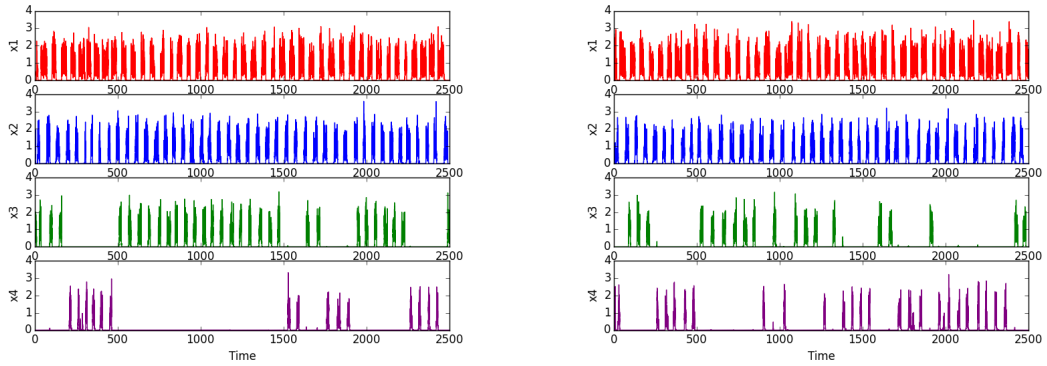

Figure 5.7: Plots of stochastic trajectories with parameters from Case 5 where Gaussian white noise is four-dimensional. On the left, the initial condition $(0.2, 0.3, 0.7, 0.2)$ was used leading to the Q_3 cycled being favored in the underlying ODE. On the right, the initial condition $(0.2, 0.3, 0.2, 0.7)$ was used leading to the Q_4 cycled being favored.

of simulating Equation 5.2 with these two initial conditions. In both cases, trajectories bounce back and forth between the two cycles and spend "blocks" of time in each cycle, although each trajectory spends more time in the cycle that their respective ODE is attracted to. Kirk and Silber noted similar behavior when additive noise was used [ASK03].

5.5 Summary

The aim of this chapter was to study a simple example of a heteroclinic network to determine if noise can cause trajectories starting near one cycle of the network to switch and visit the other cycle for periods of time. Generally, for a heteroclinic cycle to be stable, the ratio of the contracting eigenvalue to the corresponding unstable eigenvalue must be greater than unity at each fixed point. We gave an example of an ODE system for which a system of heteroclinic cycles sharing a common edge can be induced. We showed that the stochastically perturbed system (Equation 5.2) admits a positive global solution, the distribution of solutions has finite first and second moments, and the solution is stochastically bounded.

Moreover, we showed that when the stochastic perturbations is one-dimensional, trajectories are unable to change cycles, but when the noise is four independent Brownian motions, trajectories are more easily able to switch cycles. We hypothesize that higher dimensional noise induces more variability in the solutions although it is surprising that one-dimensional noise is incapable of causing solutions to change cycles. Unlike the additive noise case, the strength of noise needs to be higher in order for switching to occur. This is due to the fact that the size of the noise scales with the values of $x_i(t)$ but along the shared edge, several of the $x_i(t)$'s are near zero and a large strength of noise constant is required to overcome this.

Relating these results back to neuroscience, this work suggests that noise modeled as one-dimensional (e.g. temperature fluctuations on neuron activity levels) has minimal effects on the ability for the dynamical system to reach an unreachable state, and this fact is in agreement with previous theory showing that although it is a source of noise, it is relatively minor in the scope of its effect [MK99a]. As stated earlier, an example of a four dimensional noise source could be demographic stochasticity and variability among the neural network itself. This is supported by theory and experiments showing that in a network of neurons, there are fluctuations in spiking patterns generated by the network itself [vVS97, KZ02]. Thus, there is biological justification that four-dimensional fluctuations play a much larger role in causing trajectories to change cycles.

5.6 Acknowledgments

We would like to thank Sadique Sheik for his assistance in programming. This work has been supported by the U. S. Office of Naval Research (ONR) under Grant No. N00014-13-1-0205.

Chapter 5, in full, is a reprint of the material currently being prepared for submis-

sion for publication to journal to be determined. The dissertation/thesis author was the primary investigator and author of this paper.

Chapter 6

Conclusion

6.1 Summary

In this thesis, we first looked at the biology behind neurons and what causes them to spike. We saw that this was caused by voltage-gated ion channels that open and close as functions of the voltage. Moreover, we wrote down an equation which models such a spike known as the Hodgkin-Huxley equation. This powerful equation representing a conductance-based model is one of the hallmarks of computational neuroscience which allows us to gain insight into the mechanisms which lead to neural spiking. However, the Hodgkin-Huxley model assumes the presence of infinitely many ion channels so that fluctuations in the fraction of open channels remain undetected by the model. Real neurons only have finitely many channels; hence, the purpose of this thesis was to understand what effects microscopic fluctuations in the fraction of open channels (channel noise) has on macroscopic properties of small neural networks.

To study the role of channel noise in small neural networks, we first looked at several models which account for these fluctuations. Generally, the protein channels in the neural membrane can be found in various configuration states. In some of these

configurations, the channel is considered “open” in that it is conducting while the channel is considered “closed” in the remaining states. It is assumed that the state configurations can be modeled as a Markov Chain so that the transition from one state to another is not dependent upon its previous states. We then looked at several methods to simulate the Markov Chain model; however, simulating such a model is computationally expensive and is unfeasible for network simulations. For this reason we looked at several stochastic differential equations which sought to approximate the Markov Chain model but were much more computationally efficient. These models we referred to as the Fox and Lu channel noise model (Eqn. 2.1), the subunit noise model (Eqn. 2.2), and the current noise model (Eqn. 2.2). The majority of the thesis is based on the Fox and Lu model due to its accurate approximation of the Markov Chain model.

We first looked at the first spike latency of a neuron modeled by the Fox and Lu model when subjected to random synaptic input from other neurons. First spike latency is an important aspect of neurons as it is believed to be strongly related to neural coding, and unlike the deterministic models, the first spike latency of the stochastic neuron is now a distribution of times rather than a fixed time that depends on both the membrane area and the rate of synaptic input. Despite the two sources of randomness, certain statistical properties (the mean, median, and IQR) of the first spike latency distributions could be well predicted from a simple linear regression knowing solely the rate of synaptic input and the membrane area. However, the standard deviation could not be well predicted. We then compared these results to the subunit noise model. The two primary differences were that the subunit noise model had a bigger delay in the mean and median first spike latency, and the standard deviation of the first spike latency distribution could be accurately predicted from a linear regression. Because of the known inaccuracies in the subunit noise model, and the accuracy of the Fox and Lu model where the standard deviation of the first spike latency distribution can not be readily predicted, we proposed that the IQR

would be a better indicator of spike timing variation than the standard deviation.

One area where spike timing is important is in the study of neural synchronization. Neural synchronization has been tied to a number of conditions such as epilepsy, Parkinson's disease, and Alzheimer's disease, and hence this is a blooming area of research. Our goal was to study what role channel noise can induce on the synchronization of small neural networks. In our work, we showed that when channel noise is introduced, the long-term expected degree of synchronization matches that of completely independent Poisson neurons. Moreover, we were able to derive an explicit formula to calculate this synchronization value. We then compared our results to the subunit noise model and we saw that while the same degree of synchronization is reached, it does so on a much faster time scale.

Lastly, one of the major research areas of neuroscience is the buildup from individual neurons to cognition. Here, we have introduced a mathematical structure known as a stable heteroclinic channel which has been suggested as a potential mathematical model for cognition. A stable heteroclinic channel is a collection of saddle points of a dynamical system and the orbits that connect them. We then subjected the model to noise and found that in the case of one-dimensional noise (such as an environmental noise), noise maintains the behavior of trajectories in the stable heteroclinic channel. In the case of high-dimensional noise, noise can actually cause the system to reach fixed points (states of the system) unattainable in the deterministic system.

Ultimately, this thesis has helped shape the understanding of the role that microscopic channel state fluctuations has on macroscopic neural network properties. Moreover, this thesis should shed light on the idea that channel noise is an important biological noise that should be incorporated into the study of neuron models.

6.2 Future Directions

In this section, we will look at ways to extend our work of modeling channel noise to include more features of neurons and to extend the work to larger networks.

6.2.1 Effects of Dendritic Noise

Throughout this dissertation, we looked at the role channel noise has in terms of first spike latency and neural synchronization and noticed some large effects. The channel noise we looked at is a result of sodium and potassium channels in the neural membrane primarily found on the axon. Another important region of the neuron where channels are found is in the dendrites which are the sites of neural communication with the presynaptic neurons. Perhaps even more importantly, changes in dendritic connections is a phenomenon known as synaptic plasticity and has been thought to be the basis of human learning [GKNP14, BP98]. This leads to several questions. First, how does the inclusion of dendritic channel noise affect first spike latency and synchronization? For example, if dendritic noise on average delays the effects of post synaptic potential changes, then that could effectively cancel out the increase in firing that our simulations of channel noise predicted.

As an application of spike timing, how does channel noise affect learning? Based on the study by Bi and Poo [BP98], spike timing is strongly tied to changes in synaptic connections with neurons that fire closer together resulting in larger synaptic changes. As we have shown, channel noise decreases the time it takes for a neuron to fire, and hence may increase learning in a process known as stochastic facilitation. This however ignored the role of stochasticity in dendritic channels, and the role of this source of noise may be important.

6.2.2 Improving the Fox and Lu Model

Despite the improvements in computational efficiency over the Markov Chain Model, the Fox and Lu model is a challenge for large scale simulations due to the computational costs of calculating the square root of the diffusion matrix. While the subunit noise model was designed to help circumvent this problem, we have noted some discrepancies where this subunit noise model does not accurately reflect the Markov Chain model dynamics. Recently, a proposed model by Odio and Soudry was shown to replicate the Markov Chain model with high accuracy and bypass the square root computation [OS12]. This has the potential to expand the results from the Fox and Lu model to larger scale networks where computational costs are frequently expensive.

The stochastic dynamics of the gating variables are given by the following matrices:

$$\begin{aligned} C\dot{V} &= I_{inj}(t) + I_{syn}(t) - \bar{g}_{Na} y_{31}(V - E_{Na}) - \bar{g}_K x_4 (V - E_K) - \bar{g}_L (V - E_L) \\ \dot{\mathbf{x}} &= A_K(V)\mathbf{x} + \frac{1}{\sqrt{N_K}} \overline{S_K}(V, \mathbf{x}) \bar{\xi}_K \\ \dot{\mathbf{y}} &= A_{Na}(V)\mathbf{y} + \frac{1}{\sqrt{N_{Na}}} \overline{S_{Na}}(V, \mathbf{y}) \bar{\xi}_{Na}. \end{aligned} \tag{6.1}$$

The matrices A_K and A_{Na} are identical to the Fox and Lu model. The diffusion matrices $\overline{S_K}(V, \mathbf{x})$ and $\overline{S_{Na}}$ are different and hence are indicated with a bar to distinguish them from the Fox and Lu definitions. The diffusion matrices are given by:

$$\overline{S_K(V,x)} = \begin{bmatrix} \sqrt{4\alpha_n x_0 + \beta_n x_1} & 0 & 0 & 0 \\ -\sqrt{4\alpha_n x_0 + \beta_n x_1} & \sqrt{3\alpha_n x_1 + 2\beta_n x_2} & 0 & 0 \\ 0 & -\sqrt{3\alpha_n x_1 + 2\beta_n x_2} & \sqrt{2\alpha_n x_2 + 3\beta_n x_3} & 0 \\ 0 & 0 & -\sqrt{2\alpha_n x_2 + 3\beta_n x_3} & \sqrt{\alpha_n x_3 + 4\beta_n x_4} \\ 0 & 0 & 0 & -\sqrt{\alpha_n x_3 + 4\beta_n x_4} \end{bmatrix}$$

and

$$\overline{S_{Na}(V,y)} = \begin{bmatrix}
\sqrt{3\alpha_m y_{00}+\beta_m y_{10}} & 0 & 0 & \sqrt{\alpha_h y_{00}+\beta_h y_{01}} & 0 & 0 & 0 & 0 & 0 & 0 \\
-\sqrt{3\alpha_m y_{00}+\beta_m y_{10}} & \sqrt{2\alpha_m y_{10}+2\beta_m y_{20}} & 0 & 0 & \sqrt{\alpha_h y_{10}+\beta_h y_{11}} & 0 & 0 & 0 & 0 & 0 \\
0 & -\sqrt{2\alpha_m y_{10}+2\beta_m y_{20}} & \sqrt{\alpha_m y_{20}+3\beta_m y_{30}} & 0 & 0 & \sqrt{\alpha_h y_{20}+\beta_h y_{21}} & 0 & 0 & 0 & 0 \\
0 & 0 & -\sqrt{\alpha_m y_{20}+3\beta_m y_{30}} & 0 & 0 & 0 & \sqrt{\alpha_h y_{30}+\beta_h y_{31}} & 0 & 0 & 0 \\
0 & 0 & 0 & -\sqrt{\alpha_h y_{00}+\beta_h y_{01}} & 0 & 0 & 0 & \sqrt{3\alpha_m y_{01}+\beta_m y_{11}} & 0 & 0 \\
0 & 0 & 0 & 0 & -\sqrt{\alpha_h y_{10}+\beta_h y_{11}} & 0 & 0 & -\sqrt{3\alpha_m y_{01}+\beta_m y_{11}} & \sqrt{2\alpha_m y_{11}+2\beta_m y_{21}} & 0 \\
0 & 0 & 0 & 0 & 0 & -\sqrt{\alpha_h y_{20}+\beta_h y_{21}} & 0 & 0 & -\sqrt{2\alpha_m y_{11}+2\beta_m y_{21}} & \sqrt{\alpha_m y_{21}+3\beta_m y_{31}} \\
0 & 0 & 0 & 0 & 0 & 0 & -\sqrt{\alpha_h y_{30}+\beta_h y_{31}} & 0 & 0 & -\sqrt{\alpha_m y_{21}+3\beta_m y_{31}}
\end{bmatrix}$$

Additionally, $\bar{\xi}_K$ and $\bar{\xi}_{Na}$ are vectors of four and ten independent Gaussian white noise terms, respectively. We attempted to simulate this model to understand how the

Kuramoto order parameter compares between this model and the Fox and Lu model. While the results displayed similarities, we note that this particular stochastic differential equation system was more susceptible to numerical integration errors. While these errors were substantially reduced using a smaller time step, the necessity of using a smaller time step negated the benefit of no longer needing to take a matrix square root of the Fox and Lu model. However, it remains possible that an alternative integration scheme would result in a faster simulation time for this model.

Alternative deterministic models exist which were designed to match the Hodgkin-Huxley dynamics in exchange for lesser biological plausibility. For example, the adapative exponential integrate and fire model (AdEx) was shown to match the Hodgkin-Huxley dynamics with 96% accuracy [BG05]. However, the equations remove the concepts of sodium and potassium ion channels. It does remain possible that one could place an additive noise term with a proper scaling term (similar to the current noise model in Sec. 2.2) such that the dynamics of a stochastic AdEx (or similar) model matches that of the Fox and Lu model. This would be a tremendous advancement for studying channel noise on larger neural network systems.

Appendix A

Simulation Schemes

Consider a stochastic differential equation of the form $dx(t) = f(x(t))dt + g(x(t))dW(t)$ with $0 \leq t \leq T$ and $x(0) = x_0$. Here, $x(t) \in \mathbb{R}^m$ for all t, $W(t)$ is a d-dimensional Brownian motion, $f : \mathbb{R}^m \to \mathbb{R}^m$, and $g : \mathbb{R}^m \to \mathbb{R}^{m \times d}$. The derivation of the following schemes used in this thesis can be found in [Gar88], but we show the main result here.

A.1 Euler-Maruyama

The Euler-Maruyama method takes the following steps to approximate solutions to the stochastic differential equation:

1. Partition the interval $[0, T]$ into N equal subintervals of width Δt ($\Delta t = T/N$)
2. Define $Y_0 = x_0$
3. Recursively define $Y_{k+1} = Y_k + f(Y_k)\Delta t + g(Y_k)\Delta W_k$ where $\Delta W_k = W(t_{k+1}) - W(t_k)$.

The random variables ΔW_k are independent and identically distributed normal random variables of mean zero and variance Δt.

A.2 Fourth-Order Stochastic Runge Kutta

As before, divide the interval into N equal subintervals of width Δt and let $Y_0 = x_0$. Then define the following iteration:

$$Y_k = Y_{k-1} + \tfrac{1}{6}\left\{(F_0 + 2F_1 + 2F_2 + F_3)\,\Delta t + (G_0 + 2G_1 + 2G_2 + G_3)\,\Delta W_n\right\}$$

with

$$\begin{aligned}
F_0 &= f(Y_{k-1}) \\
F_1 &= f\left(Y_{k-1} + \frac{1}{2}F_0\Delta t + \frac{1}{2}G_0\Delta W_n\right) \\
F_2 &= f\left(Y_{k-1} + \frac{1}{2}F_1\Delta t + \frac{1}{2}G_1\Delta W_n\right) \\
F_3 &= f\left(Y_{k-1} + F_2\Delta t + \frac{1}{2}G_2\Delta W_n\right) \\
G_0 &= g(Y_{k-1}) \\
G_1 &= g\left(Y_{k-1} + \frac{1}{2}F_0\Delta t + \frac{1}{2}G_0\Delta W_n\right) \\
G_2 &= g\left(Y_{k-1} + \frac{1}{2}F_1\Delta t + \frac{1}{2}G_1\Delta W_n\right) \\
G_3 &= g\left(Y_{k-1} + F_2\Delta t + \frac{1}{2}G_2\Delta W_n\right)
\end{aligned}$$

Appendix B

Proofs

B.1 Proof of Existence of Unique, Global Solution of Eqn. 5.2

We first prove that there exists a positive, global solution (i.e. Equation 5.2 does not explode in finite time). To do so, we will need the following lemma: For any $z > 0$, $z^2 \leq 4\left(\frac{1}{2}z^2 - \log z + 1\right) - (6 - 2\log 2)$.

Suppose each $W_i(t)$ is a one-dimensional Wiener process independent of each other and defined over the complete probability space $(\Omega, \mathbb{F}, P)$ with a filtration $\{\mathbb{F}_t\}_{t\geq 0}$ satisfying the usually conditions (i.e. that is is increasing and right continuous, and F_0 contains all P-null sets.) Since the coefficients of (5.2) are locally Lipschitz continuous, for any initial value $x_0 \in \mathbb{R}^4_+ = \left\{(x_1, x_2, x_3, x_4) \in \mathbb{R}^4 : x_1, x_2, x_3, x_4 > 0\right\}$, there is a unique local solution $x(t)$ on $t \in [0, \tau_\varepsilon)$ where τ_ε is the explosion time [Lud73]. In order to show that the solution is global, we must show that $\tau_\varepsilon = \infty$ a.s.

We choose a sufficiently large number $k_0 > 0$ such that each $x_i(t)$ starts within the interval $\left(\frac{1}{k_0}, k_0\right)$. Thus we define the stopping time for all $k \geq k_0$:

$$\tau_k = inf\left\{t \in [0,\tau_\varepsilon) : \min_{1\le i\le n} x_i(t) \le \frac{1}{k} or \max_{1\le i\le n} x_i(t) \ge k\right\} \tag{B.1}$$

where $\inf\emptyset = \infty$. Clearly τ_k is increasing as $k \to \infty$. Set τ_∞ to be $\lim_{k\to\infty}\tau_k$, whence $\tau_\infty \le \tau_\varepsilon$ a.s. Since our goal is to show that $\tau_\varepsilon = \infty$, it suffices to show that $\tau_\infty = \infty$ a.s. Suppose the statement is false. Then there exists two constants, $T > 0$ and $\varepsilon \in (0,1)$, such that:

$$P(\tau_\infty \le T) > \varepsilon \tag{B.2}$$

Then there exists an integer $k_1 \ge k_0$ such that

$$P(\tau_k \le T) > \varepsilon \tag{B.3}$$

for all $k \ge k_1$.

Define a C^2-function V: $\mathbb{R}^4_+ \to \mathbb{R}_+$ by

$$V(x) = \sum_{i=1}^{n}\left(\frac{1}{2}x_i^2 + 1 - \log(x_i)\right) \tag{B.4}$$

By applying Ito's Lemma to our function $V(x)$ and (5.2), we get:

$$
\begin{aligned}
dV(X_t) &= \left[\left(x_1^2-1\right)\left(1-x_1^2-x_2^2-x_3^2-x_4^2-c_{21}x_2^2+e_{31}x_3^2+e_{41}x_4^2\right)\right. \\
&+ \left(x_2^2-1\right)\left(1-x_1^2-x_2^2-x_3^2-x_4^2+e_{12}x_1^2-c_{32}x_3^2-c_{42}x_4^2\right) \\
&+ \left(x_3^2-1\right)\left(1-x_1^2-x_2^2-x_3^2-x_4^2-c_{13}x_1^2+e_{23}x_2^2-c_{43}x_4^2\right) \\
&+ \left(x_4^2-1\right)\left(1-x_1^2-x_2^2-x_3^2-x_4^2-c_{14}x_1^2+e_{24}x_2^2-c_{34}x_3^2\right) \\
&+ \left.\sum_{i=1}^{4}\frac{\sigma_i^2x_i^2+\sigma_i^2}{2}\right]dt+\sum_{i=1}^{4}\sigma_i\left(x_i^2-1\right)dW_t \\
&= \left[\left(5-e_{12}+c_{13}+c_{14}+\frac{\sigma_1^2}{2}\right)x_1^2+\left(5+c_{21}-e_{23}-e_{24}+\frac{\sigma_2^2}{2}\right)x_2^2\right. \\
&+ \left(5-e_{31}+c_{32}+c_{34}+\frac{\sigma_3^2}{2}\right)x_3^2+\left(5-e_{41}+c_{42}+c_{43}+\frac{\sigma_4^2}{2}\right)x_4^2 \\
&+ \left(e_{12}-c_{21}-2\right)x_1^2x_2^2+\left(e_{31}-c_{13}-2\right)x_1^2x_3^2+\left(e_{41}-c_{14}-2\right)x_1^2x_4^2 \\
&+ \left(e_{23}-c_{32}-2\right)x_2^2x_3^2+\left(e_{24}-c_{42}-2\right)x_2^2x_4^2-\left(c_{43}+c_{34}+2\right)x_3^2x_4^2 \\
&+ \left.\left(-4+\sum_{i=1}^{4}\frac{\sigma_i^2}{2}\right)\right]dt+\sum_{i=1}^{4}\sigma_i\left(x_i^2-1\right)dW_t
\end{aligned}
$$

Under the assumption $c_{ij}/e_{ji}>1$ for each i and j, we have:

$$
dV(X_t)\leq a_0+a_1x_1^2+a_2x_2^2+a_3x_3^2+a_4x_4^2dt+\sum_{i=1}^{4}\sigma_i(x_i^2-1)dW_t \tag{B.5}
$$

where $a_0=\left(-4+\sum_{i=1}^{4}\frac{\sigma_i^2}{2}\right)$, $a_1=5-e_{12}+c_{13}+c_{14}+\frac{\sigma_1^2}{2}$, $a_2=5+c_{21}-e_{23}-e_{24}+\frac{\sigma_2^2}{2}$, $a_3=5-e_{31}+c_{32}+c_{34}+\frac{\sigma_3^2}{2}$, and $a_4=5-e_{41}+c_{42}+c_{43}+\frac{\sigma_4^2}{2}$. Using the Lemma and defining $a_5=\max\{a_1,a_2,a_3,a_4\}$, we can write:

$$
\sum_{i=1}^{4}a_ix_i^2\leq 4a_5V(X_t) \tag{B.6}
$$

Combining this with (B.5), we can write:

$$\begin{aligned} dV(X_t) &\leq (a_0 + a_5 V(X_t))dt + \sum_{i=1}^{4} \sigma_i (x_i^2 - 1) dW(t) \\ &\leq a_6(1 + V(X_t))dt + \sum_{i=1}^{4} \sigma_i (x_i^2 - 1) dW(t) \end{aligned} \tag{B.7}$$

where $a_6 = \max\{a_0, 4a_5\}$. Therefore, if $t_1 \leq T$,

$$\int_0^{\tau_k \wedge t_1} dV(X_t) \leq \int_0^{\tau_k \wedge t_1} a_6(1 + V(X_t))dt + \int_0^{\tau_k \wedge t_1} \sum_{i=1}^{n} \sigma_i (x_i^2 - 1) dW(t) \tag{B.8}$$

This implies that:

$$\begin{aligned} E\left[V\left(X(\tau_k \wedge t_1)\right)\right] &\leq V(X_0) + E\left[\int_0^{\tau_k \wedge t_1} a_6(1 + V(X_t))dt\right] \\ &\leq V(X_0) + a_6 t_1 + a_6 E\left[\int_0^{\tau_k \wedge t_1} V(X_t)dt\right] \\ &\leq V(X_0) + a_6 T + a_6 E\left[\int_0^{t_1} V\left(X(\tau_k \wedge t)\right)dt\right] \\ &= V(X_0) + a_6 T + a_6 \int_0^{t_1} E\left[V\left(X(\tau_k \wedge t)\right)\right]dt \end{aligned} \tag{B.9}$$

Applying Gronwall's Inequality, we get:

$$E\left[V\left(X(\tau_k \wedge T)\right)\right] \leq \left(V(X_0) + a_6 T\right) e^{a_6 T} \equiv a_7 \tag{B.10}$$

Set $\Omega_k = \{\tau_k \leq T\}$ for $k \geq k_1$. By our assumption (B.3), we have $P(\Omega_k) > \varepsilon$. Note that for every $\omega \in \Omega_k$, there is at least one i for which $x_i(\tau_k, \omega)$ equals either k or $\frac{1}{k}$, and hence $V(X_{\tau_k})$ is no less than the smaller of $k^2 + 1 - \log k$ and $\frac{1}{k^2} + 1 - \log\frac{1}{k} = \frac{1}{k^2} + 1 + \log k$. Consequently, we have:

$$V(X_{\tau_k}) \geq \left(k^2+1-\log k\right) \wedge \left(\frac{1}{k^2}+1+\log k\right) \tag{B.11}$$

It follows that from B.3 and B.10:

$$a_7 \geq E\left[1_{\Omega_k}(\omega)V\left(X(\tau_k,\omega)\right)\right] \geq \varepsilon\left[\left(k^2+1-\log k\right) \wedge \left(\frac{1}{k^2}+1+\log k\right)\right] \tag{B.12}$$

where 1_{Ω_k} is the indicator function of Ω_k. Letting $k \to \infty$, we obtain the contradiction $\infty > a_7 = \infty$, and hence $\tau_\infty = \infty$ a.s. Thus, (5.2) has a unique global positive solution and never explodes in any finite time with probability 1.

B.2 Proof of Finite First and Second Moments of Eqn. 5.2

Our next goal is to prove that the distribution of all possible paths of Equation 5.2 has finite mean and variance, and is bounded by a universal constant for all time.
Consider the function $V(X_t,t) = e^t \sum_{i=1}^4 x_i(t)^2$. Applying Ito's Lemma to Equation 5.2 yields:

$$\begin{aligned} dV &= 2e^t\left[\frac{1}{2}+\sum_{i=1}^4\left(2+\frac{1}{2}\sigma_i x_i^2\right)+(e_{12}-c_{21}-2)x_1^2x_2^2\right. \\ &+ (e_{31}-c_{13}-2)x_1^2x_3^2+(e_{41}-c_{14}-2)x_1^2x_4^2+(e_{23}-c_{32}-2)x_2^2x_3^2 \\ &+ \left.(e_{24}-c_{42}-2)x_2^2x_4^2+(-c_{34}-c_{43}-2)x_3^2x_4^2-\sum_{i=1}^4 x_i^4\right]dt \\ &+ 2e^t\sum_{i=1}^4 \sigma_i x_i^2 dW_t \end{aligned} \tag{B.13}$$

Using the hypothesis, there exists a $K > 0$ such that:

$$dV \leq Ke^t dt + 2e^t \sum_{i=1}^{4} \sigma_i x_i^2 dW_t \tag{B.14}$$

Integrating and taking expectations gives:

$$\begin{aligned} E\left[e^{t\wedge\tau_k}\sum_{i=1}^{4} x_i(t\wedge\tau_k)^2\right] - \sum_{i=1}^{4} x_i(0)^2 &\leq E\left[\int_0^{t\wedge\tau_k} Ke^s ds\right] \\ &\leq E\left[\int_0^{t} Ke^s ds\right] \\ &= K\left(e^t - 1\right) \end{aligned} \tag{B.15}$$

The previous proof showed that $\lim_{k\to\infty}\tau_k = \infty$. Thus, taking $k \to \infty$ gives:

$$E\left[e^t \sum_{i=1}^{4} x_i(t)^2\right] - \sum_{i=1}^{4} x_i(0)^2 \leq K\left(e^t - 1\right) \tag{B.16}$$

This implies:

$$E\left[\sum_{i=1}^{4} x_i(t)^2\right] \leq e^{-t}\sum_{i=1}^{4} x_i(0)^2 + K\left(1 - e^{-t}\right) \leq K < \infty \tag{B.17}$$

Taking $sup_{t\geq 0}$ gives the desired result.

B.3 Proof of Stochastic Boundedness of Eqn. 5.2

We say the solution to Equation 5.2 is stochastically bounded if for any $\varepsilon > 0$, there is a constant $H \equiv H_\varepsilon$ such that for any $x_0 \in \mathbb{R}^4_+$, we have:

$$\limsup_{t\to\infty} P\left(|x(t)| \leq H\right) > 1 - \varepsilon \tag{B.18}$$

We prove that Equation 5.2 is stochastically bounded.

Note that $E\left[|x(t)|^2\right] \leq 4E\left[\sum_{i=1}^{4} x_i(t)^2\right] \leq K < \infty$. Using Chebyshev's Inequality, we have that for $H > 0$,

$$P\left(|x(t)| > H\right) \leq \frac{sup_{t\geq 0} E\left[|x(t)|^2\right]}{H^2} \leq \frac{K}{H^2} \tag{B.19}$$

By choosing H sufficiently large, the result follows.

Appendix C

Python Code

The following is the Python code used to study the synchronization of a small network of Fox and Lu neurons. The code was run in Python version 2.7.10 and produces a plot of the mean synchronization (and standard deviation) vs. time results.

```
import scipy as sp
import numpy as np
import pylab as plt
from scipy import linalg
import math
from math import factorial

NS=10 #Number of Simulations
NN=3 #Number of Neurons in Model

dt=0.01
T = sp.arange(0.0, 3000.0, dt)
nt = len(T)  # total number of time steps

# Constants
C  =   1.0 # membrane capacitance, in uF/cm^2
```

```
gNa = 120.0 # maximum conducances, in mS/cm^2
gK  =  36.0
gL  =   0.3
ENa =  50.0 # Nernst reversal potentials, in mV
EK  = -77
EL  = -54.387

area = 300 #Membrane Area
NK = 18*area
NNa = 60*area

#Coupling Terms
Vr = 20
w = 1
e12 = e23 = e31 = 0
e11 = e22 = e33 = 0
e21 = 0.1
e32 = 0.1
e13 = 0.1

E = np.array([[e11, e12, e13], [e21, e22, e23], [e31, e32, e33]])

def alpham(V): return (0.1*V+4.0)/(1.0 - sp.exp(-0.1*V-4.0))
def betam(V):  return 4.0*sp.exp(-(V+65.0) / 18.0)
def alphah(V): return 0.07*sp.exp(-(V+65.0) / 20.0)
def betah(V):  return 1.0/(1.0 + sp.exp(-0.1*V-3.5))
def alphan(V): return (0.01*V+0.55)/(1.0 - sp.exp(-0.1*V-5.5))
def betan(V):  return 0.125*sp.exp(-(V+65.0) / 80.0)
def psp(V,s): return ((5*(1-s))/(1+sp.exp(-(V+3)/8)))-s

def mysqrtm(D):
```

```
    S = []
    for d in D:
        u,s,v = linalg.svd(d)
        S.append(u*np.sqrt(s)*v)
    return np.array(S)

def ANa(V):
    P = np.zeros((NN,8,8))

    P[:,0,0] = -3*alpham(V)-alphah(V)
    P[:,0,1] = betam(V)
    P[:,0,4] = betah(V)

    P[:,1,0] = 3*alpham(V)
    P[:,1,1] = -2*alpham(V)-betam(V)-alphah(V)
    P[:,1,2] = 2*betam(V)
    P[:,1,5] = betah(V)

    P[:,2,1] = 2*alpham(V)
    P[:,2,2] = -alpham(V)-2*betam(V)-alphah(V)
    P[:,2,3] = 3*betam(V)
    P[:,2,6] = betah(V)

    P[:,3,2] = alpham(V)
    P[:,3,3] = -3*betam(V)-alphah(V)
    P[:,3,7] = betah(V)

    P[:,4,0] = alphah(V)
    P[:,4,4] = -3*alpham(V)-betah(V)
    P[:,4,5] = betam(V)
```

```
    P[:,5,1] = alphah(V)
    P[:,5,4] = 3*alpham(V)
    P[:,5,5] = -2*alpham(V)-betam(V)-betah(V)
    P[:,5,6] = 2*betam(V)

    P[:,6,2] = alphah(V)
    P[:,6,5] = 2*alpham(V)
    P[:,6,6] = -alpham(V)-2*betam(V)-betah(V)
    P[:,6,7] = 3*betam(V)

    P[:,7,3] = alphah(V)
    P[:,7,6] = alpham(V)
    P[:,7,7] = -3*betam(V)-betah(V)

    return P


def AK(V):
    P = np.zeros((NN,5,5))

    P[:,0,0] = -4*alphan(V)
    P[:,0,1] = betan(V)

    P[:,1,0] = 4*alphan(V)
    P[:,1,1] = -3*alphan(V)-betan(V)
    P[:,1,2] = 2*betan(V)

    P[:,2,1] = 3*alphan(V)
    P[:,2,2] = -2*alphan(V)-2*betan(V)
    P[:,2,3] = 3*betan(V)
```

```
    P[:,3,2] = 2*alphan(V)
    P[:,3,3] = -alphan(V)-3*betan(V)
    P[:,3,4] = 4*betan(V)

    P[:,4,3] = alphan(V)
    P[:,4,4] = -4*betan(V)

    return P

def DNa(V,Y,N):
        D = np.zeros((NN,8,8))
        y00 = Y[:,0]
        y10 = Y[:,1]
        y20 = Y[:,2]
        y30 = Y[:,3]
        y01 = Y[:,4]
        y11 = Y[:,5]
        y21 = Y[:,6]
        y31 = Y[:,7]

        D[:,0,0] = (3*alpham(V) + alphah(V))*y00 + betam(V)*y10 +
            betah(V)*y01
        D[:,0,1] = -3*alpham(V)*y00 - betam(V)*y10
        D[:,0,2] = 0
        D[:,0,3] = 0
        D[:,0,4] = -(alphah(V)*y00 + betah(V)*y01)
        D[:,0,5] = 0
        D[:,0,6] = 0
        D[:,0,7] = 0

        D[:,1,0] = D[:,0,1]
```

```
D[:,1,1] = (betam(V)+2*alpham(V))*y10 + 2*betam(V)*y20 + 3*
    alpham(V)*y00 + alpham(V)*y10 + betah(V)*y11
D[:,1,2] = -(2*alpham(V)*y10 + 2*betam(V)*y20)
D[:,1,3] = 0
D[:,1,4] = 0
D[:,1,5] = -(alphah(V)*y10 + betah(V)*y11)
D[:,1,6] = 0
D[:,1,7] = 0

D[:,2,0] = D[:,0,2]
D[:,2,1] = D[:,1,2]
D[:,2,2] = (2*betam(V) + alpham(V))*y20 + 3*betam(V)*y30 + 2*
    alpham(V)*y10 + alphah(V)*y20 + betah(V)*y21
D[:,2,3] = -(alpham(V)*y20+3*betam(V)*y30)
D[:,2,4] = 0
D[:,2,5] = 0
D[:,2,6] = -(alphah(V)*y20+betah(V)*y21)
D[:,2,7] = 0

D[:,3,0] = D[:,0,3]
D[:,3,1] = D[:,1,3]
D[:,3,2] = D[:,2,3]
D[:,3,3] = 3*betam(V)*y30 + alpham(V)*y20 + alphah(V)*y30 +
    betah(V)*y31
D[:,3,4] = 0
D[:,3,5] = 0
D[:,3,6] = 0
D[:,3,7] = -(alphah(V)*y30 + betah(V)*y31)

D[:,4,0] = D[:,0,4]
D[:,4,1] = D[:,1,4]
```

```
D[:,4,2] = D[:,2,4]
D[:,4,3] = D[:,3,4]
D[:,4,4] = 3*alpham(V)*y01 + betam(V)*y11 + betah(V)*y01 +
    alphah(V)*y00
D[:,4,5] = -(3*alpham(V)*y01 + betam(V)*y11)
D[:,4,6] = 0
D[:,4,7] = 0

D[:,5,0] = D[:,0,5]
D[:,5,1] = D[:,1,5]
D[:,5,2] = D[:,2,5]
D[:,5,3] = D[:,3,5]
D[:,5,4] = D[:,4,5]
D[:,5,5] = (betam(V) + 2*alpham(V))*y11 + 2*betam(V)*y21 + 3*
    alpham(V)*y01 + betah(V)*y11 + alphah(V)*y10
D[:,5,6] = -(2*alpham(V)*y11+2*betam(V)*y21)
D[:,5,7] = 0

D[:,6,0] = D[:,0,6]
D[:,6,1] = D[:,1,6]
D[:,6,2] = D[:,2,6]
D[:,6,3] = D[:,3,6]
D[:,6,4] = D[:,4,6]
D[:,6,5] = D[:,5,6]
D[:,6,6] = (2*betam(V) + alpham(V))*y21 + 3*betam(V)*y31 + 2*
    alpham(V)*y11 + betah(V)*y21 + alphah(V)*y20
D[:,6,7] = -(alpham(V)*y21+3*betam(V)*y31)

D[:,7,0] = D[:,0,7]
D[:,7,1] = D[:,1,7]
D[:,7,2] = D[:,2,7]
```

```
        D[:,7,3] = D[:,3,7]
        D[:,7,4] = D[:,4,7]
        D[:,7,5] = D[:,5,7]
        D[:,7,6] = D[:,6,7]
        D[:,7,7] = 3*betam(V)*y31 + alpham(V)*y21 + betah(V)*y31 +
            alphah(V)*y30

        D = D/(N);
        return D

def DK(V,X,N):

    D = np.zeros((NN,5,5))

    D[:,0,0] = 4*alphan(V)*X[:,0] + betan(V)*X[:,1]
    D[:,0,1] = -(4*alphan(V)*X[:,0] + betan(V)*X[:,1])

    D[:,1,0] = -(4*alphan(V)*X[:,0]+betan(V)*X[:,1])
    D[:,1,1] = (4*alphan(V)*X[:,1]+(3*alphan(V)+ betan(V))*X[:,1] +
        2*betan(V)*X[:,2])
    D[:,1,2] = -(2*betan(V)*X[:,2] + 3*alphan(V)*X[:,1])

    D[:,2,1] = -(2*betan(V)*X[:,2]+3*alphan(V)*X[:,1])
    D[:,2,2] = (3*alphan(V)*X[:,1] + (2*alphan(V) + 2*betan(V))*X
        [:,2] + 3*betan(V)*X[:,3])
    D[:,2,3] = -(3*betan(V)*X[:,3]+2*alphan(V)*X[:,2])

    D[:,3,2] = -(3*betan(V)*X[:,3]+2*alphan(V)*X[:,2])
    D[:,3,3] = (2*alphan(V)*X[:,2] + (alphan(V)+ 3*betan(V))*X[:,3] +
         4*betan(V)*X[:,4])
    D[:,3,4] = -(4*betan(V)*X[:,4]+alphan(V)*X[:,3])
```

```
    D[:,4,3] = -(4*betan(V)*X[:,4]+alphan(V)*X[:,3])
    D[:,4,4] = (alphan(V)*X[:,3]+4*betan(V)*X[:,4])

    M = 1/N * D

    return M

# Take Matrix square roots numerically using SVD
def SNa(V,Y,NNa): return mysqrtm(DNa(V,Y,NNa))
def SK(V,X,N): return mysqrtm(DK(V,X,NK))

#  Potassium (K = element name)
def I_KSDE(V,x): return gK  * x[:,4] * (V - EK)

# Sodium Current
def I_NaSDE(V,y): return gNa * y[:,7] * (V - ENa)

#  Leak Current
def I_L(V): return gL * (V - EL)

# External current
def I_inj(t):
    return 10.0

#Define Factorial Function
def nCr(n,r):
    if r<=n:
        numerator=factorial(n)
        denominator=(factorial(r)*factorial(n-r))
        answer=numerator/denominator
```

```
        return answer
    if r>n:
        return 0

#Equilibrium Equations
def x0bar(V): return nCr(4,0)*((alphan(V)**0)*(betan(V)**(4-0)))/((
    alphan(V)+betan(V))**4)
def x1bar(V): return nCr(4,1)*((alphan(V)**1)*(betan(V)**(4-1)))/((
    alphan(V)+betan(V))**4)
def x2bar(V): return nCr(4,2)*((alphan(V)**2)*(betan(V)**(4-2)))/((
    alphan(V)+betan(V))**4)
def x3bar(V): return nCr(4,3)*((alphan(V)**3)*(betan(V)**(4-3)))/((
    alphan(V)+betan(V))**4)
def x4bar(V): return nCr(4,4)*((alphan(V)**4)*(betan(V)**(4-4)))/((
    alphan(V)+betan(V))**4)

def y00bar(V): return (nCr(3,0)*(alpham(V)**0 * betam(V)**(3-0))*(
    alphah(V)**0 * betah(V)**(1-0)))/((alpham(V)+betam(V))**3 *(alphah
    (V)+betah(V)))
def y10bar(V): return (nCr(3,1)*(alpham(V)**1 * betam(V)**(3-1))*(
    alphah(V)**0 * betah(V)**(1-0)))/((alpham(V)+betam(V))**3 *(alphah
    (V)+betah(V)))
def y20bar(V): return (nCr(3,2)*(alpham(V)**2 * betam(V)**(3-2))*(
    alphah(V)**0 * betah(V)**(1-0)))/((alpham(V)+betam(V))**3 *(alphah
    (V)+betah(V)))
def y30bar(V): return (nCr(3,3)*(alpham(V)**3 * betam(V)**(3-3))*(
    alphah(V)**0 * betah(V)**(1-0)))/((alpham(V)+betam(V))**3 *(alphah
    (V)+betah(V)))
def y01bar(V): return (nCr(3,0)*(alpham(V)**0 * betam(V)**(3-0))*(
    alphah(V)**1 * betah(V)**(1-1)))/((alpham(V)+betam(V))**3 *(alphah
    (V)+betah(V)))
```

```
def y11bar(V): return (nCr(3,1)*(alpham(V)**1 * betam(V)**(3-1))*(
    alphah(V)**1 * betah(V)**(1-1)))/((alpham(V)+betam(V))**3 *(alphah
    (V)+betah(V)))
def y21bar(V): return (nCr(3,2)*(alpham(V)**2 * betam(V)**(3-2))*(
    alphah(V)**1 * betah(V)**(1-1)))/((alpham(V)+betam(V))**3 *(alphah
    (V)+betah(V)))
def y31bar(V): return (nCr(3,3)*(alpham(V)**3 * betam(V)**(3-3))*(
    alphah(V)**1 * betah(V)**(1-1)))/((alpham(V)+betam(V))**3 *(alphah
    (V)+betah(V)))

#Create Initial Conditions
V = np.zeros((nt,NN))
X = np.zeros((nt,NN,5))
Y = np.zeros((nt,NN,8))
S = np.zeros((nt,NN))

V[0,:] = -65.0

X[0,:,1] = x1bar(V[0,:]) #x1
X[0,:,2] = x2bar(V[0,:]) #x2
X[0,:,3] = x3bar(V[0,:]) #x3
X[0,:,4] = x4bar(V[0,:]) #x4
X[0,:,0] = 1-X[0,:,1:].sum()

Y[0,:,1] = y10bar(V[0,:]) #y1
Y[0,:,2] = y20bar(V[0,:]) #y2
Y[0,:,3] = y30bar(V[0,:]) #y3
Y[0,:,4] = y01bar(V[0,:]) #y4
Y[0,:,5] = y11bar(V[0,:]) #y5
Y[0,:,6] = y21bar(V[0,:]) #y6
Y[0,:,7] = y31bar(V[0,:]) #y7
```

```
Y[0,:,0] = 1-Y[0,:,1:].sum()

alef = 5.0/(1+sp.exp(-(V[0,:]+3)/8.0))
S[0,:] = alef/(alef+1)

R = np.zeros((NS,len(T)))

#Euler-Maruyama method
for a in xrange(NS):
    print a
    for i in xrange(1,nt):
        X[i-1,:,0] = 1-X[i-1,:,1:].sum(axis=1)
        Y[i-1,:,0] = 1-Y[i-1,:,1:].sum(axis=1)
        V[i,:]= V[i-1,:] + dt*(I_inj(i-1)-I_NaSDE(V[i-1,:],Y[i-1,:])
            - I_KSDE(V[i-1,:],X[i-1,:]) - I_L(V[i-1,:])) + dt*((Vr-V[i
            -1,:])/w * np.dot(E,S[i-1,:]))

        #Potassium Channels
        ak = AK(V[i-1])
        z = np.array([np.dot(ak[l], X[i-1][l]) for l in xrange(NN)])
        sk = SK(V[i-1],X[i-1],NK)
        s = np.array([np.dot(sk[l], np.random.normal(0,1,size=5)) for
            l in xrange(NN)])
        X[i,:,:]= X[i-1,:]+dt*(z)+np.sqrt(dt)*s
        X[i,:,0] = 1-X[i,:,1:].sum(axis=1)

        #Sodium Channels
        ana = ANa(V[i-1])
        p = np.array([np.dot(ana[l],Y[i-1][l]) for l in xrange(NN)])
        sna = SNa(V[i-1],Y[i-1],NNa)
        q = np.array([np.dot(sna[l], np.random.normal(0,1,size=8))
```

```
        for l in xrange(NN)])
    Y[i,:,:]= Y[i-1,:,:]+dt*(p)+np.sqrt(dt)*q
    Y[i,:,0] = 1-Y[i,:,1:].sum(axis=1)

    #Coupling Term
    S[i,:] = S[i-1,:]+dt*psp(V[i-i,:],S[i-1,:])

V1 = V[:,0]
V2 = V[:,1]
V3 = V[:,2]

def spikeDetect(V, t, spike_thresh):
    '''
    Spike time given membrane potential
    '''
    spkt = t[sp.logical_and(V[:-1] < spike_thresh, V[1:] >=
        spike_thresh)]
    return spkt

spkt1 = spikeDetect(V1,T,0) #Detect times of spikes occuring of
    the $1^{st}$ neuron
spkt2 = spikeDetect(V2,T,0)
spkt3 = spikeDetect(V3,T,0)

spktN = [spkt1, spkt2, spkt3]

#Calculate Synchronicity Function
def phi(spkt, t):
    bx = spkt<t #Create vector of True/False
    m = np.sum(bx) #Count the number of True Elements
    try:
```

```
                p= 2*np.pi*(m-1)+2*np.pi*((t-spkt[m-1])/(spkt[m]-spkt
                    [m-1]))
        except:
                return 0
        return p

    def sync(t):
        r = 0
        for i in xrange(NN):
                r = r + np.exp(1j*phi(spktN[i],t))
        r = abs((1.0/NN)*r)
        return r

    for i,t in enumerate(T):
        R[a,i] = sync(t)

R_avg = R.mean(axis=0)
R_var = R.var(axis=0)
err = np.sqrt(R_var)/np.sqrt(NS)

plt.plot(T, R_avg, 'purple', label='Mean $R(t)$')
plt.fill_between(T, R_avg-err,R_avg+err,alpha=0.5,facecolor='#C165FA'
    )
plt.show()
```

Bibliography

[ABMV93] M Abeles, H Bergman, E Margalit, and E Vaadia. Spatiotemporal firing patterns in the frontal cortex of behaving monkeys. *Journal of neurophysiology*, 70(4):1629–1638, 1993.

[ABV+05] Juan A Acebrón, Luis L Bonilla, Conrad J Pérez Vicente, Félix Ritort, and Renato Spigler. The kuramoto model: A simple paradigm for synchronization phenomena. *Reviews of modern physics*, 77(1):137, 2005.

[ACM14] Kamal Abuhassan, Damien Coyle, and Liam Maguire. Compensating for thalamocortical synaptic loss in Alzheimer's disease. *Frontiers in Computational Neuroscience*, 8, 2014.

[Ada03] Robert K Adair. Noise and stochastic resonance in voltage-gated ion channels. *Proceedings of the National Academy of Sciences*, 100(21):12099–12104, 2003.

[AKR08] Adrian Ponce Alvarez, Bjorg Kilavik, and Alexa Riehle. Dynamic sequences of states in ensembles of motor cortical neurons. In *Deuxième conférence française de Neurosciences Computationnelles," Neurocomp08"*, 2008.

[AM14] Evan G Antzoulatos and Earl K Miller. Increases in functional connectivity between prefrontal cortex and striatum during category learning. *Neuron*, 83(1):216–225, 2014.

[ANGSRD08] L Alonso-Nanclares, J Gonzalez-Soriano, JR Rodriguez, and J DeFelipe. Gender differences in human cortical synaptic density. *Proceedings of the National Academy of Sciences*, 105(38):14615–14619, 2008.

[APBV94] M Abeles, Y Prut, H Bergman, and E Vaadia. Synchronization in neuronal transmission and its importance for information processing. In *Temporal coding in the brain*, pages 39–50. Springer, 1994.

[APD06] Ehsan Arabzadeh, Stefano Panzeri, and Mathew E Diamond. Deciphering the spike train of a sensory neuron: counts and temporal patterns in the rat whisker pathway. *The Journal of Neuroscience*, 26(36):9216–9226, 2006.

[AS94] Christina Allen and Charles F Stevens. An evaluation of causes for unreliability of synaptic transmission. *Proceedings of the National Academy of Sciences*, 91(22):10380–10383, 1994.

[ASK03] Dieter Armbruster, Emily Stone, and Vivien Kirk. Noisy heteroclinic networks. *Chaos: An Interdisciplinary Journal of Nonlinear Science*, 13(1):71–79, 2003.

[AZR04] VS Afraimovich, VP Zhigulin, and MI Rabinovich. On the origin of reproducible sequential activity in neural circuits. *Chaos: An Interdisciplinary Journal of Nonlinear Science*, 14(4):1123–1129, 2004.

[BBL+16] RR Borges, FS Borges, EL Lameu, AM Batista, KC Iarosz, IL Caldas, RL Viana, and MAF Sanjuán. Effects of the spike timing-dependent plasticity on the synchronisation in a random hodgkin–huxley neuronal network. *Communications in Nonlinear Science and Numerical Simulation*, 34:12–22, 2016.

[BDB+06] Cyrus P Billimoria, Ralph A DiCaprio, John T Birmingham, LF Abbott, and Eve Marder. Neuromodulation of spike-timing precision in sensory neurons. *The Journal of neuroscience*, 26(22):5910–5919, 2006.

[BG05] Romain Brette and Wulfram Gerstner. Adaptive exponential integrate-and-fire model as an effective description of neuronal activity. *Journal of neurophysiology*, 94(5):3637–3642, 2005.

[BGB09] Brett L Benedetti, Stanislaw Glazewski, and Alison L Barth. Reliable and precise neuronal firing during sensory plasticity in superficial layers of primary somatosensory cortex. *The Journal of neuroscience*, 29(38):11817–11827, 2009.

[BGP00] Pietro-Luciano Buono, Martin Golubitsky, and Antonio Palacios. Heteroclinic cycles in rings of coupled cells. *Physica D: Nonlinear Phenomena*, 143(1):74–108, 2000.

[BKH+03] EH Baeg, YB Kim, K Huh, I Mook-Jung, HT Kim, and MW Jung. Dynamics of population code for working memory in the prefrontal cortex. *Neuron*, 40(1):177–188, 2003.

[BP98] Guo-qiang Bi and Mu-ming Poo. Synaptic modifications in cultured hippocampal neurons: dependence on spike timing, synaptic strength,

and postsynaptic cell type. *The Journal of Neuroscience*, 18(24):10464–10472, 1998.

[BR09] Christian Bick and Mikhail I Rabinovich. Dynamical origin of the effective storage capacity in the brains working memory. *Physical review letters*, 103(21):218101, 2009.

[Bru09] Ian C Bruce. Evaluation of stochastic differential equation approximation of ion channel gating models. *Annals of biomedical engineering*, 37(4):824–838, 2009.

[BRVSW91] William Bialek, Fred Rieke, RR de Ruyter Van Steveninck, and David Warland. Reading a neural code. *Science*, 252(5014):1854–1857, 1991.

[BS09] Tiago Branco and Kevin Staras. The probability of neurotransmitter release: variability and feedback control at single synapses. *Nature Reviews Neuroscience*, 10(5):373–383, 2009.

[BS13] Valentino Braitenberg and Almut Schüz. *Anatomy of the cortex: statistics and geometry*, volume 18. Springer Science & Business Media, 2013.

[BSRSR15] Alex Bukoski, DA Steyn-Ross, and Moira L Steyn-Ross. Channel-noise-induced critical slowing in the subthreshold hodgkin-huxley neuron. *Physical Review E*, 91(3):032708, 2015.

[Buz06] Gyorgy Buzsaki. *Rhythms of the Brain*. Oxford University Press, 2006.

[BWF+08] Nadine Becker, Corette J Wierenga, Rosalina Fonseca, Tobias Bonhoeffer, and U Valentin Nägerl. Ltd induction causes morphological changes of presynaptic boutons and reduces their contacts with spines. *Neuron*, 60(4):590–597, 2008.

[Cas03] José Manuel Casado. Synchronization of two hodgkin–huxley neurons due to internal noise. *Physics Letters A*, 310(5):400–406, 2003.

[CD83] John R Clay and LOUIS J DeFelice. Relationship between membrane excitability and single channel open-close kinetics. *Biophysical journal*, 42(2):151–157, 1983.

[CON10] Robert C Cannon, Cian O'Donnell, and Matthew F Nolan. Stochastic ion channel gating in dendritic neurons: morphology dependence and probabilistic synaptic activation of dendritic spikes. *PLoS computational biology*, 6(8):e1000886, 2010.

[CW96] Carson C Chow and John A White. Spontaneous action potentials due to channel fluctuations. *Biophysical journal*, 71(6):3013–3021, 1996.

[DA+03] Peter Dayan, LF Abbott, et al. Theoretical neuroscience: computational and mathematical modeling of neural systems. *Journal of Cognitive Neuroscience*, 15(1):154–155, 2003.

[DMS94] Alain Destexhe, Zachary F Mainen, and Terrence J Sejnowski. An efficient method for computing synaptic conductances based on a kinetic model of receptor binding. *Neural computation*, 6(1):14–18, 1994.

[DMS98] Alain Destexhe, Zachary F Mainen, and Terrence J Sejnowski. Kinetic models of synaptic transmission. *Methods in neuronal modeling*, 2:1–25, 1998.

[DvHK+08] Mathew E Diamond, Moritz von Heimendahl, Per Magne Knutsen, David Kleinfeld, and Ehud Ahissar. 'where'and'what'in the whisker sensorimotor system. *Nature Reviews Neuroscience*, 9(8):601–612, 2008.

[DW05] Alan D Dorval and John A White. Channel noise is essential for perithreshold oscillations in entorhinal stellate neurons. *Journal of Neuroscience*, 25(43):10025–10028, 2005.

[ECFW15] Tatiana A Engel, Warasinee Chaisangmongkon, David J Freedman, and Xiao-Jing Wang. Choice-correlated activity fluctuations underlie learning of neuronal category representation. *Nature Communications*, 6, 2015.

[FA11] Juergen Fell and Nikolai Axmacher. The role of phase synchronization in memory processes. *Nature reviews neuroscience*, 12(2):105–118, 2011.

[FK52] P Fatt and B Katz. Spontaneous subthreshold activity at motor nerve endings. *The Journal of physiology*, 117(1):109–128, 1952.

[FL94] Ronald F Fox and Yan-nan Lu. Emergent collective behavior in large numbers of globally coupled independently stochastic ion channels. *Physical Review E*, 49(4):3421, 1994.

[FL07] A Aldo Faisal and Simon B Laughlin. Stochastic simulations on the reliability of action potential propagation in thin axons. *PLoS computational biology*, 3(5):e79, 2007.

[FM85] Hugo Gil Ferreira and Michael W Marshall. *The biophysical basis of excitability*. Cambridge University Press, 1985.

[Fri97] Karl J Friston. Transients, metastability, and neuronal dynamics. *Neuroimage*, 5(2):164–171, 1997.

[Fri05] Pascal Fries. A mechanism for cognitive dynamics: neuronal communication through neuronal coherence. *Trends in cognitive sciences*, 9(10):474–480, 2005.

[FVPB08] Christian Finke, Jürgen Vollmer, Svetlana Postnova, and Hans Albert Braun. Propagation effects of current and conductance noise in a model neuron with subthreshold oscillations. *Mathematical biosciences*, 214(1):109–121, 2008.

[FWL05] A Aldo Faisal, John A White, and Simon B Laughlin. Ion-channel noise places limits on the miniaturization of the brains wiring. *Current Biology*, 15(12):1143–1149, 2005.

[Gar88] Thomas C Gard. *Introduction to stochastic differential equations*. M. Dekker, 1988.

[GGMK09] Carl Gold, Cyrille C Girardin, Kevan AC Martin, and Christof Koch. High-amplitude positive spikes recorded extracellularly in cat visual cortex. *Journal of neurophysiology*, 102(6):3340–3351, 2009.

[GIFSB11] Joshua H Goldwyn, Nikita S Imennov, Michael Famulare, and Eric Shea-Brown. Stochastic differential equation models for ion channel noise in hodgkin-huxley neurons. *Physical Review E*, 83(4):041908, 2011.

[Gil77] Daniel T Gillespie. Exact stochastic simulation of coupled chemical reactions. *The journal of physical chemistry*, 81(25):2340–2361, 1977.

[GKES89] Charles M Gray, Peter König, Andreas K Engel, and Wolf Singer. Oscillatory responses in cat visual cortex exhibit inter-columnar synchronization which reflects global stimulus properties. *Nature*, 338(6213):334–337, 1989.

[GKNP14] Wulfram Gerstner, Werner M Kistler, Richard Naud, and Liam Paninski. *Neuronal dynamics: From single neurons to networks and models of cognition*. Cambridge University Press, 2014.

[GMdL10] Aryn H Gittis, Setareh H Moghadam, and Sascha du Lac. Mechanisms of sustained high firing rates in two classes of vestibular nucleus neurons: differential contributions of resurgent na, kv3, and bk currents. *Journal of neurophysiology*, 104(3):1625–1634, 2010.

[Gol99] Ian Gold. Does 40-hz oscillation play a role in visual consciousness? *Consciousness and cognition*, 8(2):186–195, 1999.

[GR93] David Golomb and John Rinzel. Dynamics of globally coupled inhibitory neurons with heterogeneity. *Physical review E*, 48(6):4810, 1993.

[GRSB12] Joshua H Goldwyn, Jay T Rubinstein, and Eric Shea-Brown. A point process framework for modeling electrical stimulation of the auditory nerve. *Journal of neurophysiology*, 108(5):1430–1452, 2012.

[GSB11] Joshua H Goldwyn and Eric Shea-Brown. The what and where of adding channel noise to the hodgkin-huxley equations. *PLoS Comput Biol*, 7(11):e1002247, 2011.

[H$^+$01] Bertil Hille et al. *Ion channels of excitable membranes*, volume 507. Sinauer Sunderland, MA, 2001.

[HBB07] Constance Hammond, Hagai Bergman, and Peter Brown. Pathological synchronization in Parkinson's disease: networks, models and treatments. *Trends in Neurosciences*, 30(7):357–364, 2007.

[Hei04] Peter Heil. First-spike latency of auditory neurons revisited. *Current opinion in neurobiology*, 14(4):461–467, 2004.

[HFM$^+$04] Sheriar G Hormuzdi, Mikhail A Filippov, Georgia Mitropoulou, Hannah Monyer, and Roberto Bruzzone. Electrical synapses: a dynamic signaling system that shapes the activity of neuronal networks. *Biochimica et Biophysica Acta (BBA)-Biomembranes*, 1662(1):113–137, 2004.

[HH52] Alan L Hodgkin and Andrew F Huxley. A quantitative description of membrane current and its application to conduction and excitation in nerve. *The Journal of physiology*, 117(4):500, 1952.

[Hig01] Desmond J Higham. An algorithmic introduction to numerical simulation of stochastic differential equations. *SIAM review*, 43(3):525–546, 2001.

[Hir82] Morris W Hirsch. Systems of differential equations which are competitive or cooperative: I. limit sets. *SIAM Journal on Mathematical Analysis*, 13(2):167–179, 1982.

[Hir85] Morris W Hirsch. Systems of differential equations that are competitive or cooperative ii: Convergence almost everywhere. *SIAM Journal on Mathematical Analysis*, 16(3):423–439, 1985.

[Hir88] Morris W Hirsch. Systems of differential equations which are competitive or cooperative: Iii. competing species. *Nonlinearity*, 1(1):51, 1988.

[HL98] Neil R Hardingham and Alan U Larkman. The reliability of excitatory synaptic transmission in slices of rat visual cortex in vitro is temperature dependent. *The Journal of Physiology*, 507(1):249–256, 1998.

[HSM93] Neal A Hessler, Aneil M Shirke, and Roberto Malinow. The probability of transmitter release at a mammalian central synapse. 1993.

[IR09] Nikita S Imennov and Jay T Rubinstein. Stochastic population model for electrical stimulation of the auditory nerve. *IEEE Transactions on Biomedical Engineering*, 56(10):2493–2501, 2009.

[Izh03] Eugene M Izhikevich. Simple model of spiking neurons. *IEEE Transactions on neural networks*, 14(6):1569–1572, 2003.

[Izh04] Eugene M Izhikevich. Which model to use for cortical spiking neurons? *IEEE transactions on neural networks*, 15(5):1063–1070, 2004.

[JA94] Staffan Johansson and Peter Arhem. Single-channel currents trigger action potentials in small cultured hippocampal neurons. *Proceedings of the National Academy of Sciences*, 91(5):1761–1765, 1994.

[JB04] Roland S Johansson and Ingvars Birznieks. First spikes in ensembles of human tactile afferents code complex spatial fingertip events. *Nature neuroscience*, 7(2):170–177, 2004.

[JdCJ+13] Premysl Jiruska, Marco de Curtis, John GR Jefferys, Catherine A Schevon, Steven J Schiff, and Kaspar Schindler. Synchronization and desynchronization in epilepsy: controversies and hypotheses. *The Journal of physiology*, 591(4):787–797, 2013.

[JFS+07] Lauren M Jones, Alfredo Fontanini, Brian F Sadacca, Paul Miller, and Donald B Katz. Natural stimuli evoke dynamic sequences of states in sensory cortical ensembles. *Proceedings of the National Academy of Sciences*, 104(47):18772–18777, 2007.

[JKCK05] Junghyo Jo, Hyuk Kang, Moo Young Choi, and Duk-Su Koh. How noise and coupling induce bursting action potentials in pancreatic β-cells. *Biophysical journal*, 89(3):1534–1542, 2005.

[JMPR71] JJB Jack, S Miller, R Porter, and SJ Redman. The time course of minimal excitatory post-synaptic potentials evoked in spinal motoneurones by group la afferent fibres. *The Journal of physiology*, 215(2):353–380, 1971.

[KCBF99] WAA Kunze, N Clerc, PP Bertrand, and JB Furness. Contractile activity in intestinal muscle evokes action potential discharge in guinea-pig myenteric neurons. *The Journal of Physiology*, 517(2):547–561, 1999.

[KHZ16] Qi Kang, BingYao Huang, and MengChu Zhou. Dynamic behavior of artificial hodgkin–huxley neuron model subject to additive noise. *IEEE transactions on cybernetics*, 46(9):2083–2093, 2016.

[Koc04] Christof Koch. *Biophysics of computation: information processing in single neurons*. Oxford university press, 2004.

[Kru97] Martin Krupa. Robust heteroclinic cycles. *Journal of Nonlinear Science*, 7(2):129–176, 1997.

[KS94] Vivien Kirk and Mary Silber. A competition between heteroclinic cycles. *Nonlinearity*, 7(6):1605, 1994.

[KS98] Christof Koch and Idan Segev. *Methods in neuronal modeling: from ions to networks*. MIT press, 1998.

[KZ02] Werner M Kistler and Chris I De Zeeuw. Dynamical working memory and timed responses: the role of reverberating loops in the olivocerebellar system. *Neural computation*, 14(11):2597–2626, 2002.

[LBB+12] EL Lameu, CAS Batista, AM Batista, K Iarosz, RL Viana, SR Lopes, and J Kurths. Suppression of bursting synchronization in clustered scale-free (rich-club) neuronal networks. *Chaos: An Interdisciplinary Journal of Nonlinear Science*, 22(4):043149, 2012.

[LBZ+00] Harvey Lodish, Arnold Berk, S Lawrence Zipursky, Paul Matsudaira, David Baltimore, and James Darnell. Molecular cell biology 4th edition. *National Center for Biotechnology InformationÕs Bookshelf*, 2000.

[LD+94] Gilles Laurent, Hananel Davidowitz, et al. Encoding of olfactory information with oscillating neural assemblies. *SCIENCE-NEW YORK THEN WASHINGTON-*, pages 1872–1872, 1994.

[LKT06] Stefano Luccioli, Thomas Kreuz, and Alessandro Torcini. Dynamical response of the hodgkin-huxley model in the high-input regime. *Physical Review E*, 73(4):041902, 2006.

[LM11] Chen-Chung Lee and John C Middlebrooks. Auditory cortex spatial sensitivity sharpens during task performance. *Nature neuroscience*, 14(1):108–114, 2011.

[LSF+01] Gilles Laurent, Mark Stopfer, Rainer W Friedrich, Misha I Rabinovich, Alexander Volkovskii, and Henry DI Abarbanel. Odor encoding as an active, dynamical process: experiments, computation, and theory. *Annual review of neuroscience*, 24(1):263–297, 2001.

[Lud73] Arnold Ludwing. Stochastic differential equations: Theory and applications, 1973.

[MB12] PS Mandal and M Banerjee. Multiplicative-noise can suppress chaotic oscillation in lotka-volterra type competitive model. *Mathematical Modelling of Natural Phenomena*, 7(06):23–46, 2012.

[ME96] Robert P Morse and Edward F Evans. Enhancement of vowel coding for cochlear implants by addition of noise. *Nature medicine*, 2(8):928–932, 1996.

[Mel91] Ian Melbourne. An example of a nonasymptotically stable attractor. *Nonlinearity*, 4(3):835, 1991.

[MG01] Frank Moss and Stan Gielen. *Neuro-informatics and neural modelling*, volume 4. Gulf Professional Publishing, 2001.

[MG11] Orjan G Martinsen and Sverre Grimnes. *Bioimpedance and bioelectricity basics*. Academic press, 2011.

[MK99a] Amit Manwani and Christof Koch. Detecting and estimating signals in noisy cable structures, i: Neuronal noise sources. *Neural computation*, 11(8):1797–1829, 1999.

[MK99b] Amit Manwani and Christof Koch. Detecting and estimating signals in noisy cable structures, ii: information theoretical analysis. *Neural Computation*, 11(8):1831–1873, 1999.

[MRMA04] Hiroyuki Mino, Jay T Rubinstein, Charles A Miller, and Paul J Abbas. Effects of electrode-to-fiber distance on temporal neural response with electrical stimulation. *IEEE transactions on biomedical engineering*, 51(1):13–20, 2004.

[MRW02] Hiroyuki Mino, Jay T Rubinstein, and John A White. Comparison of algorithms for the simulation of action potentials with stochastic sodium channels. *Annals of biomedical engineering*, 30(4):578–587, 2002.

[MT96] Henry Markram and Misha Tsodyks. Redistribution of synaptic efficacy between neocortical pyramidal neurons. 1996.

[NPR+99] Alexander Neiman, Xing Pei, David Russell, Winfried Wojtenek, Lon Wilkens, Frank Moss, HA Braun, MT Huber, and K Voigt. Synchronization of the noisy electrosensitive cells in the paddlefish. *Physical Review Letters*, 82(3):660, 1999.

[OE05] Mahmut Ozer and N Hakan Ekmekci. Effect of channel noise on the time-course of recovery from inactivation of sodium channels. *Physics Letters A*, 338(2):150–154, 2005.

[ON14] Cian ODonnell and Matthew F Nolan. Stochastic ion channel gating and probabilistic computation in dendritic neurons. In *The Computing Dendrite*, pages 397–414. Springer, 2014.

[Ope14] CNX OpenStax. Anatomy & physiology. *Human Anatomy & Physiology*, 2014.

[OR87] Lance M Optican and Barry J Richmond. Temporal encoding of two-dimensional patterns by single units in primate inferior temporal cortex. iii. information theoretic analysis. *Journal of Neurophysiology*, 57(1):162–178, 1987.

[OS12] Patricio Orio and Daniel Soudry. Simple, fast and accurate implementation of the diffusion approximation algorithm for stochastic ion channels with multiple states. *PloS one*, 7(5):e36670, 2012.

[OUPG09] Mahmut Ozer, Muhammet Uzuntarla, Matjaž Perc, and Lyle J Graham. Spike latency and jitter of neuronal membrane patches with stochastic hodgkin–huxley channels. *Journal of theoretical biology*, 261(1):83–92, 2009.

[PAF+97] Dale Ed Purves, George J Augustine, David Ed Fitzpatrick, Lawrence C Katz, et al. *Neuroscience.* Sunderland, MA, US: Sinauer Associates, 1997.

[Pal03] Antonio Palacios. Heteroclinic cycles in coupled systems of difference equations. *The Journal of Difference Equations and Applications*, 9(7):671–686, 2003.

[PILK12] Antonio Palacios, Visarath In, Patrick Longhini, and Andy Kho. Symmetry induced heteroclinic cycles in coupled sensor devices. Technical report, SPACE AND NAVAL WARFARE SYSTEMS CENTER PACIFIC SAN DIEGO CA, 2012.

[PPD01] Rasmus S Petersen, Stefano Panzeri, and Mathew E Diamond. Population coding of stimulus location in rat somatosensory cortex. *Neuron*, 32(3):503–514, 2001.

[PYT13] Oleksandr V Popovych, Serhiy Yanchuk, and Peter A Tass. Self-organized noise resistance of oscillatory neural networks with spike timing-dependent plasticity. *Scientific reports*, 3:2926, 2013.

[RES+97] Pieter R Roelfsema, Andreas K Engel, Wolf Singer, et al. Visuomotor integration is associated with zero time-lag synchronization among cortical areas. *Nature*, 385(6612):157, 1997.

[RF98] Jens C Rekling and Jack L Feldman. Prebötzinger complex and pacemaker neurons: hypothesized site and kernel for respiratory rhythm generation. *Annual review of physiology*, 60(1):385–405, 1998.

[RHL08] Misha Rabinovich, Ramon Huerta, and Gilles Laurent. Neuroscience. transient dynamics for neural processing. *Science (New York, NY)*, 321(5885):48–50, 2008.

[RHVA08] Mikhail I Rabinovich, Ramón Huerta, Pablo Varona, and Valentin S Afraimovich. Transient cognitive dynamics, metastability, and decision making. *PLoS computational biology*, 4(5):e1000072, 2008.

[RKS03] Pieter R Roelfsema, Paul S Khayat, and Henk Spekreijse. Subtask sequencing in the primary visual cortex. *Proceedings of the National Academy of Sciences*, 100(9):5467–5472, 2003.

[RMSB10] Mikhail I Rabinovich, Mehmet K Muezzinoglu, Irina Strigo, and Alexander Bystritsky. Dynamical principles of emotion-cognition interaction: mathematical images of mental disorders. *PloS one*, 5(9):e12547, 2010.

[Row07] Peter Rowat. Interspike interval statistics in the stochastic hodgkin-huxley model: Coexistence of gamma frequency bursts and highly irregular firing. *Neural Computation*, 19(5):1215–1250, 2007.

[RS99] Alex Reyes and Bert Sakmann. Developmental switch in the short-term modification of unitary epsps evoked in layer 2/3 and layer 5 pyramidal neurons of rat neocortex. *The Journal of neuroscience*, 19(10):3827–3835, 1999.

[RT95] Edmund T Rolls and Martin J Tovee. Sparseness of the neuronal representation of stimuli in the primate temporal visual cortex. *Journal of Neurophysiology*, 73(2):713–726, 1995.

[RTV13] Mikhail Rabinovich, Irma Tristan, and Pablo Varona. Neural dynamics of attentional cross-modality control. *PloS one*, 8(5):e64406, 2013.

[RVTA14] Mikhail I Rabinovich, Pablo Varona, Irma Tristan, and Valentin S Afraimovich. Chunking dynamics: heteroclinics in mind. *Frontiers in computational neuroscience*, 8, 2014.

[RWDRvSB99] F Rieke, D Warland, R De Ruyter van Steveninck, and W Bialek. Exploring the neural code, 1999.

[S+02] Ross Sheldon et al. *A first course in probability*. Pearson Education India, 2002.

[SD93] Adam F Strassberg and Louis J DeFelice. Limitations of the hodgkin-huxley formalism: effects of single channel kinetics on transmembrane voltage dynamics. *Neural computation*, 5(6):843–855, 1993.

[SFS98] Elad Schneidman, Barry Freedman, and Idan Segev. Ion channel stochasticity may be critical in determining the reliability and precision of spike timing. *Neural computation*, 10(7):1679–1703, 1998.

[SFV03] B Spagnolo, A Fiasconaro, and D Valenti. Noise induced phenomena in lotka-volterra systems. *Fluctuation and Noise Letters*, 3(02):L177–L185, 2003.

[SG05] Alfons Schnitzler and Joachim Gross. Normal and pathological oscillatory communication in the brain. *Nature reviews neuroscience*, 6(4):285–296, 2005.

[SGH01] Gerhard Schmid, Igor Goychuk, and P Hänggi. Stochastic resonance as a collective property of ion channel assemblies. *EPL (Europhysics Letters)*, 56(1):22, 2001.

[Sin93] Wolf Singer. Synchronization of cortical activity and its putative role in information processing and learning. *Annual review of physiology*, 55(1):349–374, 1993.

[SJ60] Robert GD Steel and H James. Principles and procedures of statistics: with special reference to the biological sciences. Technical report, New York, US: McGraw-Hill, 1960.

[SLN10] B Sengupta, SB Laughlin, and JE Niven. Comparison of langevin and markov channel noise models for neuronal signal generation. *Physical Review E*, 81(1):011918, 2010.

[SLYH08] Antti Saarinen, Marja-Leena Linne, and Olli Yli-Harja. Stochastic differential equation model for cerebellar granule cell excitability. *PLoS Comput Biol*, 4(2):e1000004, 2008.

[SM13] Brett A Schmerl and Mark D McDonnell. Channel-noise-induced stochastic facilitation in an auditory brainstem neuron model. *Physical Review E*, 88(5):052722, 2013.

[SNN+03] Kevin M Spencer, Paul G Nestor, Margaret A Niznikiewicz, Dean F Salisbury, Martha E Shenton, and Robert W McCarley. Abnormal neural synchrony in schizophrenia. *The Journal of Neuroscience*, 23(19):7407–7411, 2003.

[SSR05] Julian Seifter, David Sloane, and Austin Ratner. *Concepts in medical physiology*. Lippincott Williams & Wilkins, 2005.

[SSR15] Yevgeniy B Sirotin, Roman Shusterman, and Dmitry Rinberg. Neural coding of perceived odor intensity. *eneuro*, 2(6):ENEURO–0083, 2015.

[SW79] Erik Skaugen and Lars Walløe. Firing behaviour in a stochastic nerve membrane model based upon the hodgkinhuxley equations. *Acta Physiologica*, 107(4):343–363, 1979.

[Szy11] Brett Szymik. A nervous journey. asu - ask a biologist, 2011.

[TFM+96] Simon Thorpe, Denis Fize, Catherine Marlot, et al. Speed of processing in the human visual system. *nature*, 381(6582):520–522, 1996.

[TJ12] Henry C Tuckwell and Jürgen Jost. Analysis of inverse stochastic resonance and the long-term firing of hodgkin–huxley neurons with gaussian white noise. *Physica A: Statistical Mechanics and its Applications*, 391(22):5311–5325, 2012.

[TK02] Matthew C Tresch and Ole Kiehn. Synchronization of motor neurons during locomotion in the neonatal rat: predictors and mechanisms. *Journal of Neuroscience*, 22(22):9997–10008, 2002.

[TLK07] Alessandro Torcini, Stefano Luccioli, and Thomas Kreuz. Coherent response of the hodgkin–huxley neuron in the high-input regime. *Neurocomputing*, 70(10):1943–1948, 2007.

[TS97] Igor Timofeev and Mircea Steriade. Fast (mainly 30–100 hz) oscillations in the cat cerebellothalamic pathway and their synchronization with cortical potentials. *The Journal of physiology*, 504(1):153–168, 1997.

[TW05] Henry C Tuckwell and Frederic YM Wan. Time to first spike in stochastic hodgkin–huxley systems. *Physica A: Statistical Mechanics and its Applications*, 351(2):427–438, 2005.

[UOG12] M Uzuntarla, M Ozer, and DQ Guo. Controlling the first-spike latency response of a single neuron via unreliable synaptic transmission. *The European Physical Journal B*, 85(8):1–8, 2012.

[US06] Peter J Uhlhaas and Wolf Singer. Neural synchrony in brain disorders: relevance for cognitive dysfunctions and pathophysiology. *Neuron*, 52(1):155–168, 2006.

[US10] Peter J Uhlhaas and Wolf Singer. Abnormal neural oscillations and synchrony in schizophrenia. *Nature reviews neuroscience*, 11(2):100–113, 2010.

[VGT05] Rufin VanRullen, Rudy Guyonneau, and Simon J Thorpe. Spike times make sense. *Trends in neurosciences*, 28(1):1–4, 2005.

[VHIAD07] Moritz Von Heimendahl, Pavel M Itskov, Ehsan Arabzadeh, and Mathew E Diamond. Neuronal activity in rat barrel cortex underlying texture discrimination. *PLoS Biol*, 5(11):e305, 2007.

[VISGR+12] Francisco J Vidal-Iglesias, Jose Solla-Gullon, Antonio Rodes, Enrique Herrero, and Antonio Aldaz. Understanding the nernst equation and other electrochemical concepts: An easy experimental approach for students. *Journal of Chemical Education*, 89(7):936–939, 2012.

[VROS03] MCW Van Rossum, Brendan J O'Brien, and Robert G Smith. Effects of noise on the spike timing precision of retinal ganglion cells. *Journal of neurophysiology*, 89(5):2406–2419, 2003.

[vVS97] Carl van Vreeswijk and H Sompolinsky. Irregular firing in cortical circuits with inhibition/excitation balance. In *Computational Neuroscience*, pages 209–213. Springer, 1997.

[vWBD12] Bernadette van Wijk, Peter J Beek, and Andreas Daffertshofer. Neural synchrony within the motor system: what have we learned so far? *Frontiers in human neuroscience*, 6:252, 2012.

[WKAK98] John A White, Ruby Klink, Angel Alonso, and Alan R Kay. Noise from voltage-gated ion channels may influence neuronal dynamics in the entorhinal cortex. *Journal of neurophysiology*, 80(1):262–269, 1998.

[WPDC10] Qing Yun Wang, MATJAŽ PERC, Zhi Sheng Duan, and Guan Rong Chen. Spatial coherence resonance in delayed hodgkin–huxley neuronal networks. *International Journal of Modern Physics B*, 24(09):1201–1213, 2010.

[WR83] W John Wilbur and John Rinzel. A theoretical basis for large coefficient of variation and bimodality in neuronal interspike interval distributions. *Journal of Theoretical Biology*, 105(2):345–368, 1983.

[WRK00] John A White, Jay T Rubinstein, and Alan R Kay. Channel noise in neurons. *Trends in neurosciences*, 23(3):131–137, 2000.

[Zad96] Anthony Zador. When is an integrate-and-fire neuron like a poisson neuron? 1996.

[ZJ04] Shangyou Zeng and Peter Jung. Mechanism for neuronal spike generation by small and large ion channel clusters. *Physical Review E*, 70(1):011903, 2004.

[ZSN+15] Yanfang Zuo, Houman Safaai, Giuseppe Notaro, Alberto Mazzoni, Stefano Panzeri, and Mathew E Diamond. Complementary contributions

of spike timing and spike rate to perceptual decisions in rat s1 and s2 cortex. *Current Biology*, 25(3):357–363, 2015.

[ZSR+10] Ariel Zylberberg, Diego Fernández Slezak, Pieter R Roelfsema, Stanislas Dehaene, and Mariano Sigman. The brain's router: a cortical network model of serial processing in the primate brain. *PLoS computational biology*, 6(4):e1000765, 2010.

[ZY09] C Zhu and G Yin. On hybrid competitive lotka–volterra ecosystems. *Nonlinear Analysis: Theory, Methods & Applications*, 71(12):e1370–e1379, 2009.